

Cell Density Monitoring and Control of Microencapsulated CHO cell cultures

Harriet Emma Cole

Bachelor of Science in Life Technologies, Major in Biotechnology

A dissertation submitted in fulfilment of the
requirements for the award of
Doctor of Philosophy (PhD)

To the



Dublin City University

Faculty of Science and Health, School of Biotechnology,

Supervisor: Professor Ian W. Marison

July 2015

Declaration

I hereby certify that this material, which I now submit for assessment on the programme of study leading to the award of Doctor of Philosophy is entirely my own work, that I have exercised reasonable care to ensure that the work is original, and does not to the best of my knowledge breach any law of copyright, and has not been taken from the work of others save and to the extent that such work has been cited and acknowledged within the text of my work.

Signed:

Harriet Emma Cole, Student ID: 11212634

July 2015

Table of Contents

Declaration	i
List of Figures	vii
List of Tables	xiv
Acknowledgements	xv
Abstract	xvii
Chapter 1 Introduction	- 1 -
1.1. Context of study and problem statement	- 2 -
1.1.1. Introduction.....	- 2 -
1.1.2. Problem statement.....	- 3 -
1.1.3. Funding resources.....	- 4 -
1.2. The present study.....	- 4 -
1.2.1. Aim of the thesis.....	- 4 -
1.2.2. Research questions	- 5 -
1.2.3. Thesis outline	- 5 -
Chapter 2 The application of dielectric spectroscopy and biocalorimetry for the monitoring of biomass in immobilized mammalian cell cultures	- 6 -
2.1. Introduction.....	- 7 -
2.2. Biomass monitoring methods	- 8 -
2.3. Dielectric spectroscopy	- 9 -
2.3.1. Cell suspension an RC-circuit?	- 9 -
2.3.2. Cell Suspension characterization.....	- 12 -
2.3.3. Successful applications.....	- 16 -
2.4. Biocalorimetry	- 17 -
2.4.1. Cellular metabolism.....	- 17 -
2.4.2. Calorimeters	- 17 -
2.4.3. Principles of bench scale calorimetry	- 18 -

2.4.4. Bench Scale biocalorimetry applications.....	- 19 -
2.5. Conclusions	- 20 -
Chapter 3 Materials and Methods in Cell culturing, cell encapsulation and culture analysis	- 22 -
3.1. Cell culture and Inoculum development.....	- 23 -
3.1.1. Cell line.....	- 23 -
3.1.2. Cell culture media.....	- 23 -
3.1.3. Thawing cells.....	- 24 -
3.1.4. Cell maintenance and inoculum development	- 24 -
3.1.5. Cell banking.....	- 25 -
3.2. Bioreactors and culture settings	- 25 -
3.3. Cell microencapsulation in alginate-poly-L-lysine-alginate microcapsules	- 26 -
3.3.1. Bioencapsulation principles.....	- 26 -
3.3.2. Calcium alginate poly-L-lysine microcapsules	- 28 -
3.3.3. Procedure.....	- 30 -
3.4. Off-line cell culture analysis	- 30 -
3.4.1. Microcapsule break-up method for off-line line cell quantification.....	- 31 -
3.4.2. Metabolite and protein quantification.....	- 31 -
3.5. Off-line microcapsule characterisation	- 32 -
3.5.1. Capsule size measurements	- 32 -
3.5.2. Texture analyser	- 32 -
3.5.3. Membrane and pore size evolution analysis.....	- 33 -
3.5.4. 3-D cell viability estimation within microcapsules by confocal microscopy.....	- 33 -
Chapter 4 Development of a reliable data acquisition system for real time monitoring of mammalian cell cultures	- 34 -
4.1. Introduction.....	- 35 -
4.1.1. Design criteria.....	- 35 -
4.1.2. Selection of a programming environment	- 37 -

4.1.3. Different applications and available monitoring and controlling mammalian cell cultures	- 38 -
4.1.4. Basic programming in LabVIEW:.....	- 39 -
4.1.5. Software and modules.....	- 39 -
4.1.6. Hardware:.....	- 39 -
4.2. Cell culture monitoring code description.....	- 40 -
4.2.1. Implementing the Cole-Cole model.....	- 43 -
4.2.1. Project development for monitoring cultures in the eRC1	- 46 -
4.3. Outcome and conclusion.....	- 48 -
Chapter 5 The Application of Dielectric Spectroscopy for Monitoring the Viable Cell Density of Microencapsulated CHO Cell Cultures	- 50 -
5.1. Introduction.....	- 51 -
5.2. Effect of the microcapsules on the dielectric signal	- 52 -
5.3. CHO-DP12 dielectric characterisation	- 53 -
5.3.1. Cole-Cole modelling.....	- 53 -
5.3.2. Viable cell density and capacitance <i>C</i> 580 <i>kHz</i> correlation	- 58 -
5.4. The monitoring of batch cultures	- 61 -
5.5. Outcome and conclusion.....	- 66 -
Chapter 6 Application of biocalorimetry combined with dielectric spectroscopy for the monitoring of microencapsulated CHO perfusion cultures	- 68 -
6.1. Introduction.....	- 69 -
6.2. Culture predictions and applicability of bench scale biocalorimetry	- 71 -
6.3. eRC1 installation for perfusion culture operation.....	- 73 -
6.4. Validation of biocalorimetry as monitoring method	- 74 -
6.4.1. Signal resolution	- 74 -
6.4.2. Influence of the feed on the signal.....	- 76 -
6.4.3. Method validation for CHO cell cultures	- 77 -
6.5. Online monitoring of perfusion cultures	- 78 -
6.5.1. Perfusion method	- 78 -

6.5.2. Perfusion cultures cell density and metabolite analysis	- 79 -
6.5.3. Microcapsule colonisation and limitations	- 82 -
6.6. Conclusion and outlook.....	- 83 -
Chapter 7 Design of a simple feed control based on capacitance data in microencapsulated fed-batch cultures	- 85 -
7.1. Introduction.....	- 86 -
7.2. Control strategy.....	- 87 -
7.2.1. Control strategy design	- 87 -
7.2.2. Implementation in LabVIEW	- 88 -
7.3. Preliminary fed-batch results.....	- 92 -
7.3.1. Culture method and simulation	- 92 -
7.3.2. Results.....	- 94 -
7.3.3. Implications of lactate concentrations upon the cell development.....	- 96 -
7.3.4. Culture outcome.....	- 98 -
7.4. Reduction of the initial glucose concentration to increase duration of control	- 99 -
7.4.1. Culture method and simulation	- 99 -
7.4.2. Culture results.....	- 101 -
7.5. Conclusions and outlook.....	- 103 -
Chapter 8 Outcome, Outlook and Conclusion.....	- 104 -
8.1. Introduction.....	- 105 -
8.2. Findings of the study	- 106 -
8.2.1. Elaboration of an automated monitoring and feed control program	- 106 -
8.2.2. Are dielectric spectroscopy and macrocalorimetry valid methods to monitor microencapsulated CHO cell cultures?	- 106 -
8.3. Theoretical implications	- 108 -
8.4. Limitations of the study and recommendations for future research.....	- 108 -
8.5. Conclusion	- 109 -
A. Appendix.....	I
a. Publications.....	I

b. Oral presentations.....	I
c. Posters.....	I
d. The LabVIEW monitoring and control VI	II
i. The necessary software installed on the computer	II
ii. Necessary software and sub-modules installed on CompactRIO	II
iii. User manual (for Fed-Batch cultures, more complete version).....	III
iv. Acquisition VI Code.....	VII
v. Main DAq FEDBatch VI.....	IX
vi. Cole Cole modelling of frequency scans	X

CD: LabVIEW software and elaborated VIs

List of Figures

- Figure 2.1. Electric diagram of a resistor capacitor circuit. Symbols from left to right: AC voltage source, resistor and a capacitor - 9 -
- Figure 2.2. Polarization of the dielectric when under an electrical field - 10 -
- Figure 2.3. The response electrical field amplitude is smaller and shifted from the emitted field. The simulated RC-circuit is built with a 2Ω resistor, a 412 pF/cm capacitor. The generator voltage is set at 2 Volts alternating at a frequency of 500 kHz..... - 11 -
- Figure 2.4. Electrical field generated by the electrodes (blue) polarises the cells. The polarised cells then emit an electrical field in response which can be detected by the receiving electrodes (red) (Brandon Downey and Lisa Graham, 2013)..... - 11 -
- Figure 2.5. Schematic diagram showing the charge migration within a cell suspension when an electrical current is applied. The positive charge migrates towards the negative electrode and the negative charge towards the positive electrode. Unlike cell debris and solid particles, intact cells entrap ions which consequently polarize them..... - 12 -
- Figure 2.6. The polarisation of a cell at a given electrical frequency is dependent on the cell size - 13 -
- Figure 2.7. At low frequencies, the cells have a sufficient amount of time to polarise, therefore, the time shift is significant and the amplitude between the driven and response field is small. At the characteristic frequency ωc , the amplitude difference is greater and the time lag smaller, and at high frequencies no cells polarise, so little signal is measured - 14 -

Figure 2.8. Parameters determined through the curve fit Equation (2.6) and Equation (2.7) into experimental data (Dabros et al., 2009c).....	- 15 -
Figure 2.9 Diagram of the eRC1, Mettler Toledo Reaction Calorimeter	- 19 -
Figure 3.1 Neubauer Haemocytometer counting chamber. Highlighted is one of the 4 large squares that were to be counted for estimating the viable cell density and viability and corresponded to a volume of 100 nL.....	- 24 -
Figure 3.2 Microcapsules offer an optimal environment for the cells to develop. The semi-permeable membrane allows the inflow of essential nutriment such as glucose or L-glutamine, dissolved O ₂ , and the egress of waste by-products (lactate, ammonia) CO ₂ . The microcapsule membrane pore size can be engineered to allow diffusion or retention of large proteins such as recombinant antibodies.....	- 26 -
Figure 3.3 Diagram of the encapsulator set-up. The alginate-cell suspension is aseptically connected to the sterile vibrating chamber. The suspension is extruded through the nozzle by pressurising the alginate-cell containing bottle. Two other bottles are also aseptically connected: one for the waste collection and one for recuperating the manufactured microcapsules.	- 28 -
Figure 3.4 Molecular structure of alginate A: Sodium alginate molecular structure showing both β-D-mannuronic acid and α-L-guluronic acid residues; B: Egg box model; C: sodium alginate complex with Ca ²⁺ (Gombotz and Wee, 1998)	- 29 -
Figure 3.5 Poly-L-lysine monomer.....	- 29 -
Figure 4.1 Example of a bioreactor setup. Different <i>apparati</i> send continuous signal to a central computer which repeatedly gathers data from different variables such as DO, pH, biomass, temperature, and mass of additional liquid components (base and feed bottles). Peristaltic pumps are controlled (dashed lines) either by signal sent by computer or by an external controller. Cell cultures are usually an isothermal process and the broth's temperature is controlled by heating or cooling the fluid within the reactor's jacket	- 35 -
Figure 4.2 User-interface, or Front panel, displaying the evolution of the different monitored variables of an encapsulated CHO-DP12 perfusion culture; Perfusion culture 3, at the end of culture on the closing of day 9.	- 36 -
Figure 4.3 Data flow programming. a. Simple mathematical program and b. it's data flow equivalent: A and B are performed in parallel, however, C cannot be executed until the both values have been calculated.	- 38 -

Figure 4.4	Flow chart of the data acquisition program, (daq = data acquisition, BM= Biomass monitor).....	- 41 -
Figure 4.5	LabVIEW code of the Cole-Cole equation, Equation (2.6)	- 44 -
Figure 4.6	LabVIEW code of the Iteration of the three equation with three unknowns: The cell number per unit volume N_v , the cell radius r and the culture media conductivity σ_e	- 45 -
Figure 4.7	Screen shot of a frequency scan undertaken on day 12 of the second perfusion culture, in the RC1. The cell count on that day revealed that the culture had a density of $14.5 \cdot 10^6$ cells \cdot mL ⁻¹ . The average cell radius measured on that day was 6.2 μ m.....	- 46 -
Figure 5.1	Capacitance and Conductivity frequency scans of a homogenously agitated 50% (V/V) alginate bead suspension in a MOPS buffer compared those performed in MOPS solution in the absence of beads.....	- 53 -
Figure 5.2	Evolution of the characteristic frequency ω_c throughout a 12 day culture (blank circles) and error bars determined at $\Phi=95\%$	- 54 -
Figure 5.3	Capacitance measurements over the pre-set 25 frequencies performed on different encapsulated cell densities. Each scan was modelled with the Cole-Cole equation and fitted in the LabVIEW VI using the Levenberg-Marquardt algorithm (each density is expressed in (mio) million cells per mL).....	- 55 -
Figure 5.4	Conductivity measurements over the pre-set 25 frequencies performed on different encapsulated cell densities. Each scan was modelled with the adapted Cole-Cole equation and fitted in the LabVIEW VI using the Levenberg-Marquardt algorithm (each density is expressed in (mio) million cells per mL).....	- 56 -
Figure 5.5	Linear correlation between the results of a frequency scan and the offline VCD determination method. A: The number of viable cells per unit volume; B: The permittivity difference $\Delta\epsilon$	- 58 -
Figure 5.6	Linear correlation between the viable cell density with the capacitance. The correlation coefficient is equal to $R= 0.9996$	- 59 -
Figure 5.7	Linear regression of on-line capacitance plotted against viable cell density per mL in A: suspension cell cultures; B: in encapsulated cultures (solid line). The area between the dashed lines represents the confidence band ($\phi = 95\%$, $N= 13$ for the suspension cultures and $N= 17$ for encapsulated cultures).....	- 60 -

- Figure 5.8 Evolution of the viable cell density determined with on-line (—) and off-line (◊) methods for A: cell suspension culture, and B: encapsulated cell culture - 62 -
- Figure 5.9 Daily frequency scans modelled using the Cole-Cole equation and fitted in LabVIEW VI using the Levenberg-Marquardt algorithm. The vertical lines represent the characteristic angular frequency ω_c - 62 -
- Figure 5.10 Typical evolution of metabolite concentrations during an encapsulated culture. A: Glucose and lactate concentrations and viable cell density with respect to the total working volume evolution. Glucose (61.5%) was converted to lactate up until glucose depletion on Day 7. B: L-Glutamine and ammonia concentrations. L-glutamine was totally consumed between days 0 and 4. After L-glutamine depletion, the ammonia concentration remained constant until day 7 and then increased once again. The depletion of L-glutamine did not appear to influence cell growth..... - 64 -
- Figure 5.11 Cell growth evolution within microcapsules; a: Day 0: cells were homogeneously dispersed (magnification 40X); b: Day 3, small colonies start to form (magnification 40X); c: Day 7, the average capsule colonisation reached 1.8 % of the total theoretical colonization potential (magnification 40X)d: Day 7, magnification 400 x showed cells forming close contacts with one another to create aggregates - 66 -
- Figure 6.1. Diagram of a perfusion culture setup. (A) Schematic representation of a perfusion culture for suspension cells in a stirred tank reactor. A cell retention system, such as a microfilter, is necessary to separate the cells from spent media. (B) Schematic representation of a perfusion culture for immobilized cells. The microcarriers or microcapsules are sufficiently large to be retained within the vessel by a wire mesh..... - 69 -
- Figure 6.2 Confocal image of calcium-alginate poly-L-lysine-alginate microcapsules and membranes, on Day 0, immediately after inoculation. The average microcapsule radius is 260 μm and the membrane, 18 μm . The stained cells fluoresce green if viable, or red if dead..... - 71 -
- Figure 6.3 Capacitance (A) and heat flow (B) predictions throughout the exponential phase, assuming the cells duplicate at the maximum growth rate $\mu_{\text{max}} = 0.64 \text{ day}^{-1}$, and the stationary phase, when the full microcapsule colonisation potential is achieved..... - 72 -
- Figure 6.4 Perfusion culture equipment setup. The fresh media is pumped to a smaller bottle to preheat the feed before being supplied to the cells. At

	the same rate, spent medium is removed and collected in a third bottle.	
	It must be noted that the set-up only has one peristaltic pump.	- 73 -
Figure 6.5	Heat flow baseline measurements over a three day period. The standard deviation is evaluated at 0.061 W.....	- 75 -
Figure 6.6	Linear relationship between the measured heat flow rate and the tested feed rates ranging from 0.276 to 5 L·day ⁻¹	- 76 -
Figure 6.7	Metabolic heat flow rate and viable cell density are linearly correlated. The linear regression is constructed with a slope $a = 74.77 \cdot 10^{-11} \text{ W} \cdot \text{cell}^{-1}$ and a correlation coefficient of $R = 0.99$	- 77 -
Figure 6.8	The viable cell density evolution throughout the whole culture time estimated by offline cell counts, dielectric spectroscopy and calorimetry. The peaks in the viable cell density signal determined by calorimetry were caused by sampling.	- 80 -
Figure 6.9	Metabolite concentration during the batch and perfusion phases of the culture. The perfusion phase is initiated on day 4 with a feed rate of 1.7 L·days ⁻¹	- 80 -
Figure 6.10	Evolution of glucose and L-glutamine to number of cells yields $Y_{X/S}$, and the produced lactate and ammonia to cells yields, $Y_{P/X}$, over the whole culture period, expressed in [$\text{cells} \cdot \text{mmol}^{-1}$] and [$\text{mmol} \cdot \text{cell}^{-1}$] respectively.....	- 81 -
Figure 6.11	Accumulated recombinant IgG1 manufactured in an encapsulated perfusion culture. After 12 days, 2.4 g of IgG1 was produced by $14.5 \cdot 10^6 \text{ cells} \cdot \text{mL}^{-1}$ in a 1.4L culture.	- 82 -
Figure 6.12	Typical microcapsule structural proprieties (A) and microcapsule to working volume ratio (B) development throughout a perfusion culture.....	- 82 -
Figure 6.13	Photograph of the remaining intact microcapsules on day 12 suggesting near to full packing has been reached	- 83 -
Figure 7.1	Flow chart of the feed control feature inserted within the previously designed LabVIEW VI (Small box, right corner. The red box displays the location where the new code is inserted)	- 89 -
Figure 7.2	Front panel of the Main DAq FEDBatch VI with added culture parameters that allowed the transfer of the VI to monitor and control various types of fed-batch cultures.....	- 90 -
Figure 7.3	LabVIEW code for creating or replacing the buffer file, saving the 2-D array and calculating the growth rate (A). Below in B, is the implementation of equation (7.1), in a case structure to allow the operator to decide when to start the feed.....	- 91 -

Figure 7.4	Predicted evolution of the culture variables throughout the microcapsule colonisation period, from inoculation to full microcapsule colonisation. The model was constructed admitting that no lag phase or growth inhibition could be observed and using equations (7.3) to (7.11) in Table 7.1.....	- 93 -
Figure 7.5	Evolution of the cell density and supplementation of feed throughout the whole fed-batch culture. A: Development of the viable cell density estimated by dielectric spectroscopy and off line microscopic cell counts; B: Volume of feed medium added to the culture during the fed-batch phase	- 94 -
Figure 7.6	Comparison between the feed and growth rates calculated in LabVIEW and recorded in the data acquisition text file during the fed-batch phase of the culture	- 95 -
Figure 7.7	Evolution of the glucose and lactate concentrations (A) and L-glutamine and ammonia concentrations (B) throughout the first controlled feed fed-batch culture.....	- 95 -
Figure 7.8	Glucose and L-glutamine catabolic pathways, which take place in the mitochondrion, lysing glucose and L-glutamine into lactate and ammonia. ACL, ATP-citrate lyase; ACC, acetyl-CoA carboxylase; FAS, fatty acid synthase; ME, malic enzyme; Ac-CoA, acetyl-CoA; Mal-CoA, malonyl-CoA; MDH, malate dehydrogenase; LDH-A, lactate dehydrogenase-A; GLS, glutaminase. Adapted from (Zagari, 2012)	- 96 -
Figure 7.9	Effect of the initial lactate concentration on viable cell density (A), growth rate (B) and the produced lactate (C)	- 97 -
Figure 7.10	Predicted evolution of the culture variables throughout the second feed controlled culture, from inoculation until when the reactor would be completely filled. The model was constructed admitting that no lag phase or growth inhibition could be observed. The grey dashed-dot-dashed line represents the expected culture time based on the produced lactate concentration when would have reached 50 mM.....	- 100 -
Figure 7.11	Evolution of the cell density and feed supplementation throughout the entire culture time of the second fed-batch culture. A: Development of the viable cell density estimated by dielectric spectroscopy and off line microscopic cell counts; B: Volume of feed medium added to the culture during the fed-batch phase.....	- 101 -

Figure 7.12 Evolution of glucose and lactate concentrations (A) and L-glutamine and ammonia concentrations (B) throughout the second adapted controlled feed fed-batch culture.....	- 102 -
Figure 7.13 Production of rIgG1 (A), and evolution of the packed microcapsule to working volume (B) of the second adapted fed-batch.....	- 103 -
Figure A.1 Code for the acquisition of the signals received from the pH controller, DO controller, ambient temperature pt100 and calorimeter eRC1.....	VII
Figure A.2 Sub-VI to obtain and read the signal sent by the eRC1	VII
Figure A.3 Code for the acquisition of the signals received from the Biomass Monitor	VIII
Figure A.4 Sub-VI to obtain and read the signal sent by the Biomass Monitor from ABER Instruments.....	VIII
Figure A.5 Code of the Main Data Acquisition VI. This VI codes for saving the data into a text file after calculating an average and adding the new data point to the time chart. In addition, in the FEDbatch VI, the growth rate and the feed rate are calculated	IX
Figure A.6 Code for the frequency scans modelling using the Cole Cole equations, and iteration to determine the cell radius, cell number per unit volume and the conductivity of the medium.....	X
Figure A.7 Code of the Cole Cole formula used to fit capacitance values	XI
Figure A.8 Code of the Cole Cole formula used to fit conductivity values.....	XI

List of Tables

Table 2.1.	Direct and Indirect methods for biomass estimation and its applicability to immobilized cell cultures	- 8 -
Table 3.1	Elution program for the quantification of IgG ₁ by affinity HPLC.....	- 32 -
Table 4.1	Information type and respective wire code	- 39 -
Table 5.1	Parameters and respective confidence interval ($\alpha=0.05$) for the calibration model (N=10), suspension (N= 13) and encapsulated cultures (N=17) of the linear correlation $y = ax + b$, and correlation coefficient R.....	- 60 -
Table 5.2	Comparison of the growth kinetics and stoichiometric characteristics between the encapsulated and suspension CHO-DP12 cell cultures.....	- 65 -
Table 6.1	Equations used to evaluate the evolution of the biomass to substrate and product to biomass yields from day to day depending on the perfusion culture stage Nomenclature: $Y_{X/S}$ = Biomass to substrate yield, $Y_{P/X}$ = Product to biomass yield, X viable cell density, S = substrate concentration culture, S_f = substrate concentration in the feed, P= product concentration, D = Dilution rate, μ = growth rate, and t = time.....	- 70 -
Table 6.2	Monitoring encapsulated CHO-DP12 cell cultures method validation	- 77 -
Table 7.1	Equations used to simulate the potential evolution of the different measured variables of a fed-batch culture, in figures Figure 7.4 and Figure 7.10. Nomenclature: F = Feed rate, V = volume, V_0 = volume at t_0 , V_{wv} = working volume, X viable cell density (VCD), q_s = substrate consumption rate, S = substrate concentration culture, S_f = substrate concentration in the feed, P= product concentration, P_0 = product at t_0 , q_p = product production rate and t = time	- 93 -

Acknowledgements

Firstly and foremost, I would like to express my gratitude to my supervisor Professor Ian Marison under whose expertise and guidance this research and work was executed. In addition to the extensive knowledge and experience of Professor Marison in the field of biotechnology, I am grateful for the use of the infrastructures and equipment made available, which provided excellent conditions for the laboratory work undertaken for the realisation of this thesis.

Secondly, I would like to thank Mary Rafter, who from the start of this journey, helped organising meetings, annual reports, travel, accommodation and managing the purchase of all the necessary consumables and chemicals. Furthermore, I'd like to extend my gratitude to Dr. Rosaleen Devereay for all her support and encouragements.

Very special thanks go to Aurélie Demont ("Cocotte") who has not only been a good friend, but also a good partner in all the various experiments undertaken. I will never forget those "late nights", investigating different ideas listening to a wide repertoire of music! I would also like to thank Brian Freeland, who spent some of his valuable time teaching me to code in LabVIEW and helped me design the skeleton of the main VI. I would also like to show my appreciation to all the members of LIB including Dr. Micheal Whelehan, Dr. Sinead Doherty, Dr. Pirkko Muhonen, Dr. Siobhan Hennessey, Dr. Moira Schuler ("Schülerin"), Dr. Roisin Foley, Dr. Bianca Tassinari, Dr. Karen Byrne, Dr. Tanja Buch (Dr. TaBu), Sharon Conaghan, Yannick Dufour, Niamh Sheridan, Jérémy Baras, Sabrina Wiedmer and Tracy Ghidossi.

In addition, I extend my acknowledgements to Professors Alana James, Maria Sanchez Patino and Bob Zenhausern, who throughout the PhD Accelerator Experience and other conferences helped me gain confidence in my writing, and helped me understand the

structure and content of a well written thesis. I do recommend Alana's book entitled "Writing your Doctoral Dissertation or Thesis Faster: A proven Map to Success" to any PhD student.

I am extremely thankful to Fintan Thorn, who has been my rock throughout this journey and has kept me focused on the end goal. He and his family, especially his parents Dr Richard and Suzanne Thorn, and Aunt and Uncle, Adrienne Galligan and Paul Houston have made this journey a better one by believing in me and discussing different aspects of the work.

Finally, I would like to thank all my friends, my friends of the SubAqua club including Paul, Alice, Emmet, Aoibheann, Johan, Samira, John, and family but especially my parents Simon and Christl for their encouragements, understanding and support, my brothers James who has help me gain an understanding of the physics of capacitors, and William for his continuous brotherly teasing!

Abstract

Though mammalian cells play a key role in the manufacturing of recombinant glycosylated proteins, cell cultures and productivity are limited by the lack of suitable systems to enable stable perfusion culture. Microencapsulation, or entrapping cells within a semi-permeable membrane, offers the potential to generate high cell density cultures and improve the productivity by mimicking the cells natural environment. However, the cells being secluded by the microcapsules membrane are difficult to access for monitoring purposes. In this study, CHO-DP12 cells were cultured within calcium-alginate-poly-L-lysine-alginate microcapsules in two bench scale- bioreactors, including a highly sensitive bench-scale calorimeter. The different cultures were monitored by continuous real-time dielectric spectroscopy and/or heat-flow measurements. These measurements were acquired, saved and plotted as time charts for rapid culture evaluation within a LabVIEW Virtual Instrument specifically designed for this study. Findings of this study show that capacitance measurements gave real time information on the viable cell density evolution in batch, fed batch and high density perfusion cultures; and the heat flux measurements allowed to follow the cell evolution in high density perfusion cultures. More significantly, dielectric spectroscopy gave precise information throughout each stage of the culture, from inoculation to the maximum cell density reached and through the early stages of the decline phase. Based on these results, a control strategy was implemented within the tailored LabVIEW program to control the feed rate of fed-batch cultures. The feed rate was calculated directly in the Virtual Instrument in accordance with the viable cell density and growth rate measured by dielectric spectroscopy. The capability of monitoring the evolution of microencapsulated cultures brings microencapsulation technology a step towards a potential industrial application.

Chapter 1 Introduction

1.1. Context of study and problem statement

1.1.1. Introduction

Glycosylated therapeutic recombinant proteins, such as monoclonal antibodies, represented 50% of all the 151 protein based drugs approved by the FDA and EMEA by 2009, which corresponded to a multibillion US dollar market (Ferrer-Miralles et al., 2009; Martínez et al., 2012; Walsh, 2014). Glycosylated therapeutic proteins, currently may only be manufactured using mammalian cell lines and hybridoma cells. Unlike microbial cells, mammalian cells have the capacity to glycosylate, fold and undertake other post-translational modifications in a similar manner to the human cells. Without these post-translational modifications, the protein of interest would most likely lose its affinity for its target (substrate or antigen) or even completely lose its original functionality. However, cultivating these cells is more complex than microbial cells as they have a slower doubling time and generate much lower yields. It is said that microbial cells can produce a growth hormone in the order of $3 - 5 \text{ g} \cdot \text{L}^{-1}$, whereas, the expression levels found in mammalian cell rarely exceeds $500 \text{ mg} \cdot \text{L}^{-1}$ (Demain and Vaishnav, 2009; Zhu, 2012).

Additionally, mammalian cells unlike microbial cells do not have a cell wall, making them very sensitive to shear stress caused by agitation or aeration. Industrial bioprocesses are established within stirred tank reactors (STR) as they ensure homogeneity throughout the system. Turbulent eddies are generated through agitation whose intensity is dependent on the reactor and impeller geometries. These eddies distort and stretch the air bubbles, braking them into smaller units to increase the bubbles interfacial area a . Obtaining a large interfacial bubble area is important in living cell bioprocesses as this will increase the dissolved O_2 concentration. However, cells, especially animal cells are highly sensitive to shear stress: cell collisions, bubble coalescence, eddies can cause important hindrances to a bioprocess (Chisti, 2000; Doran, 1995a; Keane et al., 2003). To avoid cell damage, the bioreactor geometry and parameters such as agitation and aeration have been adapted for the cultivation of insect and mammalian cells. Consequently, the material and oxygen transfers are compromised, lowering considerably the maximum viable cell density, thus the amount of therapeutic produced per run.

Two angles may be investigated to improve a bioprocess total product yield:

- Optimising the biological host by choosing a different host cell and/or by genetic alterations. This strategy can rapidly come across biological limitations
- Optimising the production process.

This work focuses on the latter strategy, for the hosts are widely recognized by the FDA and EMEA and used since 1986 (Martínez et al., 2012; Zhou et al., 2009). Cell

immobilisation has been reported to be an efficient way to improve yields of a culture by imitating the natural environment of the cells (Verica et al., 2009a). While most techniques have used macroporous carriers, these have been shown to be limited by the heterogeneous conditions in the reactor, the desorption of cells from the supports, the requirement for serum or fibronectin pre-treatment to facilitate cell binding, and the diffusional limitations that can arise as the cells grow preferentially on the macroporous particle surface, with cells in the core becoming starved of oxygen and other nutrients (Chu and Robinson, 2001; Kong et al., 1998).

On the other hand entrapment of cells within a semi-permeable membrane through microencapsulation would enable cell growth in a protected environment with a constant volume available to the cells, thereby reducing nutrient limitations while minimising the shear stresses encountered in a bioreactor. Previous studies have shown that cell densities can exceed 10^7 cells \cdot mL $^{-1}$ if the culture contains a high number of macroporous particles and if the cells are not substrate-limited (Breguet et al., 2007a; Gugerli, 2003a; Ozturk and Kompala, 2005a; Warnock and Al-Rubeai, 2005); in other words, if the immobilised culture cell viability and density is monitored and controlled by operating the feed at the optimum feed rate.

1.1.2. Problem statement

Numerous studies have shown that microencapsulation increases the cell viability and heterologous protein production (Breguet et al., 2007b; Uludag et al., 2000; Zhang et al., 2008). Yet, being entrapped, the cells are inaccessible for evaluating the cell growth and health of a culture. Many techniques have been developed for determining the viable cell concentration and distributions within the microcapsules. These techniques require the removal of a sample for offline analysis (Catena et al., 2010; Xiao et al., 2010). Removing microcapsules means removing the total amount available space for the cells to develop, thus affecting the outcome of the maximum cell density.

With manufacturing regulations becoming increasingly more stringent, monitoring various culture variables is being promoted by the different drug regulating agencies. Since the FDA published its "Guidance for Industry PAT — A Framework for Innovative Pharmaceutical Development, Manufacturing, and Quality Assurance" initiative for Pharmaceutical cGMPs in September 2004, Process Analytical Tools (PAT) have immensely evolved (Bakeev, 2005). The FDA suggests that the adoption of such tools would help the process gain a better understanding and consequently, batch- to- batch culture variations would be better controlled. A more detailed discussion is given in chapter 2.

Nowadays, there seems to be little, or nothing written, on real-time microencapsulated biomass monitoring. This absence of online monitoring tools makes cell microencapsulation non-compliant to the FDA initiative. Finding a suitable PAT or two would not only bring microencapsulation one step forward towards industrial processes, it will also, in the meantime, give us a better understanding on the cell development and viability throughout a culture as well as enabling a feed rate control. This feed control would be assessed based on a model and the signal acquired from the online monitoring tool.

1.1.3. Funding resources

The work undertaken throughout this PhD project is related to a research project (Project Number 08/IN.1/B1949) funded by the Science Foundation Ireland (SFI) and entitled “Online Monitoring & Control of High Density Cultures” (Principle Investigator: Prof. Ian W. Marison).

1.2. The present study

1.2.1. Aim of the thesis

Like any online monitoring Process Analytical Technology (PAT), the biomass measuring PAT must be accurate, precise, reliable, sensitive and have a short response time (Carloni et al., 2009). In addition, given that the technology is going to be measuring encapsulated mammalian cell growth over a long period of time, the PAT should be non-invasive and must not require capsule breakage for cell accessibility.

Two different PAT are to be investigated:

- Dielectric spectroscopy for measuring the viable cell biovolume and/ or cell concentration
- Bench scale biocalorimetry for measuring the heat of reaction, also known as the metabolic activity of the cells.

In addition to investigating the applicability of these two chosen monitoring techniques, the thesis will discuss the potential of using either techniques to control the feed at a rate that will provide the cells with the nutrients necessary to their development. To combine process monitoring and instrument control, a data acquisition system must be first elaborated which will allow the monitoring of different aspects of a culture (pH, capacitance, temperature, etc.), save the data for further process analysis and output a potential signal to a feed pump.

1.2.2. *Research questions*

The thesis seeks to answer the following questions:

1. Can we monitor encapsulated cells by dielectric spectroscopy? And are there any necessary mathematical corrections to make?
2. Can we monitor the cell metabolic activity in a bench calorimeter, the Bio-RC1?
3. Can either dielectric spectroscopy or biocalorimetry be used as monitoring method to provide in real-time precise and accurate biomass information for a feed control?

1.2.3. *Thesis outline*

To fill the gap this thesis seeks to bridge and answer the research questions, the thesis is composed with 8 distinct chapters, including the introduction chapter. Following this introductory chapter, a literature survey is given in **Chapter 2**, with the aim to convey the importance of applying monitoring tools in mammalian cultures, especially in immobilised, and more precisely in microencapsulated cultures. The chapter then proposes two monitoring methods that will be used in this work: dielectric spectroscopy and bench scale biocalorimetry, and the reasoning for selecting the two technologies. The thesis then moves into **Chapter 3**, which presents the material and methods used throughout the work.

Chapter 4, begins the results part of the thesis by informing the reader on data acquisition programming and describes the elaborated Virtual Instruments (VI) used for undertaking the experimental work. Afterwards, the three stated research questions are explored in their own distinct chapters:

- **Chapter 5** answers whether dielectric spectroscopy can be used to monitor microencapsulated cultures; and if so, if the presence of microcapsules in high volume fractions influences the dielectric signal
- **Chapter 6** investigates the potential of using biocalorimetry to continuously estimate online the viable cell density and determines after the generation of a calibration model what are the limitations of the method
- **Chapter 7** applies dielectric spectroscopy to control a feed rate, calculated and output by the LabVIEW VI, based on a simple feed model.

Finally, the three threads are woven back together, in **Chapter 8**, to offer an answer to the general goal of this thesis which is “*Can we monitor and control microencapsulated CHO cell culture?*”.

Chapter 2 The application of dielectric spectroscopy and biocalorimetry for the monitoring of biomass in immobilized mammalian cell cultures

Summary: The aim of this second chapter is to offer an overview on the importance of monitoring and controlling immobilised mammalian cell cultures and to present the current monitoring techniques available in the literature. The chapter then presents the theory behind the two selected culture monitoring methods: dielectric spectroscopy and biocalorimetry. Mammalian cell cultures are currently the sole process type to correctly manufacture glycosylated proteins for therapeutic means. Such cultures can reveal to be complex and vary from batch to batch. Cells microencapsulation has the potential to improve manufacturing processes. However, cell entrapment hinders offline monitoring methods and not all online monitoring methods can be applicable. Dielectric spectroscopy gives direct online information on the viable cell density, and though some limitations must be considered, the technique has been reported to be a successful method to monitor other types of immobilised cell cultures. Calorimetry provides information upon the cellular metabolic activity which is closely related to cell number, growth rate and viability. Bench scale calorimetry, though no investigation has been published has a true potential, to monitor high mammalian cell density cultures. It is finally suggested to monitor both dielectric spectroscopy and calorimetry for a full comprehensive understanding of the process.

Keywords: Mammalian Cells; Bioprocess Monitoring; Immobilized Cells; Dielectric spectroscopy; Biocalorimetry.

2.1. Introduction

Mammalian cells are used in the biotechnology industry as they are capable to correctly glycosylate and undertake other post-translational modifications of a therapeutic protein (Ozturk and Hu, 2005; Tharmalingam et al., 2011; Wurm, 2004; Zhu, 2012). Though continuous cell lines such as Chinese Hamster Ovary (CHO) cells, adapted to suspension culture, are usually encountered in manufacturing processes, it is sometimes necessary or more advantageous to use immobilized systems (Tharmalingam et al., 2011). Cell immobilization or microencapsulation not only offers a structure for the cells to grow upon and improving productivity, it also eases cell retention in perfusion culture systems, see Chapter 6.

Mammalian cells, to develop, rely on multiple interconnected complex metabolic pathways, such as glycolysis, glutaminolysis and the tricarboxylic acid cycle (TCA) (Ahn and Antoniewicz, 2011; Zamorano et al., 2010). To adapt to the current *in-vitro* culturing methods, the cells had to alter their metabolism. The resulting metabolism is said to be highly deregulated and inefficient. Further amendments in the cellular metabolic activity may still be observed with any pH, temperature or metabolite concentration deviations (Cairó and Gódia, 2005; Read et al., 2010), and with the culture phase (growth or stationary phase) (Ahn and Antoniewicz, 2011). Therefore, a slight change in the process, which may not have been detected during the early stages of a culture, may induce a significant variation in the productivity of the target recombinant protein. Besides a potential deviation in the amount of produced target protein, the reproducibility of the product quality is also dependent on the reproducibility of the process (Gnoth et al., 2007).

To minimise the batch to batch variability, industries are moving towards applying different process analytical technologies (PATs) to monitor, and potentially control their bioprocesses. Since the FDA published the "Guidance for Industry PAT — A Framework for Innovative Pharmaceutical Development, Manufacturing, and Quality Assurance" initiative for Pharmaceutical cGMPs in September 2004, Process Analytical Tools have immensely evolved (Bakeev, 2005). The FDA suggests that the adoption of PAT would help gain a better understanding of the process, which could therefore be better controlled (Chen et al., 2011).

These technologies analyse the chemical or physical proprieties of fluids or gases and should be used to improve the process' design, development and control. The most commonly used sensors are pH, temperature and DO (dissolved oxygen) probes. However, they can only give limited information and control over complex systems such as cell fermentations. Many techniques exist which can potentially measure a wide range of different characteristics from biomass to metabolites and gases (Bakeev, 2005).

Biomass quantification and viability determination is a key aspect to any upstream bioprocess, as other culture variables depend on the biomass' developments (Dabros et al., 2010; Dorresteyn et al., 1996). Though cell immobilization offers many advantages, the cells are not readily accessible for culture analysis. Continuously removing a small sample of carriers or microcapsules would mean reducing the available space for the cells to colonize, thus reducing the number of cells and diminishing the global productivity.

2.2. Biomass monitoring methods

Accurate biomass monitoring and control is essential to achieve robust bioprocesses and heterologous protein production. Direct and indirect techniques exist to monitor cell growth and viability. Direct methods measure a physical propriety of a cell and its components, whereas indirect methods measure factors related to the cells and their activity (respiration, electrochemical behaviour, and/or nutrient fluctuation) Table 2.1 (Carloni et al., 2009; Potvin et al., 2012).

Table 2.1. Direct and Indirect methods for biomass estimation and its applicability to immobilized cell cultures

PAT	Measured bioprocess variable	Direct/Indirect	Applicability to immobilized cell cultures
Dielectric Spectroscopy	Capacitance	Direct	Yes
Optical Probing	Turbidimetry or nephelometry in VIS or NIR, MIR and FTIR	Direct	No
MultiWavelength Fluorescence	Cellular fluorophores (NAD(P)H, flavins and aromatic amino acids	Indirect	No
Biocalorimetry	Heat production from metabolic activity	Indirect	Yes
Off-gas analysis	Oxygen Uptake Rate (OUR) and Carbon Dioxide Evolution Rate (CER)	Indirect	Yes
Infrared sensors	Metabolite concentrations	Indirect	Yes

These technologies must not only have a linear dependence and be robust, accurate, precise, and easy to calibrate, they must also have no biological interference and endure pressure and temperature conditions of a sterilization process (Kiviharju et al., 2008). All of the methods mentioned in Table 2.1 have certain advantages, but some are not suitable for monitoring encapsulated or other immobilized cell growth and viability. Indeed some methods such as Turbidity or multi wavelength fluorescence would require liberation of the cells from their protective shells or microcarriers. Direct methods are of course preferred as they do not rely on model-based predictions (Potvin et al., 2012), making dielectric spectroscopy a preferred method for monitoring microencapsulated cells. This technique relies on the flow of ions, which can easily permeate the microcapsules membrane, in the case of microencapsulated cultures.

On the other hand, an insight on the cell metabolic activity may offer a better understanding of the bioprocess. Since CO₂ is usually used to control the mammalian cell culture pH, monitoring the carbon dioxide evolution rate (CER), Table 2.1, is not applicable. Biocalorimetry, or the online or at-line monitoring of bioreaction heat generation, may prove to be an easy but informative online monitoring method.

2.3. Dielectric spectroscopy

2.3.1. Cell suspension an RC-circuit?

Cells behave like resistor-capacitor circuits (RC-circuit) when an electrical field is applied to a cell suspension (Brandon Downey and Lisa Graham, 2013; Davey et al., 1992a). An RC-circuit contains a resistor and a capacitor in series, Figure 2.1.

A resistor is an energy loss component that transforms electrical energy into heat. A capacitor is an electrical component built with two metal plates separated by a dielectric material, capable of storing electrical charge. A dielectric material, by definition, is an insulating matter containing dipoles which polarise under an electrical field Figure 2.2. As suggested by Equation (2.1) a capacitor's ability to store charge (capacitance) is dependent on its permittivity (ability to transmit an electrical field) and geometry; where ϵ is the dielectric permittivity, A the surface of the plates, d the distance between the plates and C the capacitance.

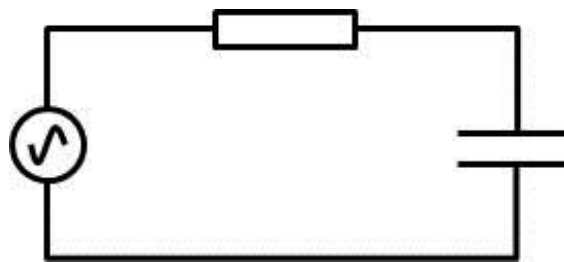


Figure 2.1. Electric diagram of a resistor capacitor circuit. Symbols from left to right: AC voltage source, resistor and a capacitor

$$C = \frac{\epsilon \cdot A}{d} \quad (2.1)$$

When a direct current (DC) passes through a capacitor, the electrical component will polarize and store charge up until its voltage matches the one of the voltage source, Figure 2.2. As soon as the capacitor is fully charge, electrical current can no longer flow through the electrical component. As soon as the fully charged capacitor is connected to another parallel circuit, it will start losing its charge and return to its native state.

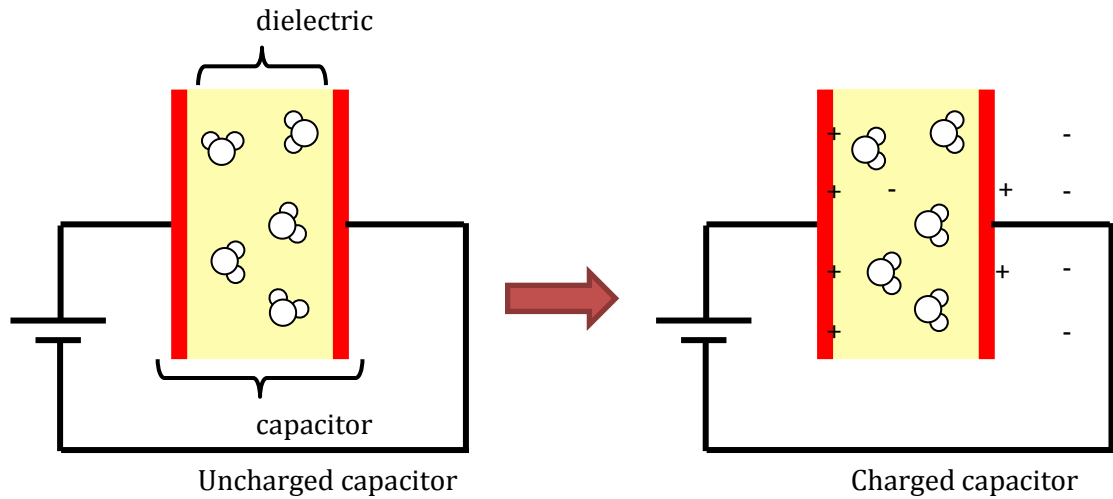


Figure 2.2. Polarization of the dielectric when under an electrical field

When an alternating current (AC) electrical field flows through a resistor-capacitor field, an amplitude reduction (caused by the resistor) and a phase lag (caused by the capacitor) can be observed between the induced and the response electrical field, Figure 2.3. An AC field is preferred to other type of alternating currents (such as step function current) for the circuit can easily be characterized through few simple equations. If the Input voltage, the resistance and the frequency are known, the amplitude reduction and the phase lag can be determined using the following sequence of equations:

First, the current flowing through the RC circuit (or of a cell suspension) is determined using Ohm and Kirchoff laws, respectively Equation (2.2) and Equation (2.3), with U being the potential (U_p of resistor, U_c of capacitor, and U_e of the generator), R the resistance, I the current, ω the angular frequency, C the capacitance and j an imaginary unit.

$$U = R \cdot I \quad (2.2)$$

$$U_e = U_p + U_c = R \cdot I + I \cdot \frac{1}{j \cdot \omega \cdot C} \rightarrow I = \frac{U_e}{R + \frac{1}{j \cdot \omega \cdot C}} = \frac{U_e \cdot j \cdot \omega \cdot C}{j \cdot \omega \cdot C + 1} \quad (2.3)$$

Then the amplitude or module $|U_c|$ emitted by the capacitor can be determined using Equation (2.4).

$$|U_c| = \sqrt{\left(\frac{1}{1 + \omega^2 \cdot R^2 \cdot C^2}\right)^2 + \left(\frac{\omega \cdot R \cdot C}{1 + \omega^2 \cdot R^2 \cdot C^2}\right)^2} \cdot U_e \quad (2.4)$$

The phase shift can also be calculated by determining the argument $arg|U_c|$ in Equation (2.5).

$$\arg|U_c| = \arctan\left(\frac{-\omega \cdot R \cdot C}{1}\right) \quad (2.5)$$

This series of equations allows the construction of an oscilloscope diagram, Figure 2.3, simulating a simple resistor-capacitor circuit constructed in series with an input voltage of 2 Volts alternating at a frequency of 500 kHz, a 2 Ω resistor and a 412 pF \cdot cm⁻¹ capacitor.

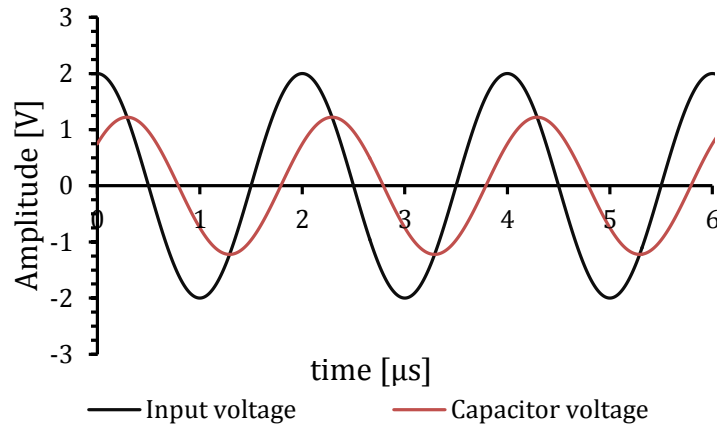


Figure 2.3. The response electrical field amplitude is smaller and shifted from the emitted field. The simulated RC-circuit is built with a 2 Ω resistor, a 412 pF/cm capacitor. The generator voltage is set at 2 Volts alternating at a frequency of 500 kHz.

When an alternating field is applied through a cell suspension, as is the case with a RC-circuit, the cell suspension responds by generating an electrical field with a smaller amplitude but at the same frequency as the input field and with a time shift. Cells may be considered to be microcapacitors since they can polarize and store charge as they are constructed with a non-conductive phospholipid membrane enclosing a conductive cytoplasm.

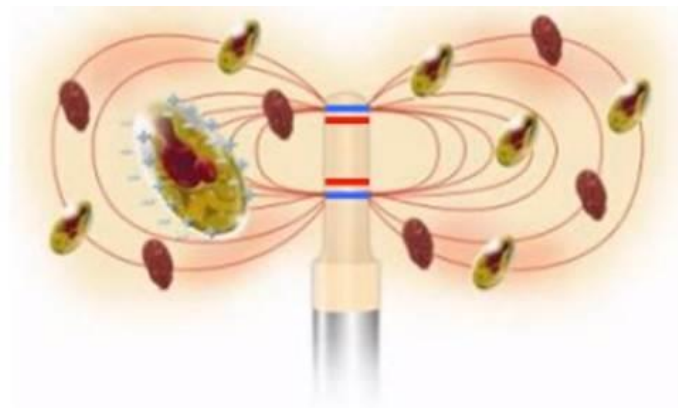


Figure 2.4. Electrical field generated by the electrodes (blue) polarises the cells. The polarised cells then emit an electrical field in response which can be detected by the receiving electrodes (red) (Brandon Downey and Lisa Graham, 2013)

In the case of an RC circuit, the component characteristics are known and the amplitude difference and the phase shift can be determined. However dielectric spectroscopy

functions conversely. The apparatus generates an alternative electric field at a standard voltage at a set frequency through the electrodes in blue Figure 2.4. The field polarises the cells, which in turn produce their own electrical field. This field is then picked-up by the probe receiving electrodes, in red Figure 2.4 (Brandon Downey and Lisa Graham, 2013). The apparatus then measures the amplitude difference between the input and response electrical fields and the phase shift. From these measurements, the cell suspension capacitance and conductivity are determined.

2.3.2. Cell Suspension characterization

As mentioned in Section 3.1, cells can store charge and can be considered to be microcapacitors. Electrically speaking, a healthy cell suspension would consist of three separate electrical regions (Carvell and Dowd, 2006a; Markx and Davey, 1999a) :

- Cell culture medium, a conductive solution containing nutrients and fermentation by-products.
- Plasma membrane which is essentially electrically insulating.
- Cytoplasm, a highly complex but structured combination of water, salts, protein, glycans, nucleic acids and, in eukaryote cells, organelles. Organelles being membrane bound cell sub-structures have an influence on the dielectric response.

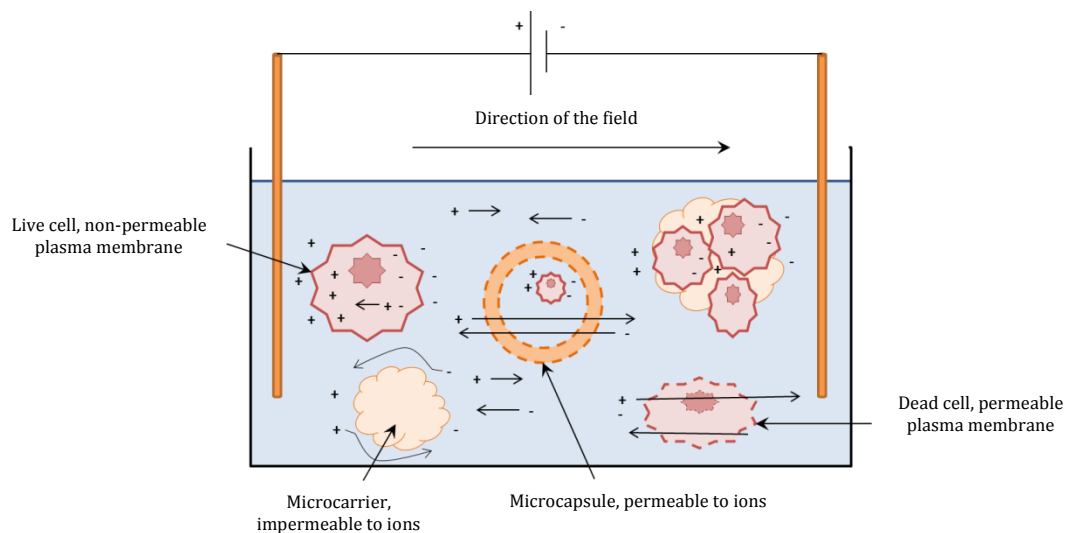


Figure 2.5. Schematic diagram showing the charge migration within a cell suspension when an electrical current is applied. The positive charge migrates towards the negative electrode and the negative charge towards the positive electrode. Unlike cell debris and solid particles, intact cells entrap ions which consequently polarize them

When alternating electrical fields are applied to a cell suspension, the ions of the cell culture medium and of the cytoplasm are forced to migrate towards the oppositely charged electrode (Davey, 1993). The ions within the cytoplasm will be entrapped by the

intact plasma membrane, hence polarizing the cell. Solid particles and cells with disrupted plasma membrane (dead cells) do not polarize and will not store charge, Figure 2.5. However, it is important to note that solid particles, if in a high enough fraction volume could reduce the measured capacitance due to a displacement of the cell containing solution. (Noll and Biselli, 1998a) .

The Biomass Monitor from Aber Instruments offers two methods to measure the dielectric characteristics of a cell culture. The first measures continuously the capacitance and the conductivity at a set frequency. The second mode scans and measures the capacitance and the conductivity over 25 pre-set frequencies ranging from $1 \cdot 10^5$ Hz to $1.95 \cdot 10^7$ Hz (Davey, 1993). The first mode is easier to implement for cell or microbial culture monitoring and data acquisition, as the displayed information is straight forward and is linearly correlated to the viable biovolume per volume unit of cell suspension. Nevertheless, the second mode, though more complex, gives more comprehensive information about the cell culture, for the ability to polarize a cell at defined electrical frequency is dependent on the cell size, Figure 2.6 (Cannizzaro et al., 2003a; Davey, 1993; Noll and Biselli, 1998a; Opel et al., 2010a).

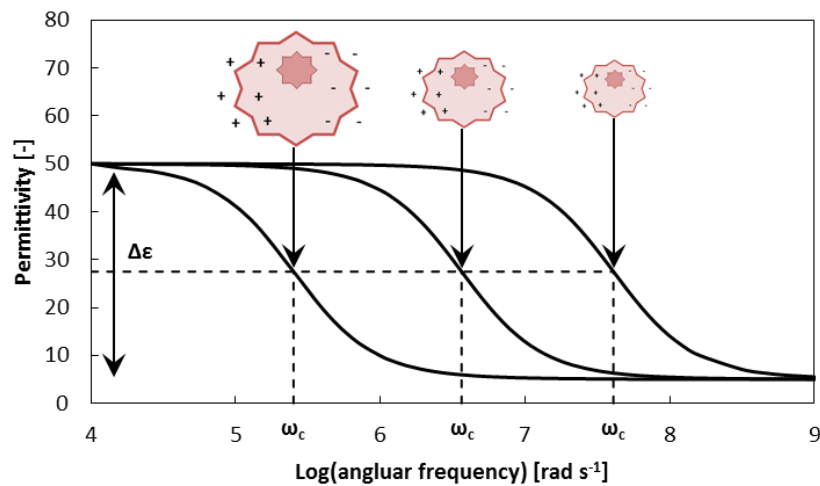


Figure 2.6. The polarisation of a cell at a given electrical frequency is dependent on the cell size

When the electrical field frequency is low, the ions have a sufficient amount of time to flow across the cytoplasm, reach the cell plasma membrane and polarise the cells before the electrical field is reversed. As the frequency increases, the number of cells that polarise diminishes. The capacitance (or permittivity) measurements are then plotted against the angular frequency in a semi logarithmic plot as represented in Figure 2.6. The chart therefore displays a β -dispersion, that is characterized by $\Delta\epsilon$, the characteristic frequency ω_c and α the slope of the β -dispersion, at $x = \omega_c$, Figure 2.8. $\Delta\epsilon$ is the permittivity difference between the high and low permittivity plateau and is linearly proportional to the viable cell density (if cell size remains constant), and the characteristic angular

frequency ω_c is the frequency at which the measured permittivity is equal to $\Delta\epsilon/2$. The characteristic angular frequency ω_c depends on the cell size. Indeed, ions require more time to reach the plasma membrane before the electrical field is reversed, Figure 2.6 and Figure 2.7 (Brandon Downey and Lisa Graham, 2013; Davey et al., 1992a).

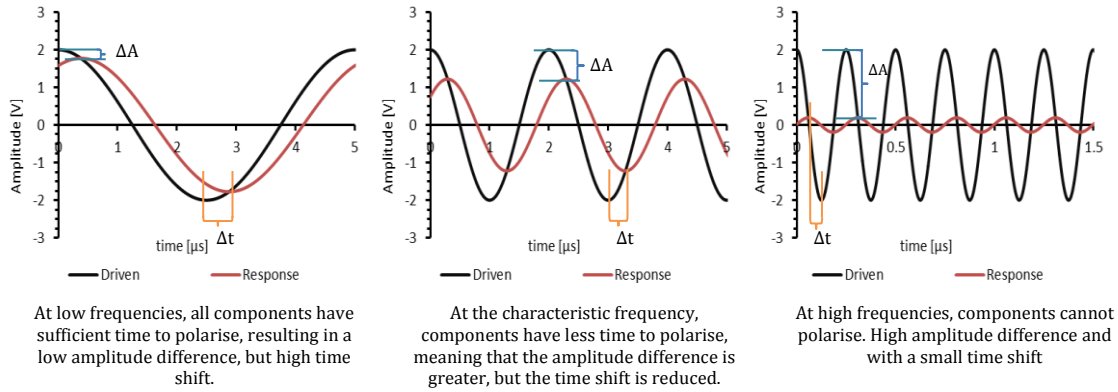


Figure 2.7. At low frequencies, the cells have a sufficient amount of time to polarise, therefore, the time shift is significant and the amplitude between the driven and response field is small. At the characteristic frequency ω_c , the amplitude difference is greater and the time lag smaller, and at high frequencies no cells polarise, so little signal is measured

The β -dispersion is modelled by the Cole-Cole equation, Equation (2.6), derives from the Debye equation, describing the polymer dielectric relaxation (Dabros et al., 2009c). It assumes that the polarization of materials diminishes exponentially when the applied field is removed. The Cole-Cole equation has an additional empirical parameter α [-]. This factor determines the dispersion slope (or material relaxation), and is dependent on cellular health, type and size.

After performing a frequency scan on a cell suspension, or after measuring the capacitance at the 25 pre-set frequencies, and plotted against the frequencies on a log-scale, a β -dispersion is drawn. Because permittivity depends solely on the material whereas the capacitance depends on both geometry and material, both frequency values and capacitance values are computed into respectively in angular frequencies and permittivity. By curve fitting using algorithms such as the Levenberg-Marquardt algorithm, the parameter $\Delta\epsilon$ [-], ω_c [$\text{rad} \cdot \text{s}^{-1}$], ϵ_∞ [-] and α [-] are defined. The permittivity difference $\Delta\epsilon$ is proportional to the culture biovolume, the characteristic frequency ω_c [$\text{rad} \cdot \text{s}^{-1}$] is highly dependent upon the cell radius, the high frequency permittivity ϵ_∞ [-] is the culture permittivity baseline (Dabros et al., 2009c; Markx et al., 1991).

$$\epsilon(\omega) = \frac{\Delta\epsilon \left(1 + \left(\frac{\omega}{\omega_c} \right)^{1-\alpha} \cdot \sin\left(\frac{\pi}{2} \cdot \alpha\right) \right)}{\left(1 + \left(\frac{\omega}{\omega_c} \right)^{2-2\alpha} + 2 \cdot \left(\frac{\omega}{\omega_c} \right)^{1-\alpha} \cdot \sin\left(\frac{\pi}{2} \cdot \alpha\right) \right)} + \epsilon_\infty \quad (2.6)$$

In parallel, the parameters $\Delta\sigma$ [$\text{mS} \cdot \text{cm}^{-1}$], $\omega_{c,2}$ [$\text{rad} \cdot \text{s}^{-1}$], α_2 [-] and σ_L [$\text{mS} \cdot \text{cm}^{-1}$] are fixed into Equation (2.7). It is highly probable that $\omega_{c,2}$ and α_2 differ from the parameter ω_c and α of Equation (2.6). The eight parameters obtained through the two parallel curve fits, illustrated in Figure 2.8, are then used in a further set of iterative equations, Equations (2.8) to (2.11), to determine cell number N_v [$\text{cells} \cdot \text{m}^3$], radius r [m] and the extracellular (or culture) conductivity σ_e [$\text{mS} \cdot \text{cm}^{-1}$].

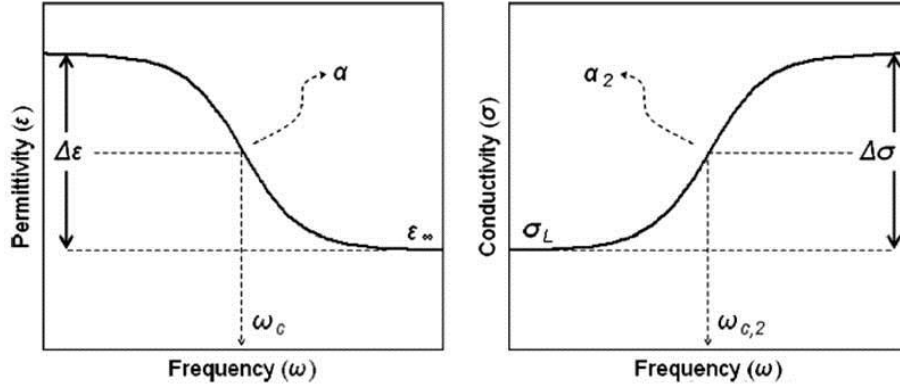


Figure 2.8. Parameters determined through the curve fit Equation (2.6) and Equation (2.7) into experimental data (Dabros et al., 2009c)

$$\sigma(\omega) = \frac{-\Delta\sigma \left(1 + \left(\frac{\omega}{\omega_{c,2}} \right)^{1-\alpha_2} \cdot \sin\left(\frac{\pi}{2} \cdot \alpha_2\right) \right)}{\left(1 + \left(\frac{\omega}{\omega_{c,2}} \right)^{2-2\alpha_2} + 2 \cdot \left(\frac{\omega}{\omega_{c,2}} \right)^{1-\alpha_2} \cdot \sin\left(\frac{\pi}{2} \cdot \alpha_2\right) \right)} + (\sigma_L + \Delta\sigma) \quad (2.7)$$

Equations (2.8), (2.9) and (2.10) contain three unknown variables and two constants, the membrane capacitance C_m [$\text{pF} \cdot \text{cm}^{-1}$] and the intracellular conductivity, or the intracellular conductivity σ_i [$\text{mS} \cdot \text{cm}^{-1}$]. The membrane capacitance C_m and the intracellular conductivity σ_i are specific to the cell line and are determined through calibration. It is suggested to begin the iteration by estimating the extracellular (or the culture) conductivity σ_e using Equation (2.11).

$$\Delta\epsilon = \frac{3N_v \cdot \pi \cdot r^4 \cdot C_m}{\epsilon_0} \quad (2.8)$$

$$\omega_c = \frac{1}{r \cdot C_m \cdot \left(\frac{1}{\sigma_i} + \frac{1}{2\sigma_e} \right)} \quad (2.9)$$

$$\sigma_e = \frac{\sigma_L}{(1-P)^{1.5}} = \frac{\sigma_L}{\left(1 - \frac{4}{3} \cdot \pi \cdot r^3 \cdot N_v \right)^{1.5}} \quad (2.10)$$

$$\sigma_e = \sigma_L + \Delta\sigma \quad (2.11)$$

2.3.3. *Successful applications*

To obtain a dielectric signal using the biomass monitor of a suspension, a conducting culture medium, an intact insulating cytoplasmic membrane and a conducting cytoplasm are required. At low volume fractions non-biological solid particles or dead cells, with permeable membrane, do not interfere with the dielectric signal (Davey et al., 1993). It has been successfully shown that suspension cultures can be monitored on-line using single frequency measurements (Justice et al., 2011a; Párta et al., n.d.) or frequency scans (Cannizzaro et al., 2003a; Opel et al., 2010a) in stirred tank reactors.

Immobilized cell cultures may vary slightly from suspension cultures as solid particles are encountered at high volume fractions and may slightly affect the signal (Carvell and Dowd, 2006a; Davey et al., 1993; Ducommun et al., 2002a). Because the microcarrier or microcapsule volume fraction should remain constant, a simple calibration of the capacitance versus the cell density in the presence of the desired volume fraction of microcarriers is necessary (El Wajgali et al., 2013a). However, attention must be drawn to microcarrier cultures, as the relationship between capacitance and cell number is only linear until the microcarrier is fully colonised. Once the cells have adhered to the entire available surface, it has been suggested that the cells change not only in size but in shape, affecting the signal (Ducommun et al., 2002a; El Wajgali et al., 2013a).

Immobilised cell cultures can be undertaken in different types of reactors. Vero cells have been cultivated in a stirred tank perfusion reactor, and successfully monitored using dielectric spectroscopy. The microcarriers were retained using a “home-made” settling glass tube (El Wajgali et al., 2013a). Different calibration curves have been established using different microcarrier densities ranging from 1.5 to 6 g · L⁻¹. No variations were reported.

In contrast to stirred tank reactors, immobilised cells can also be cultured in fluidised or packed bed reactors (Ducommun et al., 2002a; Noll and Biselli, 1998a). Sampling in such packed bed reactors for cell number determination is only possible before inoculation and at the end of the culture. Cell number determination using off-line methods is not possible, meaning a monitoring method is primordial in such cases. (Ducommun et al., 2002a) On-line capacitance gives real-time information about the culture evolution in both fluidised and packed bed reactors.

These different applications show the potential dielectric spectroscopy has to monitor microencapsulated cultures. The microcapsule semi-permeable membrane, protecting the

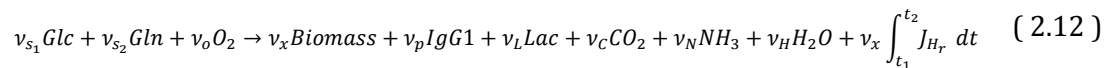
cells from the stirred tank environment, as explained in Chapter 3, would allow the ingress and egress of the ions towards the alternating poles of the emitted electrical field. The alternating flow of ions would induce a cell polarisation and depolarisation, and hence generate a dielectric signal. Nevertheless, the influence of the microcapsules, present in high volume fractions, requires investigation, see Chapter 5.

2.4. Biocalorimetry

2.4.1. Cellular metabolism

Heat production is an inevitable by-product of mammalian cell metabolic activity. To generate ATP, a cell uses catabolic pathways. The ATP is then used by the cell to synthesise larger and more complex molecules through anabolic pathways (Guan et al., 1998; von Stockar et al., 2006). Even if the cells were to be highly efficient with regards to their energy source, some energy is unavoidably lost in the form of heat. This heat loss, or heat flow, can nevertheless be stoichiometrically determined (Doran, 1995b).

Mammalian cells have a complex metabolism involving multiple substrates for carbon and energy sources (they are auxotrophic) and therefore rely on many metabolic pathways. However, a simplified model has been proposed. The stoichiometric equation, Equation (2.12), assumes that the CHO cells (*Biomass*) develop solely by metabolising glucose (*Glc*) and glutamine (*Gln*) as substrates and produce lactate (*Lac*), ammonia (NH_3) and recombinant protein (IgG_1) Equation (2.12) (Guan et al., 1998).



2.4.2. Calorimeters

The heat loss can be used to advantage for process monitoring. It has been reported that heat flow is highly correlated to the process biomass (Guan et al., 1998; Guan and Kemp, 1999; Kemp, 2000; Marison et al., 1998). Microcalorimeters were the first available calorimeters. With a high sensitivity they offer the possibility to monitor weak exothermic cultures such as mammalian cell cultures (Türker, 2004). The microcalorimeters are externally connected to the reactor (Guan et al., 1998) and continuous samples flow to the calorimetric chamber. The capacity of the calorimetric chamber ranges from (1-100 mL).

Although this heat measuring method is highly sensitive and has shown promising results in measuring the metabolic activity of CHO suspension cultures (Guan et al., 1998; Guan and Kemp, 1999), the different environments between the reactor vessel and heat measuring cell can be a major drawback (García-Payo et al., 2002; Türker, 2004). A slight change in pH, aeration, foaming or mixing can affect the cells and their metabolic activity.

In addition, though it has been previously undertaken for microbial cultures (Ma et al., 2007), the technology can be difficult or impossible to apply to immobilized cell cultures. The removal of microcapsules (or microcarriers), if not recycled, would mean a reduction in the total available space for cell colonisation, and hence a diminution in the total cell number and productivity. Finally, this technique is simply not applicable to packed-bed cultures.

Macrocalorimeters generally resemble traditional bench scale bioreactors, and are much larger with a working volume superior to 1 L (Marison et al., 1998). The sensitivity of such calorimeters can vary, especially with the working volume. At small scale, heat production can be hardly noticeable, as most of the heat is lost to the environment. This heat loss is explained by the high surface to volume ratio (Türker, 2004; Voisard et al., 2002a). However, at industrial scale, or at volumes of a few cubic meters, the surface to volume ratio is less significant, and are said to necessitate little heating and may even require cooling instead.

Different bench scale calorimeters have been designed and examined. To monitor the heat flux of a mammalian cell culture, high resolution is required. The eRC1 biocalorimeter is the most encountered macrocalorimeter as it offers a high resolution that is comparable to microcalorimeters', or to $15 \text{ [mW} \cdot \text{L}^{-1} \cdot \text{K}^{-1}]$. (García-Payo et al., 2002; Marison et al., 1998).

The RC1, Figure 2.9, was first designed to characterise the thermodynamics of chemical reactions and has been modified to perform and measure biological reactions (Bio-RC1). Unlike the at-line calorimetric system (Guan et al., 1998), the Bio-RC1, does not require any additional *ex-situ* equipment to measure the heat production of a culture, it measures the heat production in real-time, and can then apply an optimized control on the reactor temperature (García-Payo et al., 2002).

2.4.3. Principles of bench scale calorimetry

To monitor the heat flux produced during a culture the Bio-RC1 is operated in isothermal mode in which the reactor temperature T_r is set to remain constant. A silicone oil, circulating at a high rate of $2 \text{ L} \cdot \text{s}^{-1}$ through the reactor jacket, controls T_r by adapting the temperature of the jacket T_j accordingly, Figure 2.9 (Marison et al., 1998).

The reactor temperature T_r can be influenced by many parameters and the heat flow accumulated within the reactor can be characterised by the following heat balance, Equation (2.13) (Voisard et al., 2002a):

$$q_{acr} = q_r - q_j + q_s - q_g - q_e - q_f - q_a - q_{CO_2} + q_c - q_{acj} = 0 \quad (2.13)$$

q_{acr} and q_{acj} represent the heat flux accumulated within the reactor and the jacket respectively, q_r the heat flow produced by the biological reaction(s), q_j the heat flow to the jacket, q_s the heat induced by stirring, q_g the heat loss caused by gassing and evaporation, q_e the heat loss to the environment, q_f the heat flow caused by addition of a substrate or medium to the culture, q_a the addition and dissolution of either an acid and/or a base for the maintenance of a constant pH, q_{CO_2} the heat flow caused by CO₂ evaporation and q_c the heat emitted by the calibration heater. The heat flow is expressed in [W] or equivalently in [$J \cdot s^{-1}$].

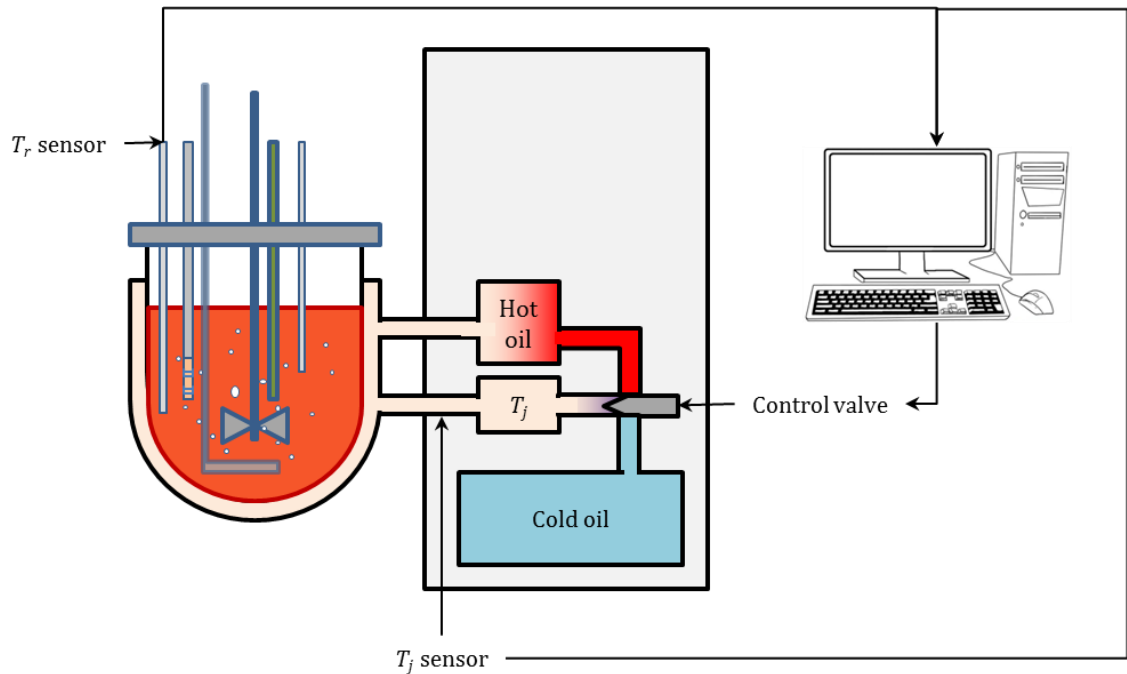


Figure 2.9 Diagram of the eRC1, Mettler Toledo Reaction Calorimeter

As the RC1 is operated in isothermal mode, and most heat fluxes are considered to remain constant throughout the whole culture period, the reaction heat q_r in the RC1 can be determined using Equations (2.13)and (2.14). U_A [$W \cdot K^{-1}$] represents the heat transfer coefficient, or global heat transfer coefficient expressed in [$W \cdot m^{-2} \cdot K^{-1}$] multiplied by the heat transfer area A [m^2].

$$q_r = U_A \cdot (T_r - T_j) \quad (2.14)$$

2.4.4. Bench Scale biocalorimetry applications

To my knowledge, no investigation in the use of bench scale biocalorimeters to monitor mammalian cell cultures has been reported to this date. A number of studies have been reported on the monitoring and possible control of microbial cultures using macrocalorimeters. Biocalorimetry has been used in many different applications, including to monitor culture metabolism and control the feed of nutrients and hence the growth

rate. By doing so, respiro-fermentative metabolism caused by overflow-metabolism in Crabtree positive organisms can be avoided (Biener et al., 2012, 2010; Schuler et al., 2012; Sivaprakasam et al., 2007; Voisard et al., 1998). In addition, a study was performed in the RC1 to determine the existence of endothermic bacterial strains (Liu et al., 2001). By cultivating *Methanosarcina barkeri* and using acetate as substrate under obligate anaerobic conditions, it was shown that the bioreaction was endothermic and yielded a heat uptake of $Y_{Q/X} = +145 \text{ kJ} \cdot \text{C} - \text{mol}^{-1}$.

Moreover, some Reaction Calorimeters have seen further structural modifications to increase the RC1 sensitivity, in order to measure the heat produced by insect cells. These modifications reduced the sensitivity to $4 \text{ mW} \cdot \text{L}^{-1}$ (García-Payo et al., 2002)! In parallel, CHO 320 were cultured in a 3 L batch culture. The culture was monitored combining microcalorimetry and dielectric spectroscopy. A flow microcalorimeter was connected *ex-situ* of the bioreactor to continuously measure the heat. After 60 hours, a heat flow rate of $10 \text{ } \mu\text{W} \cdot \text{mL}^{-1}$ for a maximum cell density of $0.6 \cdot 10^6 \text{ cells} \cdot \text{mL}^{-1}$ was obtained. It was then determined that the CHO 320 cells have a specific heat production rate of $15 \text{ pW} \cdot \text{cell}^{-1}$ (Guan et al., 1998). Based on these results, one could estimate that a 1.4 L culture, with a density cell of 3 million cells could generate a heat flux of 45 mW/L. This would therefore suggest that monitoring CHO cells metabolic activity in the RC1 should be feasible, and that the heat of reaction would be correlated with cell density, as presented in Chapter 6 of this thesis.

2.5. Conclusions

Mammalian cell cultures are complex processes and can have important batch- to-batch variations therefore, monitoring mammalian cells is gaining importance. Immobilised cell cultures have an additional barrier to real-time monitoring as the cells are not directly available for analysis. Nevertheless, both dielectric spectroscopy and biocalorimetry have important potential and are easily scalable to industrial scale. Dielectric spectroscopy offers direct viable cell number monitoring in different types of immobilized mammalian cell culture. Though a calibration may be necessary, the signal should not be influenced by the presence of the microcapsules (or microcarriers). Biocalorimetry is readily applicable at large-scale through simple heat balancing methods (Türker, 2004; Voisard et al., 2002a), but necessitates more sophisticated equipment at bench- scale. Though no studies have investigated the potential use of laboratory scale calorimeters, the RC1 calorimeter of Mettler Toledo has a resolution that would permit the successful monitoring of mammalian cell cultures.

Both dielectric spectroscopy and biocalorimetry may be used to monitor viable density of microencapsulated mammalian cell cultures. One method measures the viable biovolume concentration of the culture, whilst the other measures the metabolic activity of the living cells. Therefore, it would be ideal to combine both techniques to have a more comprehensive understanding on the cellular development of the bioprocess.

Chapter 3 **Materials and Methods in Cell culturing, cell encapsulation and culture analysis**

Summary: This chapter introduces the different methods used. The cell culture techniques as well as the procedure to manufacture the microcapsules are described. To build a model and then to validate the online data, samples were taken daily. The cells, recombinant IgG₁ and metabolites were quantified using the described methods. As the microcapsules evolve during cultures, methods to measure different variables such as microcapsule size, membrane thickness, pore size and mechanical resistance are presented. The culture conditions in the bioreactors are also briefly given, however, a more detailed set-up description is to be given.

Keywords: Cell maintenance, Bioencapsulation, Bioreactors, culture characterisation, Microcapsule characterisation

3.1. Cell culture and Inoculum development

The cells were thawed, maintained and banked following standard cell culture procedures.

3.1.1. Cell line

The cells used throughout this work were CHO-DP12. They have been adapted to serum free cell culture media and to suspension cultures. CHO-DP12 are a desoxyfolate dehydrogenase negative (dhfr⁻) cell line which has been stably co-transfected with the IgG1-dhfr^r gene. Selective pressure and high throughput screening was performed by removing hypoxanthine and thymidine from the media and adding methotrexate for gene amplification.

3.1.2. Cell culture media

Two culture media have been used to cultivate the cells. The first medium EX-CELL® 325 PF CHO is a protein-free medium for CHO Cells (SAFC biosciences, Cat#: 24340C). The medium was shipped and stored in dry powder form. Three months supply of medium was prepared according to the manufacturers' instructions. Once the medium was solubilised and the pH adjusted to pH 7, it was supplemented with 4 mM L-glutamine (Sigma Aldrich, USA, Cat # G7513) 1 µM MTX, 10 mg · L⁻¹ insulin and 10 ml · L⁻¹ GibcoR Penicillin-Streptomycin (Life Technologies, California USA, Cat#:15140-122). The solution was then sterile filtered using Stericup™ filter units (EMD Millipore, Germany, Cat# FDR-125-505M). The medium was stored at 4 °C for a maximum period of 3 months. This medium contained 3.45 g · L⁻¹ glucose.

As the work progressed, a medium with a higher glucose concentration (6 g · L⁻¹ glucose), and hence potential to generate a higher cell density, was used. EX-CELL® CHO DHFR^r shipped in its liquid form, was supplemented with 4 mM L-glutamine (Sigma Aldrich, USA, Cat # G7513) and 10 ml · L⁻¹ Penicillin-Streptomycin (Life Technologies, California USA, Cat#:15140-122). As the EX-CELL® CHO DHFR^r formulation readily includes human recombinant insulin.

Both culture media were supplemented with 500 µl · L⁻¹ of a sterilised 5x Antifoam C emulsion (Sigma Aldrich, USA, Cat# A8011) for encapsulation and bioreactor cultures to prevent foaming.

3.1.3. Thawing cells

To thaw cells, 50 mL of cell culture media was pre-heated to 37 °C. The frozen cell banks were stored in 2 ml cryovials in liquid nitrogen. Thawing was rapid as the frozen suspension contained DMSO, a toxic substance for the cells. As soon as a vial was removed from the cell bank, the cells were rapidly thawed and the 1 ml suspension was transferred into a sterile 50 ml Falcon® tube and 9 mL of fresh media added to the suspension. The cells were then spun down at $200 \times g$ for 5 minutes. The supernatant was carefully removed without disturbing the pellet and replaced with 10 mL of fresh media. The cells were counted using a Neubauer® Hæmocytometer, Figure 3.1, under an inverted microscope (Leica, Germany). Ten μl of cell suspension was mixed with 30 μl 0.4% Trypan Blue exclusion dye (Sigma Aldrich, USA, Cat# 93595). The white cells were counted as viable and the blue-stained ones as dead. The cells were diluted to $0.5 \cdot 10^6 \text{ cells} \cdot \text{ml}^{-1}$ with preheated media and transferred to a 125 ml Erlenmeyer culture flask with a vent cap (Corning, USA, Cat# 431143). The cells were incubated at 37 °C and 5% CO_2 on an IKA® KS 260 compact orbital shaker (IKA, USA) at 100 rpm .

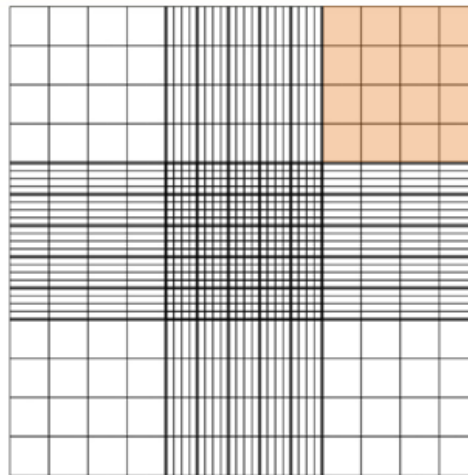


Figure 3.1 Neubauer Haemocytometer counting chamber. Highlighted is one of the 4 large squares that were to be counted for estimating the viable cell density and viability and corresponded to a volume of 100 nL

3.1.4. Cell maintenance and inoculum development

The cells were passaged every three to four days, when they were in the mid-exponential phase of growth. fresh medium (25 ml) was preheated at 37 °C. While the medium was preheating, the cells were counted, as explained in section 3.1.2. The necessary volume of viable cell suspension and fresh media was then determined to form a new 25 ml cell suspension with an initial cell density $0.3 \cdot 10^6 \text{ cells} \cdot \text{ml}^{-1}$. If the required cell suspension volume exceeded 25 % of the total volume, the suspension was centrifuged at $200 \times g$ for 5 minutes. The supernatant was carefully removed and the cell

pellet was resuspended in the 25 ml of fresh preheated medium. Cells were maintained in 125 ml Erlenmeyer culture flasks with vent caps (Corning, USA, Cat# 431143). When developing the inoculum for seeding bioreactors or for cell encapsulation, the cell suspension volume was increased to 300 ml in a 1000 ml Erlenmeyer culture flask with a vent cap (Corning, usa, Cat# 431147). The seeding density remains at $0.3 \cdot 10^6 \text{ }_{\text{v}}\text{cells} \cdot \text{ml}^{-1}$.

3.1.5. *Cell banking*

Three days prior to banking cells, 300 ml cell suspension was prepared with an initial viable cell density of $0.3 \cdot 10^6 \text{ }_{\text{v}}\text{cells} \cdot \text{ml}^{-1}$ in a 1000 ml Erlenmeyer culture flask with a vent cap (Corning, USA, Cat# 431147). It was important to ensure that the cell viability was greater than 95 %.

Medium (20 ml) containing 10% DMSO (Sigma Aldrich, USA, Cat# D2650) as prepared and preheated and up to 18 labelled cryovials. The viability and cell density of the cell suspension was determined as explained in section 3.1.3, and the volume of cells necessary to form up to 20 ml $10 \cdot 10^6 \text{ }_{\text{v}}\text{cells} \cdot \text{ml}^{-1}$ cell suspension was calculated. It was important that the viability was greater than 95%. The calculated volume of cells were centrifuged at $200 \times g$ for 5 minutes, and resuspended with up to 20 ml 10% DMSO media. A volume of the suspension (1 ml) was then aseptically distributed into the labelled cryovials. The vials were then placed in a freezing container (Thermo Fisher Scientific, USA, Nalgene® Mr. Frosty). The container was then filled with isopropanol and stored at $-80 \text{ }^{\circ}\text{C}$ for 24 hours. Four vials were then placed in the mother cell bank (liquid nitrogen tank) and the remaining vials were placed in the working cell bank (liquid nitrogen tank).

3.2. **Bioreactors and culture settings**

The cells were cultured in two bioreactors, a Minifors (Infors HT, Switzerland) and a biocalorimeter eRC1 (Mettler Toledo, USA). Both bioreactors were equipped with a 2.5 L culture vessel. For suspension cultures, the reactors were seeded at $0.3 \cdot 10^6 \text{ }_{\text{v}}\text{cells ml}^{-1}$, and in the case of encapsulated cultures, the vessels were inoculated with 25 % (v/v) packed microcapsules. The microcapsules contained at $0.7 \cdot 10^6 \text{ }_{\text{v}}\text{cells ml}^{-1}_{\text{capsules}}$.

The culture conditions were monitored and controlled to a set-point of $37 \text{ }^{\circ}\text{C}$ and pH 7.2. The pH was controlled by CO_2 addition to the headspace or by addition of 2 M NaOH to the medium, which was mixed using a marine impeller set at 100 rpm. Air was sparged into the culture medium at 0.01 vvm and the headspace aerated at 0.1 vvm.

The viable cell density was monitored using a Biomass monitor (ABER Instruments, UK). The frequency at which the capacitance was continuously measured was set at 580 kHz, dual frequency with polarisation correction. Frequency scans were performed daily to obtain information on the cell morphology.

The bioreactor vessels and components were prepared, filled with deionized water and sterilised one day prior to inoculation. After the vessel was cooled to the operating temperature and the deionised water was replaced with the working volume of media to allow stabilisation of the dielectric probe. The capacitance value displayed on the biomass monitor was “zeroed” after stabilisation of the signal.

3.3. Cell microencapsulation in alginate-poly-L-lysine-alginate microcapsules

3.3.1. Bioencapsulation principles

Bioencapsulation consists in entrapping active biologicals such as cells or enzymes within a semi-permeable membrane. The technology is used in many applications such as enzyme immobilisation, cell transplantation or large scale recombinant protein production (Orive et al., 2004a; Uludag et al., 2000; Zhao et al., 2013).

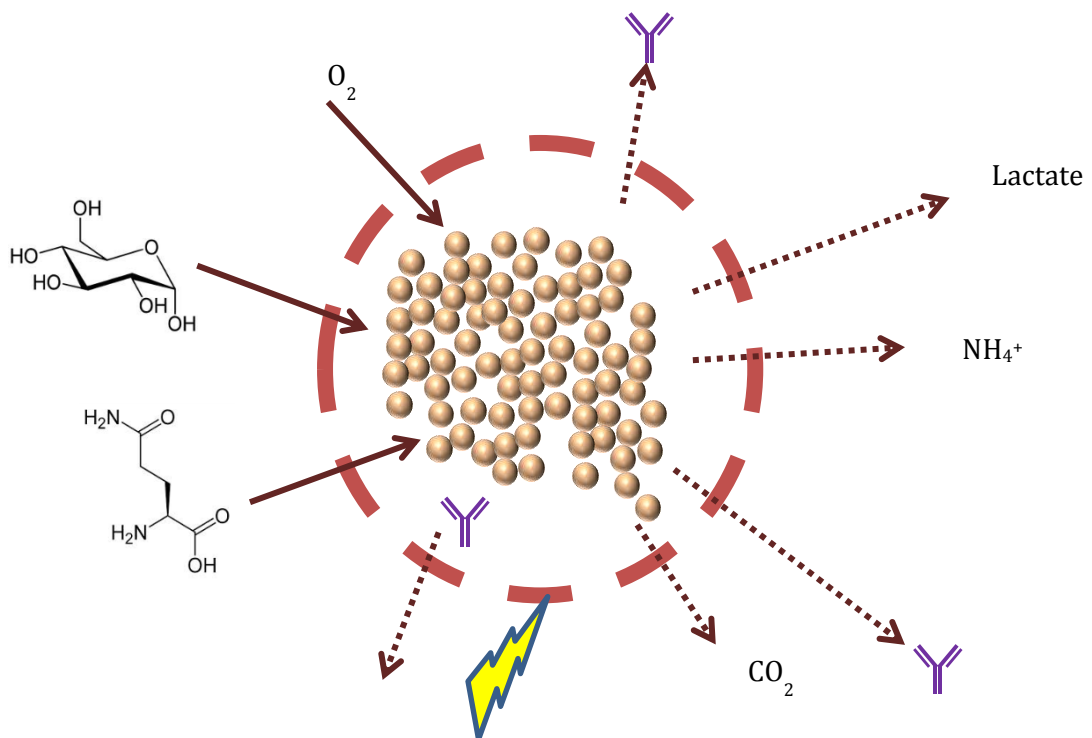


Figure 3.2 Microcapsules offer an optimal environment for the cells to develop. The semi-permeable membrane allows the inflow of essential nutrients such as glucose or L-glutamine, dissolved O₂, and the egress of waste by-products (lactate, ammonia) CO₂. The microcapsule membrane pore size can be engineered to allow diffusion or retention of large proteins such as recombinant antibodies.

Considerations regarding the microcapsule manufacturing method and the choice of polymers and reagents need to be made for the encapsulation of cells for large scale recombinant protein production. The manufacturing process must be easily scaled-up to produce large volumes of bio-microcapsules. Furthermore the process and reagents should be as harmless to the cells as possible and the end product should form an environment in which the cells can proliferate and produce high quality and quantity of recombinant proteins (Gombotz and Wee, 1998; Orive et al., 2004a).

To ensure a favourable environment for cell proliferation and heterologous protein synthesis, the microcapsules have a semi-permeable membrane. The semi-permeable membrane enables the ingress of nutrients and dissolved O₂, and the waste metabolites and CO₂ excretion, whilst protecting the cells from the shear forces generated through agitation and bioreactor gassing, Figure 3.2. Nutrients and dissolved gases constantly permeate the capsule membrane by diffusion. Diffusion is a movement of matter or energy which is triggered by a material, heat or momentum disequilibrium, within a system. This movement seeks to destroy any form of gradient and to generate a homogeneous environment (Doran, 1995a). The diffusion of macromolecules through the microcapsule membrane can be controlled by formulating an adequate process.

Many bead forming techniques are available (Hübner et al., 2009; Kang et al., 2014; Uludag et al., 2000). Manufacturing microcapsules can be a complex process and the different variables such as temperature, pH, osmotic conditions, polymer choice, chemical structure, molecular weight and/or concentration may have a significant impact on the mechanical and pore size distribution (Verica et al., 2009b). The most common cell-entrapped microcapsules are produced by extruding an alginate-cell suspension through a needle or a nozzle into a bath containing suitable cations (calcium, barium, except magnesium). The beads are then coated with a polycation such as poly-L-lysine, Poly-L-ornithine or chitosan and then solubilised using a chelating agent.

The method used in this work consists in using either an Encapsulator Biotech (EncapBioSystems, Switzerland) or its predecessor the Encapsulator Inotech ie-50R (Dottikon, Switzerland) to extrude the alginate-cell suspension, as illustrated in Figure 3.3. These encapsulators permit the production of 200 ml of microcapsules with a narrow size distribution but high cell viability under aseptic conditions. The alginate-cell suspension is pumped into a vibrating chamber and then through a nozzle at a constant flow rate. The vibrating chamber (50-3000 Hz) creates a jet of droplets which are then separated by electrostatic forces of 1000-2000 Volts. The bead size can be adapted by modifying the nozzle size, the fluid laminar flow rate, the vibration frequency and the electrostatic voltage (Heinzen et al., 2004). To make small beads, a smaller nozzle, a higher debit, frequency and voltage are chosen, but to produce larger beads, a larger nozzle is chosen

and the flow rate is slowed down, along with the vibration frequency and the voltage is slightly lower.

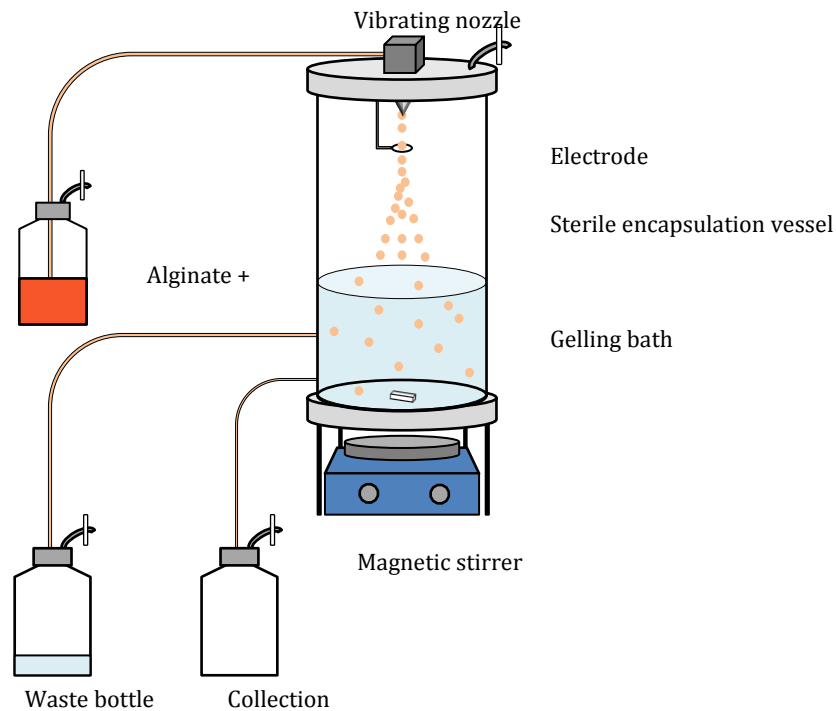


Figure 3.3 Diagram of the encapsulator set-up. The alginate-cell suspension is aseptically connected to the sterile vibrating chamber. The suspension is extruded through the nozzle by pressurising the alginate-cell containing bottle. Two other bottles are also aseptically connected: one for the waste collection and one for recuperating the manufactured microcapsules.

3.3.2. Calcium alginate poly-L-lysine microcapsules

The capsules produced were Ca^{2+} -alginate-poly-L-lysine-alginate (APLLA) microcapsules. The cells were resuspended in alginate, a polysaccharide extracted from algae. The polysaccharide is water soluble and consists of alternating chains of 1 → 4 linked α -L-guluronic acid (G) and β -D-mannuronic acid (M) Figure 3.4 A (Davidovich-Pinhas and Bianco-Peled, 2010; Gombotz and Wee, 1998). The crosslinking and gelation of the alginate occurred as soon as a Ca^{2+} or any bivalent cation (except for Mg^{2+}), replaced the Na^+ associated with the guluronic acids groups. The chemical structure of the polysaccharide plays an important role in the gelation process and the bead mechanical and chemical resistance, porosity, and swelling behaviour. It is said that to obtain optimal gelation, an alginate composed of 75% guluronic acid groups (G groups) should be used, especially if the G groups are bound together, though new evidence shows that M-G-M blocks have a positive influence on cross-linking (Davidovich-Pinhas and Bianco-Peled, 2010; Hübner et al., 2009).

Different alkaline earth cations can be used for alginate cross-linking. Though Ca^{2+} is the most commonly used cation, Ba^{2+} and Sr^{2+} form stronger alginate gels. Like other

bivalent cations such as Cu^{2+} , Mn^{2+} , Ni^{2+} , Zn^{2+} or Co^{2+} , the concentration used is limited since they may be toxic to the cells. These cations bind the α -L-guluronic acid residues, forming a well organised structure, known as the egg-box model Figure 3.4 B & C, (Gombotz and Wee, 1998).

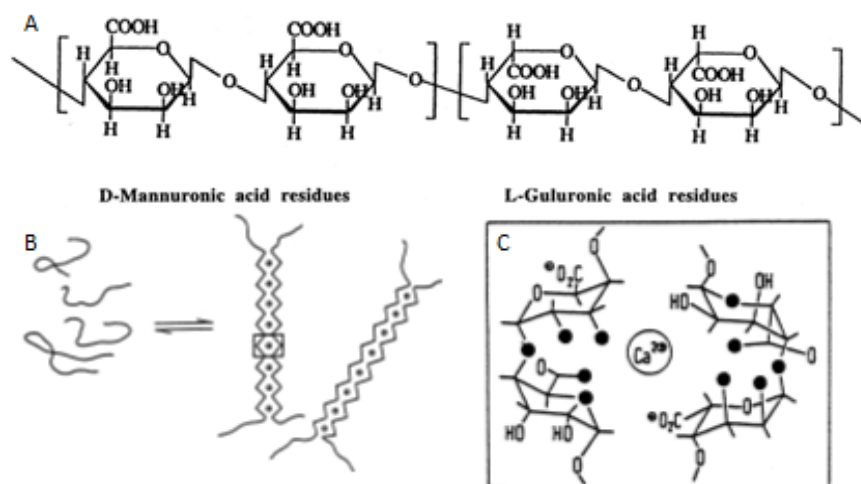


Figure 3.4 Molecular structure of alginate A: Sodium alginate molecular structure showing both β -D-mannuronic acid and α -L-guluronic acid residues; B: Egg box model; C: sodium alginate complex with Ca^{2+} (Gombotz and Wee, 1998)

After gelation, to avoid cell leakage, the alginate beads are coated with polycations, such, poly-L-lysine. Poly-L-lysine, Figure 1.4, is a homopolymer of the amino acid L-lysine. The positively charged lysine residues are chemically attracted to the negatively charged alginate. The stability of the poly-L-lysine layer depends on the alginate ratio of M groups (β -D-mannuronic acid): the more M-groups, the more efficient is the poly-L-lysine coating. The layer of poly-L-lysine is then coated once again with alginate (or polyethylenimine, PEI) to neutralise the NH_4^+ of the lysine residues that are not interacting with the alginate bead. This step is essential to avoid any unwanted protein interactions. The inner core of the capsules is then solubilised by addition of citrate. A citrate anion is a competitor for the Ca^{2+} . Once the Ca^{2+} is bound with the citrate and is removed from the alginate, the polymer is once again in its liquid form. The displacement of the Ca^{2+} ions may cause a swelling of the capsules.

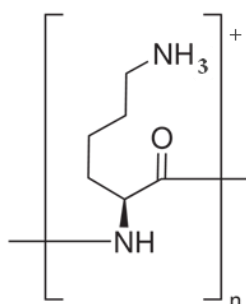


Figure 3.5 Poly-L-lysine monomer

3.3.3. Procedure

The bioreactors are inoculated with 25% (v/v) Ca²⁺-alginate-poly-L-lysine-alginate (APLLA) microcapsules containing $0.7 \cdot 10^6$ cell \cdot ml⁻¹ alginate, equivalent to 350 mL of packed microcapsules containing a total of $2.45 \cdot 10^8$ cells.

Before encapsulating the poly-L-lysine (MW: 30,000-70,000 Dalton) (PLL) (Sigma Aldrich, USA, Cat#: P2636) was labelled by adding 1.2 mg of FITC (Fluorescein isothiocyanate) to a 1.2 L solution containing 600 mg of PLL. The pH was raised to pH 8-9 by drop-wise addition of 2 M NaOH. The solution was agitated for one hour before the pH was adjusted to 7 by addition of, MOPS 10 mM, CaCl₂ 100 mM (Sigma Aldrich, USA) and acetic acid 3 M enabling an average label yield of $7.5 \cdot 10^{-4}$ mole_{FITC} \cdot mole_{lysine monomer}.

The microcapsules were produced by extruding a cell suspension in 1.5% alginate solution through an Encapsulator Biotech (Inotech, Switzerland). Cells were centrifuged at $200 \times g$ for 10 minutes and re-suspended in 400 ml of sterile filtered 1.5% (w/v) sodium alginate, 10 mM MOPS (Sigma Aldrich, USA, Cat#: M3183) and 0.85% NaCl (Merck, Germany, Cat#: 106400) buffer, pH 7. The alginate-cell suspension is then extruded through a 200 μ m \varnothing single nozzle into a stirred 1 L solution of 100 mM CaCl₂ (Sigma, USA, Cat#: C7902) in 10 mM MOPS buffer pH 7.2. After incubation for 10 minutes, the CaCl₂ solution was removed and the alginate beads washed with 500 mL 10 mM MOPS containing 0.85% NaCl. After washing, the Ca²⁺-alginate beads were placed in the labelled PLL solution for 30 minutes, at room temperature. After coating with labelled PLL the beads were washed twice for five minutes with MOPS-NaCl buffer pH 7.2, and coated with a second layer of Na-alginate by incubation in 0.03% (w/V) sodium alginate, 10 mM MOPS, 0.85% NaCl, pH 7.2 for 10 minutes. The coated beads were washed twice with MOPS-NaCl buffer and the inner Ca²⁺-alginate core solubilised by addition of a 1 L solution containing 50 mM sodium citrate (Sigma Aldrich, USA, Cat#: S1804), 10 mM MOPS, 0.45% NaCl, pH 7.4. The APLLA microcapsules were rinsed once with 500 ml MOPS-NaCl buffer, and once with 400 ml media. After removing the medium, 400 ml of fresh media was added to the microcapsules. The cell-containing microcapsules were then transferred into an inoculating bottle and aseptically connected to the bioreactor for inoculation.

3.4. Off-line cell culture analysis

The cultures were sampled daily and characterised by quantifying the total and viable cell density, recombinant IgG₁ and metabolites. The techniques were the same for cell suspension cultures and encapsulated cultures. The used methods were either previously developed in-house or by following the instruction manual distributed with the assay kits.

However, it was first necessary to develop a method to liberate the cells without affecting the cell viability.

3.4.1. Microcapsule break-up method for off-line line cell quantification

To determine the viable cell density off -line, the cells need to be liberated from the microcapsules. The microcapsule break-up method used must be rapid and gentle in order to not affect the cell viability. First, the microcapsules were separated from the medium using a cell strainer (100 μm nylon mesh) and washed with PBS. The microcapsules were then transferred to a graduated 1 ml syringe. The microcapsules were first incubated for 10 minutes in 1:1 volume 50 mM sodium citrate solution. The citrate-microcapsule suspension was then gently extruded through a 30 gauge needle. The broken microcapsule suspension was extruded twice more to ensure complete microcapsule breakage and to avoid the presence of particles which might interfere with the cell counting. The liberated cells were homogenised with care and counted microscopically using a Neubauer Haemocytometer after staining with 0.4% Trypan blue.

3.4.2. Metabolite and protein quantification

The concentration of glucose and lactate in culture samples was quantified using an HPLC (Agilent Instruments 1200, Agilent Technologies Ltd. Cork, Ireland) equipped with a refractive index detector, thermostat set to 30 °C with a Supelcogel™ C-610H column (Sigma Aldrich Ireland Ltd. Arklow, Ireland). A 0.01 M H_2SO_4 solution was used as mobile phase at a constant rate of 0.5 ml \cdot min⁻¹ for 32 minutes.

L-Glutamine and ammonia concentrations were quantified using a commercially available enzyme assay procedure (K-GLNAM, Megazyme, Ireland), in which the absorbance was measured using a microplate reader at 340 nm (Versamax, Molecular Devices, USA).

Recombinant IgG₁ was quantified using protein A affinity HPLC. The HPLC (Agilent Instruments 1200, Agilent Technologies Ltd. Cork, Ireland) was equipped with a refrigerated autosampler and a thermostatted column compartment. The column, POROS® Prepacked Protein A Affinity Colum (Life Technologies, Thermo Fisher Scientific, USA) was connected and maintained at 25 °C. Two mobile phases were prepared:

- Mobile Phase A - 20 mM sodium phosphate, 500 mM NaCl, pH 7.0
- Mobile Phase B - 50 mM sodium phosphate, 500 mM NaCl, pH 2.0

Each analysis lasted 5 minutes. The flow rate of the two mobile phases was 2 ml \cdot min⁻¹, and according to the program described in Table 3.1.25 μl of the sample was

injected 100 % of mobile phase A. The recombinant protein was detected using a UV/VIS detector set to 280 nm.

Table 3.1 Elution program for the quantification of IgG₁ by affinity HPLC

Time	% mobile phase A	% mobile phase B
0.0 → 2.5 minutes	100	0
2.5 → 3.5 minutes	0	100
3.5 → 5.0 minutes	100	0

To ensure column efficiency, the protein column must be regenerated at the beginning and the end of the process, after the calibration curve samples, after every 20 samples and at the end of the sequence. This was done by injecting $3 \times 100 \mu\text{l}$ of 2 M guanidine HCl and eluting using the mobile phase B at $2 \text{ ml} \cdot \text{min}^{-1}$. The column regeneration was followed by 3 blank analysis (3 injections of mobile phase A).

3.5. Off-line microcapsule characterisation

To have a full understanding of the evolution of microencapsulated cell cultures, different microcapsule characterisation methods were used. Microcapsules may vary in size, porosity, mechanical resistance and membrane thickness. The following methods, designed in-house, have been applied throughout this work.

3.5.1. Capsule size measurements

The microcapsule size was determined microscopically using a 40 x magnification. The microcapsules were placed on a glass slide or Petri dish and are submerged in MOPS buffer. The sample was then placed under a microscope equipped with a camera (Leica, Germany). The microcapsule diameter was calculated by triangulation using the camera imaging software (Leica Application Suite V5).

3.5.2. Texture analyser

The microcapsule mechanical resistance was determined daily, using a texture analyser (TA.XT plus Texture analyser, Stable Micro Systems, UK). The instrument was calibrated once, at the beginning of the culture. The microcapsules were first removed from the medium using a Falcon cell strainer (Falcon, Cat# 352360) and placed on a glass microscope slide. MOPS buffer was added to the capsules in sufficient amounts to cover the capsules. The capsules were spread across the slide. A uniform monolayer was formed by the use of absorbent paper on the side of the slide to remove a maximum of fluid as possible. The texture analyser probe (surface area $3.17 \times 10^7 \mu\text{m}^2$) descended at a constant rate compressing the microcapsule samples. The force required to compress the

microcapsule layer to 50% of the original height was measured. The mechanical resistance is expressed in $[g \cdot capsules^{-1}]$. Five to seven measurements were performed to obtain the statistical variability.

3.5.3. *Membrane and pore size evolution analysis*

To 100 μ l of microcapsules, 300 μ l of MW 0.05% FITC-labelled-molecule dextran solutions (10 kDa, 40 kDa, 70 kDa, 150 kDa, 250 kDa or 500 kDa) or IgG (Sigma Aldrich, USA) was added. The microcapsule suspension was incubated at room temperature with continuous mixing for 2 hours. The microcapsules were then analysed by confocal microscopy to confirm the diffusion of the dextrans or IgG into the microcapsules.

The microcapsules were analysed using a multiphoton confocal microscope (Zeiss LSM 710 and Confocor 3). The excitation wavelength was set to 488 nm and the emission wavelength at between 500 and 600 nm. The gain was adapted from 500 to 900 in order to have the maximal intensity without reaching signal saturation. The pinhole was set at 33.5 and the averaging was set to 4. The settings were kept identical for all the samples for comparison purposes and to detect any PLL leakage. The membrane width was defined as the distance between each side of the peak at 50% of peak height.

3.5.4. *3-D cell viability estimation within microcapsules by confocal microscopy*

The cell viability determined by off-line cell counts and by on-line monitoring methods (dielectric spectroscopy or biocalorimetry) was confirmed by double staining the cells with calcein and propidium iodide (Live/Dead Double staining kit, Sigma Aldrich, USA, Cat# 04511-1KT-F). Calcein (1 μ l) and 10 μ l propidium iodide in 1 ml PBS was found to be adequate for an optimal image quality. Staining solution (300 μ l) was added to 100 μ l of packed microcapsules. The suspension was then incubated at 37 °C for 2 hours before analysis using a multiphoton confocal microscope (Zeiss LSM 710 and ConfoColor 3). The excitation wavelength was set at 488 nm, since this wavelength can excite both dyes. The emission wavelength, on the other hand, was different for each dye. Calcein emits light with a wavelength between 500 and 600 nm and propidium bromide between 600 and 700 nm. The gain was adapted from 500 to 1000 for each emission wavelength, the pinhole was set to 33.5 and the averaging was set to 4. The imaging analysis comprised a 2-D plane image and a 3-D imaging, or a stack, of the microcapsule layers. This allowed a detailed visualisation of the viable and dead cells distribution across the microcapsule.

Chapter 4 Development of a reliable data acquisition system for real time monitoring of mammalian cell cultures

Summary: This chapter is about programming a software to continuously record measurements in Real-Time for cell culture monitoring purposes. Many languages are available, but LabVIEW is chosen for its graphical language, parallelism, instrument control and transferability proprieties. Two VI's (Virtual Instruments) are elaborated to monitor primarily the viable cell density and viability and other culture variables to additional information and understanding on the culture's evolution. The hardware, software and supplementary installed modules are described as well as the LabVIEW coding basics. Finally, the programs' structure and functions are explained. Though a previous LabVIEW VI was available, the program is more user friendly, adapted to the project's requirements and give a rapid insight on the culture's evolution. Furthermore, structure of the VI does allow modifications and/or addition of new components as well as a potential feed control function. Finally, the data from the frequency scans are further processed in LabVIEW and modelled by the Cole-Cole equation which may provide more accurate details on the culture's biomass state.

Keywords: Coding language, LabVIEW, Graphical language, Data acquisition, Parallelism, Realtime monitoring, Cole-Cole equation, Viable Cell density

4.1. Introduction

Bioprocesses, and more precisely mammalian cell cultures are complex and rely on many parameters to develop optimally. These parameters can be physical, (temperature or agitation), chemical (pH, metabolite and waste by-product) concentrations and biological (cell growth, cell viability). As these factors may significantly influence the productivity of a cultivation, they should be continuously monitored in real-time and controlled to improve the batch to batch reproducibility (Gnoth et al., 2007; Mark Riley, 2005).

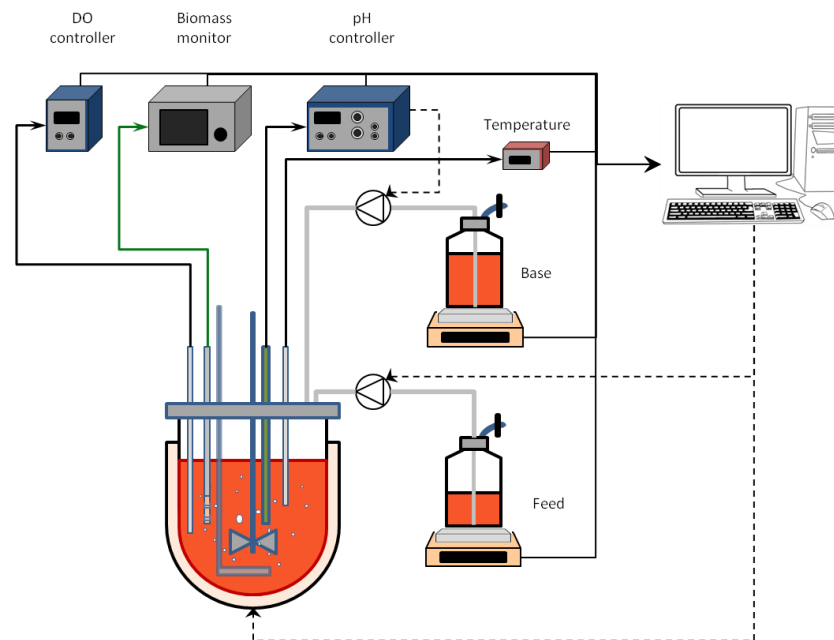


Figure 4.1 Example of a bioreactor setup. Different *apparati* send continuous signal to a central computer which repeatedly gathers data from different variables such as DO, pH, biomass, temperature, and mass of additional liquid components (base and feed bottles). Peristaltic pumps are controlled (dashed lines) either by signal sent by computer or by an external controller. Cell cultures are usually an isothermal process and the broth's temperature is controlled by heating or cooling the fluid within the reactor's jacket

As illustrated in Figure 4.1, each parameter measures a specific variable and a central computer based platform gathers the information from each signal, to analyse the evolution of the process. If necessary and programmed, a signal is output as a response to a process set point deviation (Chen et al., 2011).

4.1.1. Design criteria

A data acquisition program for culture monitoring and potential control purposes, must foremost be reliable to continuously run without interruption over a number of days or even weeks. A batch cell culture typically lasts a period of 8 days, yet it has been reported for perfusion cultures to exceed a 2 month lifespan (Sadettin & Ozturk and Dhinakar & Kompala, 2005).

The project is carried out by a group of people with different skills. It is therefore necessary for the program to have a user-friendly interface. The interface should clearly display all the program functions for all the different operations. In addition, the cultures are carried out over long periods of time including out-of-hours periods. As the main purpose of the program is to continuously monitor cell cultures, all the acquired data should be treated, saved and plotted in a time chart to rapidly inform any operator on the constant development of the culture Figure 4.2.

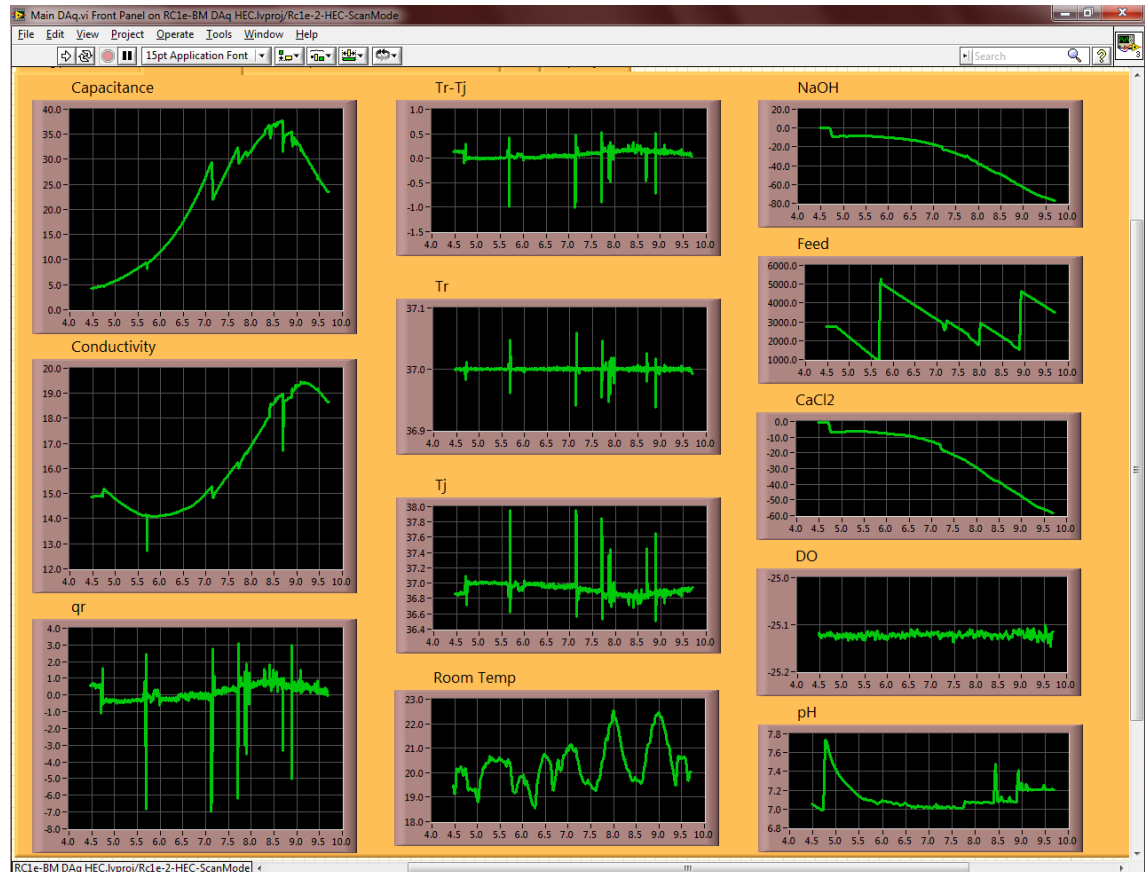


Figure 4.2 User-interface, or Front panel, displaying the evolution of the different monitored variables of an encapsulated CHO-DP12 perfusion culture; Perfusion culture 3, at the end of culture on the closing of day 9.

As a project may evolve and require the monitoring of cells cultivated in different bioreactors, the program needs to be easily transferrable and installed for different set-ups. Additional monitoring equipment and features, such as a feed control, may be required necessitating the program to be rapidly extendable or altered.

Finally, to facilitate the design and debugging of the program, the chosen language must be straightforward to comprehend. Long coded text could create confusion and become difficult to alter, especially if adaptation to a different set-up or process is required. Not all users have programming knowledge or programming skills, therefore a simple language is an essential criteria.

4.1.2. *Selection of a programming environment*

Many platforms are currently available for the conception of a laboratory data acquisition program. Each platform codes in a specific language such as C++, Java, Visual Basic, MATLAB, LabVIEW, etc. The language selection is not only based on the application but also on the developers skills (Wang et al., 2012). Unlike other coding languages such as C++ or Visual Basic that are textual, LabVIEW is a purely graphical language, which involves wiring different components together. Graphical code does not only make programming more accessible but also reduces the necessary time to develop a tailored program (Travis, 2002; Wagner et al., 2010).

MATLAB, which stands for Matrix Laboratory (Mathworks, USA), and LabVIEW, Laboratory Visual Instrument Engineering Workbench (National Instruments, USA) are often encountered in laboratories to generate robust data acquisition programs. Both environments are capable of executing similar tasks, however they differ in their area of expertise. MATLAB's core strength is to analyse and manipulate complex data, whereas LabVIEW is generally preferred to rapidly creating personalised measurement and control systems. Communication between the computer and laboratory equipment can easily be implemented as different Virtual Instruments (VI), or LABVIEW drivers, are usually provided with the equipment, or else by changing the communication settings within Windows (Wrobel et al., 2012).

LabVIEW is renowned for its capability of readings different elements of a code simultaneously (Johnston et al., 2004; Wagner et al., 2010; Wrobel et al., 2012). The concept of data flow execution, or parallelism is said to be a great advantage for acquiring data from multiple sources, for processing and evaluating data (Wagner et al., 2010), and shortening the program execution time (Johnston et al., 2004). For example, the equation in Figure 4.3 can either be calculated in three consecutive steps, by first adding a and b, followed by multiplying b and c, and then determine x by dividing the first by the second previously calculated value; or in contrast adding a and b at the same time as multiplying b with c and then dividing the value of sum by that of the multiplication.

The project will not only involve monitoring the viable cell density and other parameters of mammalian cell cultures, it also prospects to use either capacitance or heat flux measurements to control a feed rate. Because the software permits the synchronisation of different parallel processes, the decision to time and execute different tasks and its capability to communicate with most laboratory equipment, it makes LabVIEW an ideal platform for creating a robust real-time online monitoring program and control system.

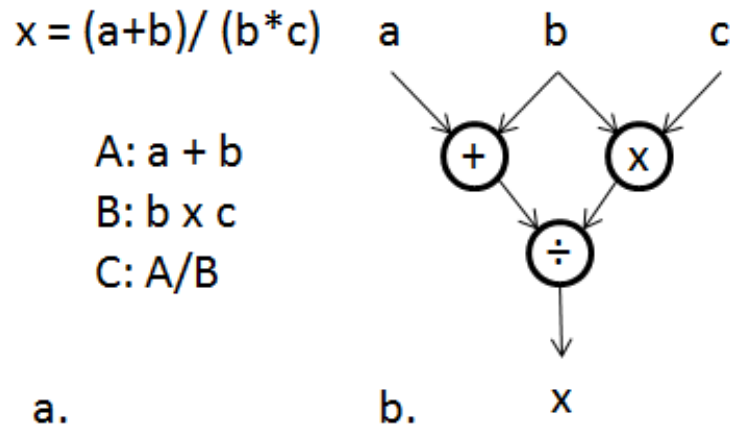


Figure 4.3 Data flow programming. a. Simple mathematical program and b. it's data flow equivalent: A and B are performed in parallel, however, C cannot be executed until the both values have been calculated.

4.1.3. *Different applications and available monitoring and controlling mammalian cell cultures*

LabVIEW has been the chosen platform to create programs for many applications of different backgrounds ranging from automotive, aerospace and defence, green energy, healthcare, geology, meteorology and bioprocessing (Andò and Carbone, 2009; Dabros et al., 2010; Wahab et al., 2014; Wali et al., 2013).

A previous data acquisition program was developed and used within the laboratory, for the monitoring and control of a yeast culture (Dabros et al., 2010, 2009a). The *Saccharomyces cerevisiae* were not only directly monitored by dielectric spectroscopy, but glucose, ethanol, ammonium, phosphate, glycerol and acetic acid were quantified by FTIR spectroscopy. Besides, most variables (capacitance, CO₂, O₂, volume reactor and feed volume) being acquired in LabVIEW, the FTIR spectra were acquired in the probe's own software ReactIR (Mettler Toledo, USA) and processed in MATLAB. The biomass determined in LabVIEW was reconciliated with the biomass density determined in MATLAB based on the culture's characteristic yields and rates. The data was then processed again in LabVIEW to determine the growth rate and used to then control a feed pump.













Though this VI was readily available, a new data acquisition system was constructed to facilitate the addition of new components and to improve the user interface. The numerical tables were replaced by time charts to give rapid visual information on the culture's trends. Nonetheless, all the equipment communication VI's were updated and used to generate the new adapted data acquisition system.

4.1.4. Basic programming in LabVIEW:

A virtual instrument, or LabVIEW program, is a compilation of different sub-VI's, wired together. When LabVIEW is launched, the front panel of a blank, or pre-existing VI is displayed. The front panel is the user-interface that contains the different controls and indicators. Many controls (buttons, switches, dials) and indicators (gages, graphs, text boxes) are available and can be freely placed to produce an interactive environment. Each sub-VI has its own front panel with its own controls and indicators. To link these controls and indicators to the main VI, they are designated as inputs and outputs in that interface.

Every element that is placed in the front panel is automatically added to the block diagram (the reverse is true as well). The block diagram is where the program is coded. The different sub-VI's or functions are connected together using various colours and size wires. The wire type is automatically selected in LabVIEW depending on the information type, Table 4.1.

Table 4.1 Information type and respective wire code

Data Type	Scalar	1-dimensional array	2 dimensional array	Data type
Blue				Numeric (Integer)
Orange				Numeric (floating-point)
Pink				String (text)
Green				Boolean (true/false)

As mentioned above the execution of the code can be timed, i.e. the speed and the period time at which a segment of the VI can be controlled using “execution structures” and timing sub-VI. These execution structures can be sequential, while or for-loops used for repeating a code until a condition is fulfilled or for a number of iterations, or case structures to read a code if and when a condition is met.

4.1.5. Software and modules

The data acquisition system is coded in LabVIEW 2010 Service Pack 1. Along with the core software, NI-RIO 3.6, NI-Serial 3.7, NI-VISA 5.2.0 and LabVIEW 2010 Real-Time are complementary modules necessary to communicate with different equipment and to save the data in text files in real-time.

4.1.6. Hardware:

- Minifors set- up

The Minifors bioreactor (Infors, HT, Switzerland) has its own data logging software Iris V.5. This software records data from all pH, DO, agitation and temperature measurements,

whilst providing a feedback control and data analysis. In parallel, the data from the biomass monitor (Biomass Monitor 220, ABER Instruments, UK) and two balances (PG3001-S Balance, Metler Toledo, USA) are acquired in LabVIEW. The Biomass Monitor is connected through a low modem RS232 cable fixed to a USB to low modem port connector. The device communicates with the computer at $38400 \text{ bits} \cdot \text{s}^{-1}$, 8 data bits with no parity and 1 stop bit. The balances were also wired to the computer using RS232 cables and USB to RS232 adaptors. The communication settings are entered in LabVIEW and are $9600 \text{ bits} \cdot \text{s}^{-1}$, 7 data *bits* with no parity and 1 stop bit.

- Reaction Calorimeter eRC1

The calorimeter is equipped with two separate computers. One computer's unique function is to control the calorimeter (agitation and temperature of the reactor and the jacket) using the iControl software (Mettler Toledo, USA). Unlike the data acquisition elaborated in the Minifors set-up, it is desirable that all data from the different sensors are acquired and processed within the one program. In addition, a pump must be connected if a controlled feed is required. For these reasons, each monitoring device is grouped onto a Real-Time Controller with 128 MB DRAM, 2 GB Storage, NI-cRIO 9014 and 8-slot chassis. The pH controller (Bioengineering, Switzerland), DO controller (Bioengineering, Switzerland) and a PT100 temperature probe are connected to a NI-9215, analog in-put module. The three balances (SG16001 and PG3001-S balances, Mettler Toledo, USA) and biomass monitor (Biomass Monitor 220, National Instruments, UK) are connected to a NI-9870, RS232 Serial Interface Module for CompactRIO. And finally, the cable connecting the calorimeter to the first computer is intercepted by a secondary RS232 to allow the recording of the data in parallel within LabVIEW and is connected to the compactRIO controller directly. All the communication settings are pre-set in LabVIEW.

4.2. Cell culture monitoring code description

Two data acquisition programs were designed for culture monitoring purposes. The first was elaborated to continuously acquire data sent by the biomass monitor and by the base and feed balances. The LabVIEW VI program runs in parallel to Infors' Minifors program Iris. In addition to its continuous data reading and recording role, the LabVIEW program also fits the Cole-Cole model within frequency scans to give further information about the cell physiological and chemical characteristics. As the project evolved towards using heat flow rates to monitor cell density and cell activity, a new VI was needed with additional monitoring features. The first VI is incorporated within the RC1 culture monitoring program.

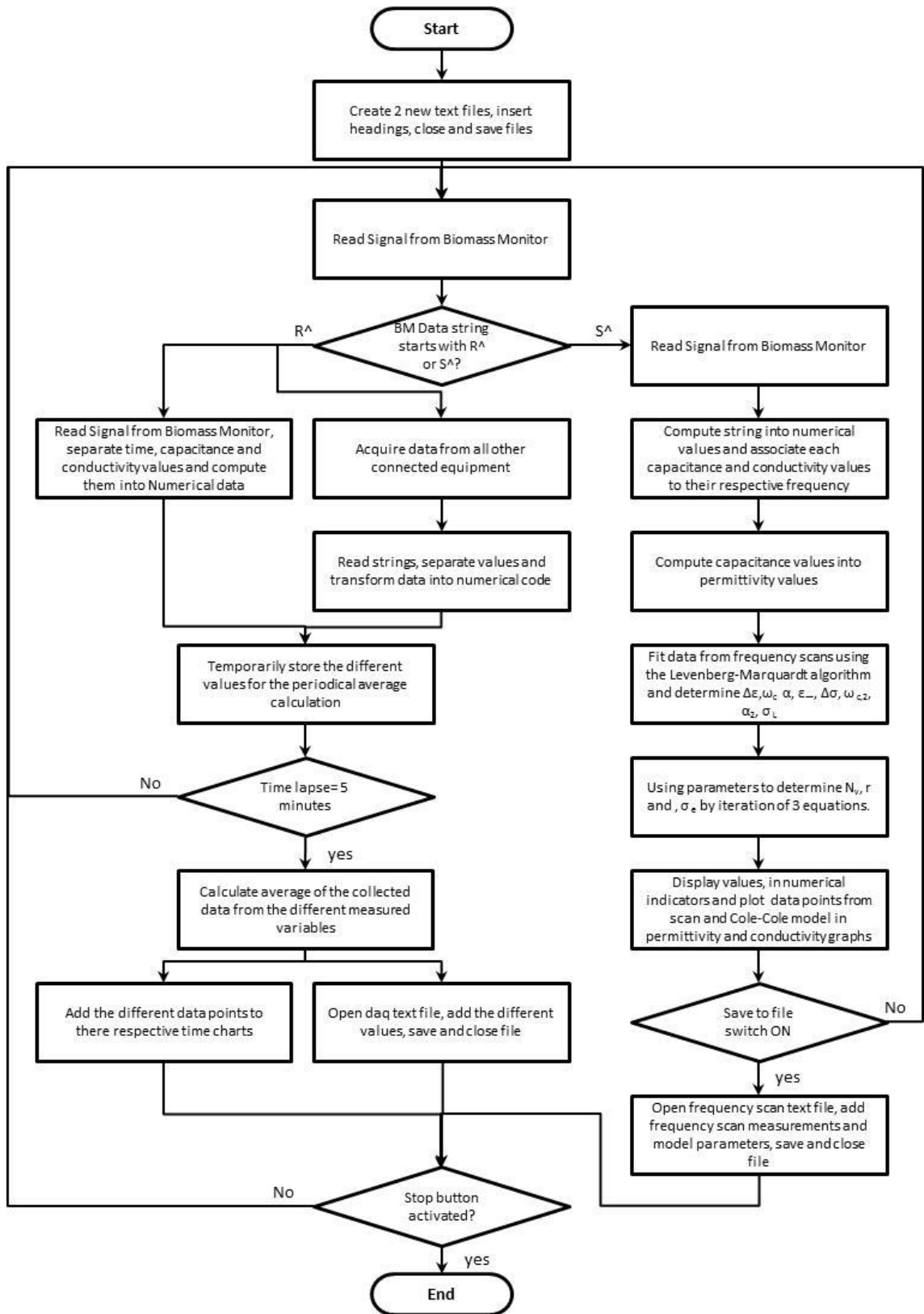


Figure 4.4 Flow chart of the data acquisition program, (daq = data acquisition, BM= Biomass monitor)

Both programs are conceived to sequentially carry out similar tasks, described in

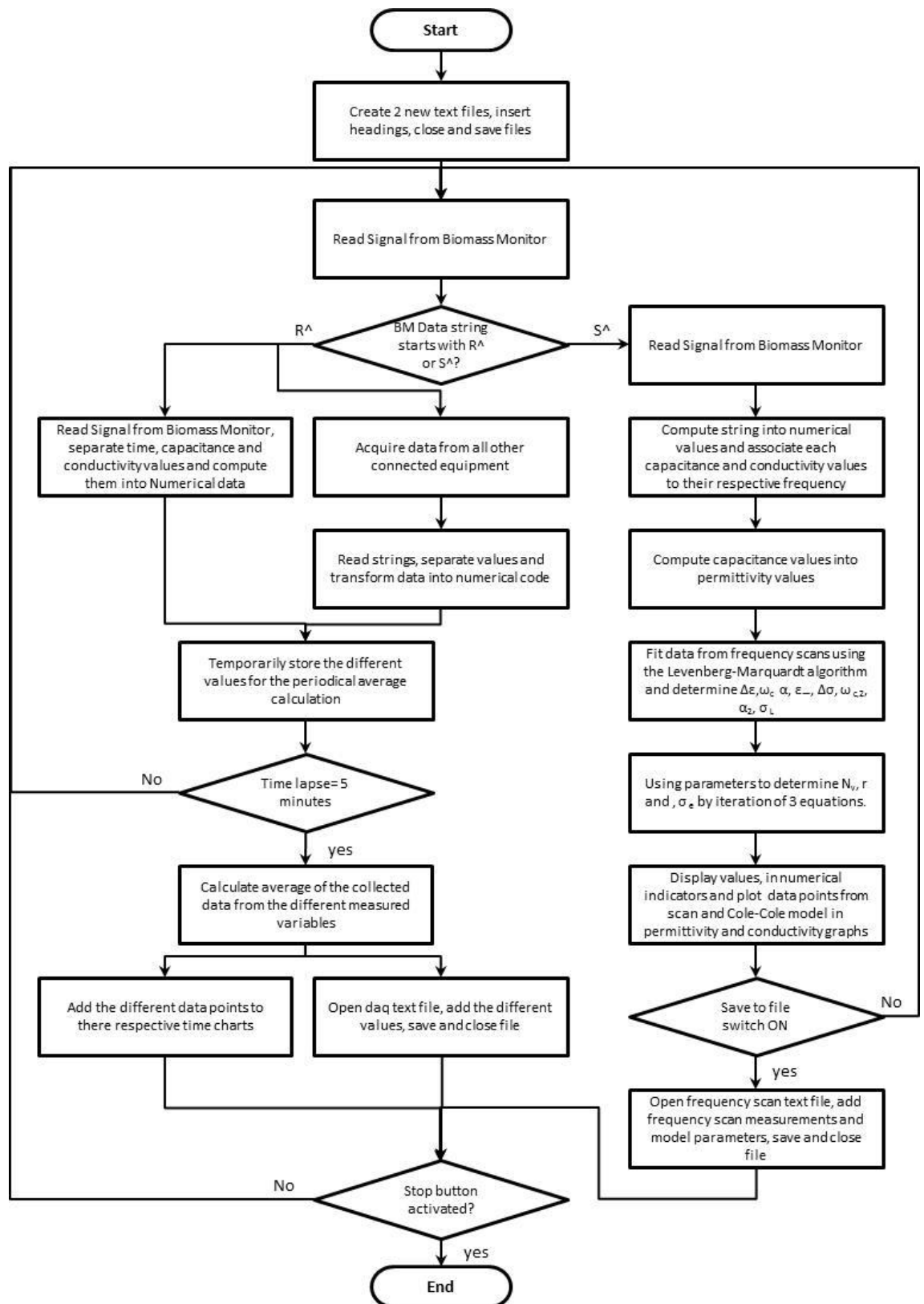


Figure 4.4. The main VI is constructed within a flat sequence structure with two time-frames to execute tasks within two distinct phases. In the first sequence, two text files are created: the data acquisition text file for saving all the continuous measurements and the frequency scan text file for saving the daily scans. Both text files are opened to insert the different headings (time, capacitance, conductivity, etc. or frequencies and Cole-Cole

equation parameters), saved and closed. The tasks of the second sequence are not read until those of the first frame are completed.

The second frame contains two distinct while-loops that execute the code repeatedly, until the STOP button is activated to end the program. The first while loop contains the code to acquire data from the different connected devices, calculate an average, add the data to the text file and add the new data points to the respective chart. The second while loop processes the data from a frequency scan and fits the capacitance and conductivity values within Cole-Cole model. The while loops run simultaneously, however the data received from the biomass monitor is treated in either loops depending on the communicated string. ABER Instruments' Biomass Monitor 210 sends two types of signal:

- ^R,01,2013-04-27 16:37:02, 0.107, 0.003,;(chan,time,c,g)
- ^S,01,2013-04-27 16:34:48, 2.509, 0.006, 1.801, -0.006, 1.962, 0.008, 2.057, 0.000, 1.897, -0.003, 1.881, -0.002, 2.081, -0.004, 1.909, 0.002, 1.832, 0.000, 1.829, 0.000, 1.824, 0.000, 1.993, 0.005, 2.244, -0.003, 2.397, 0.008, 2.087, -0.001, 1.735, 0.004, 1.676, -0.001, 1.777, 0.003, 1.791, -0.000, 1.961, -0.004, 2.040, 0.006, 2.055, 0.007, 2.320, 0.010, 2.644, 0.006, 2.587, -0.009

The first string, the R string, is transmitted to the computer when the inline monitoring screen is selected. The string is constructed with the channel number, the date and time of the acquired data, the capacitance measurement and the conductivity measurement followed by a string description. The second string, the S string is transmitted to the computer when the operator wishes to run frequency scans. The S string is composed of the channel number, the date and time and 25 pairs of capacitance and conductivity readings measured at the instrument's pre-selected 25 frequencies.

4.2.1. *Implementing the Cole-Cole model*

Frequency scans, as reported in Chapter 2, have the potential to provide further information on the viable cell density. Capacitance measurements at a single frequency are linearly proportional to the biovolume. As the cell size is dependent on the cellular health and the culture environment, it may fluctuate and falsify the estimated viable cell density (Cannizzaro et al., 2003a; Opel et al., 2010a).

Frequency scans of spherical cells such as CHO cells can be modelled through the Cole-Cole equation, Equation (2.6) and coded in Figure 4.5 (Dabros et al., 2009c; Opel et al., 2010a). The equation describes the relationship between the culture's permittivity and the angular frequency. Four parameters $\Delta\epsilon$, ω_c , α and ϵ_∞ are determined by inputting the 25 data points into the ready-made Non-Linear Curve fit VI, a "black box" containing the Levenberg Marquardt algorithm.

$$\varepsilon(\omega) = \frac{\Delta\varepsilon \left(1 + \left(\frac{\omega}{\omega_c} \right)^{1-\alpha} \cdot \sin\left(\frac{\pi}{2} \cdot \alpha\right) \right)}{\left(1 + \left(\frac{\omega}{\omega_c} \right)^{2-2\alpha} + 2 \cdot \left(\frac{\omega}{\omega_c} \right)^{1-\alpha} \cdot \sin\left(\frac{\pi}{2} \cdot \alpha\right) \right)} + \varepsilon_\infty \quad (4.1)$$

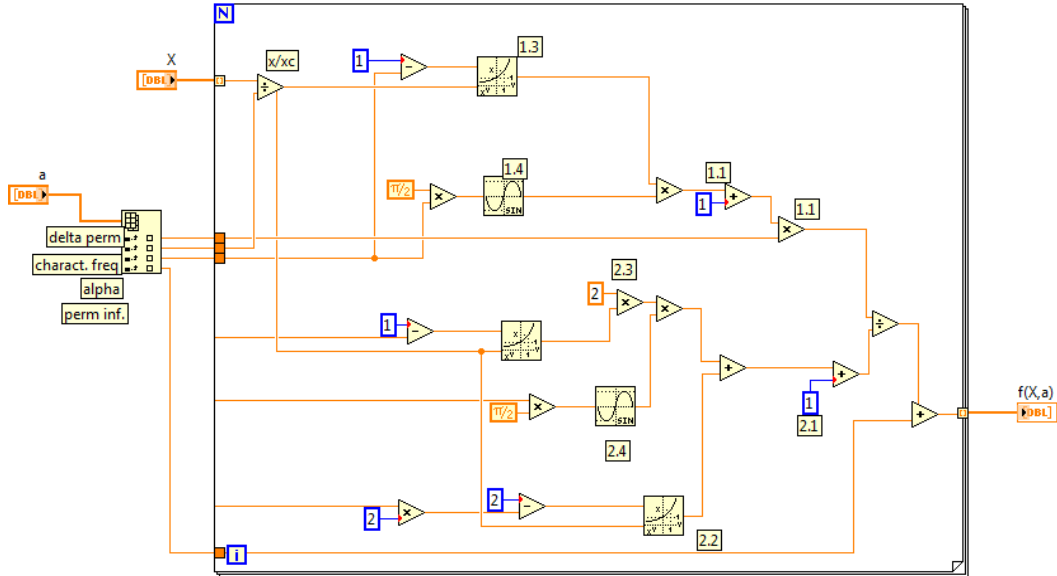


Figure 4.5 LabVIEW code of the Cole-Cole equation, Equation (2.6)

According to the capacitance and the conductivity definitions, the measured conductivity increases as the capacitance decreases. Therefore, the conductivity readings are fitted in the same manner as the capacitance values within the adapted Cole-Cole equation, Equation (2.7).

$$\sigma(\omega) = \frac{-\Delta\sigma \left(1 + \left(\frac{\omega}{\omega_{c,2}} \right)^{1-\alpha_2} \cdot \sin\left(\frac{\pi}{2} \cdot \alpha_2\right) \right)}{\left(1 + \left(\frac{\omega}{\omega_{c,2}} \right)^{2-2\alpha_2} + 2 \cdot \left(\frac{\omega}{\omega_{c,2}} \right)^{1-\alpha_2} \cdot \sin\left(\frac{\pi}{2} \cdot \alpha_2\right) \right)} + (\sigma_L + \Delta\sigma) \quad (4.2)$$

The parameter $\Delta\varepsilon$, permittivity difference between high and low frequencies, proportional to the culture's biovolume, ω_c , the characteristic frequency dependent on the cell size distribution, $\Delta\sigma$ the conductivity difference between low and high frequencies and the conductivity plateau at low frequencies σ_L are then used to solve a three equation system.

To estimate the cell number per unit volume N_v , the cell radius r and the culture media conductivity σ_e , Equations (2.8), (2.9) and (2.10), are coded within a While-Loop. Before starting the iteration, σ_e is determined using Equation (2.11). The estimated σ_e is then inserted into Equation (2.9) to calculate r . This value is used afterwards to determine N_v with Equation (2.8), which in its turn is used to find a more accurate value for σ_e . The cycle is repeated using the last σ_e value. The iteration ends when the absolute

convergence test between the last σ_e subtracted by the 7th to last σ_e is smaller than 10^{-10} . At the end of each frequency scan cycle, data points, model, equation parameters and the determined equation variables displayed as graphs and numerical indicators on the front panel, Figure 4.7.

$$\Delta\varepsilon = \frac{3N_v \cdot \pi \cdot r^4 \cdot C_m}{\varepsilon_0} \quad (4.3)$$

$$\omega_c = \frac{1}{r \cdot C_m \cdot \left(\frac{1}{\sigma_i} + \frac{1}{2\sigma_e} \right)} \quad (4.4)$$

$$\sigma_e = \frac{\sigma_L}{(1-P)^{1.5}} = \frac{\sigma_L}{\left(1 - \frac{4}{3} \cdot \pi \cdot r^3 \cdot N_v \right)^{1.5}} \quad (4.5)$$

$$\sigma_e = \sigma_L + \Delta\sigma \quad (4.6)$$

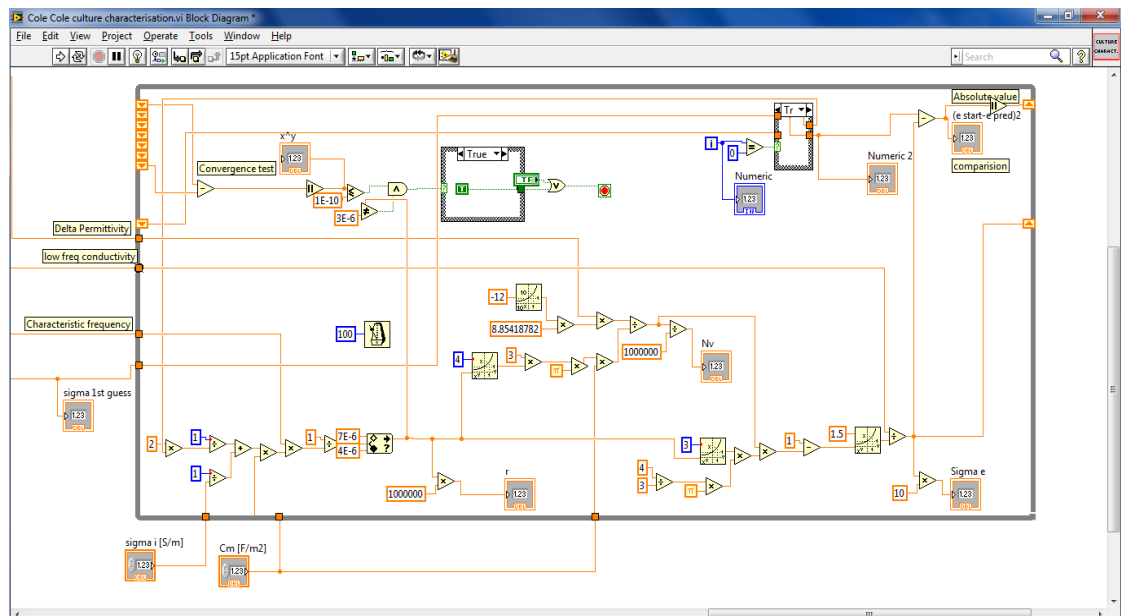


Figure 4.6 LabVIEW code of the iteration of the three equation with three unknowns: The cell number per unit volume N_v , the cell radius r and the culture media conductivity σ_e

The membrane capacitance $C_m = 0.02295 [F \cdot m^2]$ and cytoplasm conductivity $\sigma_i = 0.6524 [mS \cdot cm^{-1}]$ constants, defined in the Chapter 5, are specific to the cell line and culture settings. They are determined through calibration and inserted into their numerical control boxes, top-right in Figure 4.7.



Figure 4.7 Screen shot of a frequency scan undertaken on day 12 of the second perfusion culture, in the RC1. The cell count on that day revealed that the culture had a density of $14.5 \cdot 10^6$ cells \cdot mL⁻¹. The average cell radius measured on that day was 6.2 μ m

4.2.1. Project development for monitoring cultures in the eRC1

The VI created to monitor cultures performed in the Minifors bioreactor is limited to acquire data solely from the Biomass Monitor and two balances. The other culture variable such as temperature and pH are recorded within another parallel program. To obtain a more comprehensive and a more prompt culture analysis, all of the variables should be analysed and processed in the same manner.

Moreover, in addition to the capacitance and conductivity, mass of added base and feed to the culture, pH and reactor temperature, the jacket temperature and ambient temperature must all be monitored, if the heat flow rate produced by the cells is to be evaluated. As a result, a new project is developed. The NI CompactRIO is inserted into the project and set to Scan-mode. This means that the each I/O module is accessible in Real-Time without needing to reconfigure the FPGA (field-programmable gate array) circuit.

Six different types of monitoring devices are connected and each have different communication settings. Acquiring and processing data within one VI may lead to a complex and large VI and the timing might become difficult to manage. Two main VI are then elaborated and run in parallel.

The first VI, entitled Acquisition.vi, receives data from all the different monitoring devices. It is composed with three While-Loops. The first While-Loop acquires data from the balances, the pH and DO controllers and the PT100. The execution timing is set at 1000 ms per cycle. The pH and DO controllers and ambient temperature PT100 probe output a

voltage that is proportional to the measure variable. The voltage and pH, DO and temperature were calibrated and the calibration is coded within the VI.

The second While-Loop contains the “Read Biomass Monitor 210” VI, previously designed for the Minifors setup. The string received is deciphered into either single numerical capacitance and conductivity values or within the 25 capacitance and 25 conductivity numerical arrays. The third While-Loop is constructed with the VI previously designed by a previous peer to decrypt the information sent by the calorimeter with the reactor and jacket temperatures.

The measured values are displayed on the front panel and configured as global variables to communicate them to the second VI. The second VI, Main DAq.vi is similarly constructed as the main VI conceived for the Minifors set-up. It is composed within the same two frame flat sequence structure. As the program starts two new text files are created, opened, and the headings are inserted before saving and closing them. Like the other VI, one file saves the average data points of each variable taken up during a 5 minute period, and the other saves the data from the daily frequency scans.

The second frame is also composed with two While-Loops, one for processing the data obtained from the daily frequency scans and model them with the Cole-Cole equation. The frame has the same function to save data points after averaging the measurements made during the set 5 minutes time-frame. However, here the heat flow rate is calculated by subtracting the reactor from the jacket temperatures, $T_r - T_j$, and deducting the baseline value. The subtraction is then multiplied by the heat coefficient U_A to estimate the reaction heat flow rate. The baseline and U_A are determined prior to inoculation and manually entered into the numerical control boxes on the front panel. Time, capacitance, conductivity, pH, DO, room temperature, mass of added base, mass of added feed, reactor temperature, jacket temperature, $T_r - T_j$, reaction heat flow rate q_r are plotted, Figure 4.2 and saved into the daq text file. The project follows the diagram in

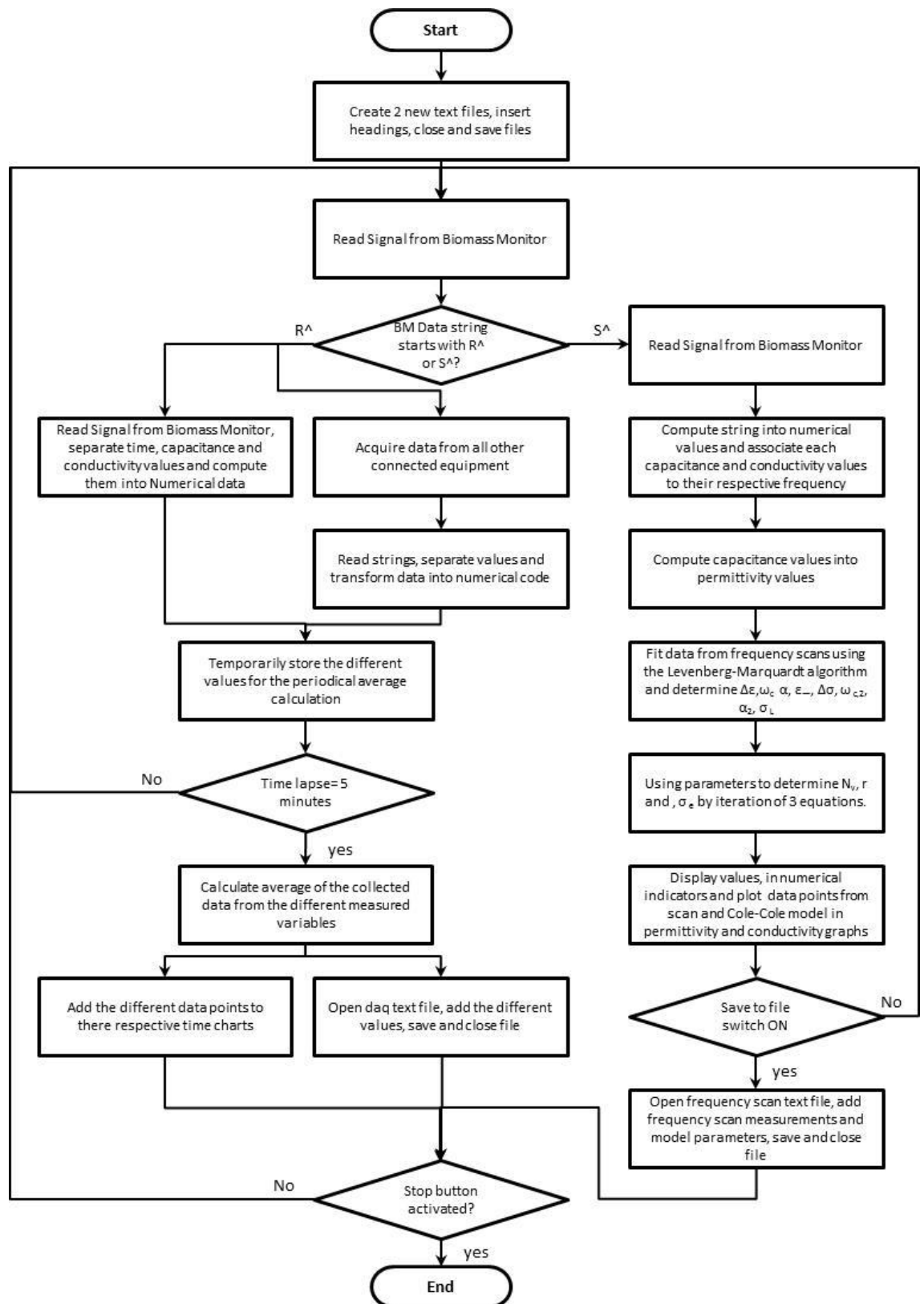


Figure 4.4.

4.3. Outcome and conclusion

Design criteria were considered before commencing the data acquisition programming, which are stability, ease to transfer from one setup to another, easy and comprehensive

code, and accessible to other researchers. LabVIEW is a platform which allows to graphically code a program, specific to a project's requirements. It is the preferred coding language to rapidly generate monitoring and control programs that allow different tasks to be executed synchronously. The graphical code is easy to learn and also permits program alterations for its transferability from one set-up to another in respect to the project development.

Two VI were designed to monitor cell cultures and successfully gave real-time information throughout each culture. The first VI was created to monitor the viable cell density, the added base for pH control and feed, if any. In addition to real-time monitoring, the VI models each performed frequency scans by fitting the Cole-Cole equation using the Levenberg Marquardt algorithm. The parameters of the model are then used to determine the cell number and cell radius in a three equation system solved within the LabVIEW program by iteration.

The second VI required a more extensive culture monitoring data acquisition VI, to uptake data from 6 different instruments with different communication settings. The first VI was used as a scaffold into which the supplementary code was input. The data points for each monitored variable (capacitance, conductivity, pH, DO, ambient temperature, reactor and jacket temperature, mass of added base and feed, etc.) were not only saved into tab-delimited text files, but also plotted into charts to give a rapid insight upon the culture's development.

Chapter 5 The Application of Dielectric Spectroscopy for Monitoring the Viable Cell Density of Microencapsulated CHO Cell Cultures

Summary: The correlation between the viable cell density of microencapsulated cultures and the online dielectric measurements is studied in this chapter. After verifying that the presence of alginate beads at high levels has little influence upon the dielectric signal, the CHO-DP12 cultures were characterised. The frequency scans were processed within the tailored LabVIEW VI and from the Cole-Cole model, the specific membrane capacitance was evaluated at $C_m = 0.02295 [pF \cdot cm^{-2}]$ and the internal conductivity at $\sigma_i = 0.6524 [mS \cdot cm^{-1}]$. In addition, to calculate the viable cell density from the capacitance signal in real-time, a calibration model was generated within the $10^5 - 10^8 \text{ }_{vcell} \cdot mL^{-1}$ range. A highly correlated model was drawn from which the slope, $a = (1.44 \cdot 10^{-6} pF \text{ }_{vcell}^{-1} \text{ } cm^{-1})$ represents the specific capacitance per cell density unit. This model was validated by the two models directly built from the online and offline results from both suspension and microencapsulated cultures. Suspension and microencapsulated batch cultures were undertaken to verify the applicability of dielectric spectroscopy to monitor all stages of a culture. A maximum cell density of $2.94 \cdot 10^6 \text{ }_{vcell} \cdot mL^{-1}$ was obtained corresponding to 1.8% of the internal volume of the microcapsules. Growth was limited by glucose depletion. Since substrate, rather than space within the core, was limiting under the conditions studied, dielectric spectroscopy has the potential to be used to design a controlled medium feed strategy to achieve very high cell densities.

Keywords: Dielectric spectroscopy; cell encapsulation; on-line monitoring; mammalian cell culture; batch culture.

5.1. Introduction

Cell microencapsulation technology consists in entrapping cells within a semi-permeable membrane. As a result, the accessibility of the cells for monitoring purposes is not straightforward. Since microcapsules are permeable to small ions, the following chapter discusses the use of dielectric spectroscopy as an on-line monitoring method, and investigates the potential use to accurately estimate the viable cell density in real-time.

Dielectric spectroscopy has been reported to be an effective method to monitor viable cell density on-line in many bioprocessing applications (Cannizzaro et al., 2003b; Carvell and Dowd, 2006b; Ducommun et al., 2002b; El Wajgali et al., 2013b; Justice et al., 2011b; Noll and Biselli, 1998b; Opel et al., 2010b). Since cells act like micro-capacitors, with conductive cytoplasm and electrically insulating cytoplasmic membranes, they polarise and store charge when an electrical field is applied (Carvell and Dowd, 2006b; Markx and Davey, 1999b). By the application of an alternating electrical field the cells depolarise as the electrical field alternates, thus generating an electrical field of their own. This electrical field is detected by the biomass monitor and the amplitude difference and time shift is analysed to determine the global capacitance of a culture (Davey et al., 1992b; Patel and Markx, 2008).

This biomass monitoring tool has been used to monitor the viable cell density of cells grown in suspension or adhering to microcarriers, in stirred tank reactors, in packed beds or in air lift reactors, as well as for the control of nutrient feeds for fed-batch and perfusion cultures (Carvell et al., 2006; Carvell and Dowd, 2006b; Justice et al., 2011b). Though dielectric spectroscopy was successfully applied to various mammalian cell culture types, following the growth of microencapsulated cultures has not previously been reported.

After determining the effect of the presence of the microcapsules in high volume fractions on both capacitance and conductivity signals, the CHO-DP12 cells were characterised. Physiological and biochemical proprieties vary between cell species and may also differ from one cell line to another. The membrane capacitance per surface unit C_m and the internal conductivity σ_i were calculated from the resulting measurements of frequency scans. The capacitance and conductivity data were then processed and modelled with the Cole-Cole equations in the designed LabVIEW VI. In addition, a calibration model was established to correlate the measured capacitance at 580 kHz and the calibration and the specific cellular capacitance obtained. These proprieties allowed a good understanding of the culture development and cell viability.

CHO-DP12 cells were then cultured in a stirred tank reactor in both suspension and encapsulated modes. The cultures were operated in batch mode to define the frequency range for operation of the dielectric spectrometer, to study the influence of the culture

medium, to define whether there was interference caused by the polyelectrolytes used in microcapsule fabrication and to evaluate whether the capacitance signal could be used to define the cell density in both suspension and microencapsulated cultures throughout the different stages and states of the cultures.

5.2. Effect of the microcapsules on the dielectric signal

Non-biological particles that cannot polarise and store charge, do not have a significant effect on the dielectric signal in low volume fractions (Davey et al., 1993). The ions of the culture media can either migrate through or around the particles depending on the electrical permeability. On the other hand, microcapsules entrapping cells can constitute up to 70 % (V/V) of a culture suspension. As a result it is possible that at high volume fractions, solids may cause a reduction of the β -dispersion.

Microcapsules are composed of a semi-permeable membrane surrounding an inner core that allows the in- and out- flow of small molecules and ions. The core is composed of water, alginate in solution, alginate complexed with calcium and other ions. Alginate beads are porous and the spherical shape is maintained by the Ca^{2+} -alginate guluronic acid complex. In both water- based and porous structures, ions should be able to flow freely with the alternating electrical field. Thus, the presence of such solids would be expected to have little effect on the β -dispersion and capacitance measurements.

In this work cultures were carried out in which the medium contained 25%(v/v) microcapsules. However, in order to determine whether the presence of microcapsules resulted in an interference in the dielectric signal, the dielectric probe was placed in a MOPS solution in the presence and absence of 50% (v/v) calcium alginate beads. Alginate beads were selected since the amount of alginate complexed in the microcapsule core depends on the amount of calcium in the medium, the amount of citrate used in the core liquefaction step and the amount of alginate lost from the core through exodiffusion. The alginate beads were produced by extruding a 1.5 % (w/v) alginate solution through a 300 μm \varnothing single nozzle into a stirred a 100 mM CaCl_2 (Sigma, USA, Cat#: C7902), 10 mM MOPS buffer pH 7, bath using a vibrating nozzle encapsulation device (Inotech, Switzerland). After gelation the beads were transferred to a 10 mM MOPS solution (Sigma Aldrich, USA, Cat#: M3183) containing 0.85% NaCl (Merck, Germany, Cat#: 106400), pH 7 to form a 200 mL 50% (V/V) suspension of calcium alginate beads. The suspension was agitated using a magnetic stirrer with the speed adapted to ensure homogenous mixing without creating a vortex. Dielectric frequency scans were performed in both the bead suspension and the MOPS buffer as a negative control.

As observed in Figure 5.1, the suspension of 50% (v/v) of calcium alginate beads showed a significantly lower conductivity. This reduction in conductivity resulted in a

small increase in the capacitance values at low frequencies, however no β -dispersion was obtained in either the MOPS solution or bead suspension. It can therefore be concluded that microcapsules or alginate beads are unlikely to have a significant effect on the capacitance measurements. It should also be noted that the encapsulated mammalian cell cultures are carried out in well agitated stirred tanks, and that repeated sampling should not alter the volume fraction of microcapsules in the reactor.

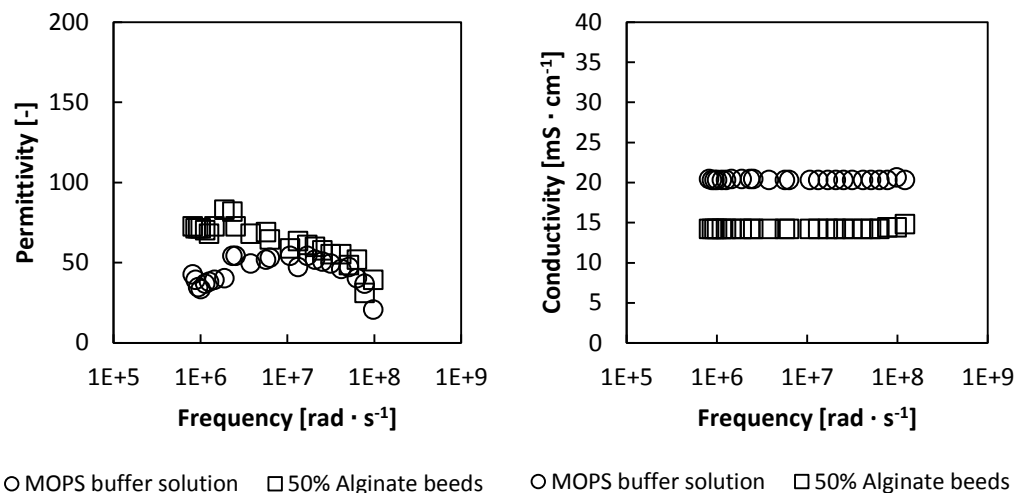


Figure 5.1 Capacitance and Conductivity frequency scans of a homogenously agitated 50% (V/V) alginate bead suspension in a MOPS buffer compared those performed in MOPS solution in the absence of beads

5.3. CHO-DP12 dielectric characterisation

The size of a healthy cell and the cytoplasmic membrane and cytoplasm electrochemical characteristics are specific to a cell species and may also vary between cell lines. In this section, the CHO-DP12 cells were characterised using the Cole-Cole model to determine the optimum frequency to measure the continuous viable cell density the specific membrane capacitance per unit area C_m [$pF \cdot cm^2$] and the cytoplasmic conductivity σ_i [$mS \cdot cm^{-1}$]. In addition, a calibration curve was established to correlate the viable cell density to the measured capacitance at the characteristic frequency.

5.3.1. Cole-Cole modelling

Frequency scans, or measuring the cell culture capacitance over a range of 25 frequencies, though more complex than measuring at a single frequency, can provide more comprehensive information on the average cells size and hence the cell number per unit volume. As the frequency increases, ions have less time to migrate between the electrodes thereby diminishing the ability of the cells to polarise. From a frequency scan, such as those displayed in Figure 5.3, a β -dispersion can be drawn.

A β -dispersion is characterised by the permittivity difference between low and high frequencies, $\Delta\epsilon$, the characteristic frequency ω_c and slope α , and modelled using the Cole-

Cole equation, Eq. (5.1). This equation (5.1) is based on the Debye equation, describing the polymer dielectric relaxation (Dabros et al., 2009b).

$$\varepsilon(\omega) = \frac{\Delta\varepsilon \left(1 + \left(\frac{\omega}{\omega_c} \right)^{1-\alpha} \cdot \sin \left(\frac{\pi}{2} \cdot \alpha \right) \right)}{\left(1 + \left(\frac{\omega}{\omega_c} \right)^{2-2\alpha} + 2 \cdot \left(\frac{\omega}{\omega_c} \right)^{1-\alpha} \cdot \sin \left(\frac{\pi}{2} \cdot \alpha \right) \right)} + \varepsilon_\infty \quad (5.1)$$

$\Delta\varepsilon$ is linearly proportional to the viable cell concentration if the cell volume distribution remains constant. The characteristic frequency ω_c is the frequency at which the measured capacitance is equal to $\Delta\varepsilon/2$. This value is dependent on the cell size distribution of a culture (Carvell and Dowd, 2006b; Davey et al., 1992b) The parameters $\Delta\varepsilon$, ω_c , ε_∞ and α obtained through curve fitting are used in a further set of iterative equations to determine cell radius r and cell number N_v .

To fully characterise the cells, data from a microencapsulated perfusion culture performed in the eRC1 calorimeter was taken. The culture is described in more detail in Chapter 6. The culture had a duration period of 12 days and 11 different cell densities ranging from $0.15 \cdot 10^6$ to $14.5 \cdot 10^6$ $\nu_{\text{cell}} \cdot \text{mL}^{-1}$ were scanned.

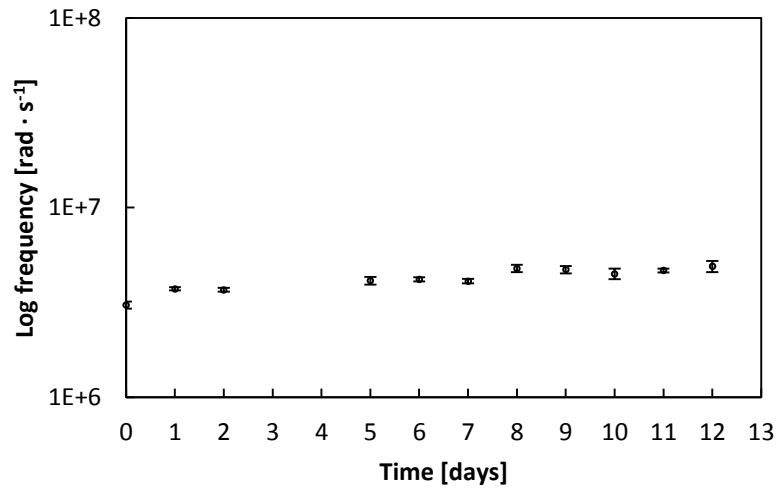


Figure 5.2 Evolution of the characteristic frequency ω_c throughout a 12 day culture (blank circles) and error bars determined at $\Phi=95\%$.

The capacitance measurements made over the 25 pre-set frequencies display a β -dispersion. The Cole-Cole model was successfully defined within the LabVIEW VI and plotted in Figure 5.3 and Figure 5.4. In parallel to the frequency scans, the cell size distribution was determined and compared with microscopic counting.

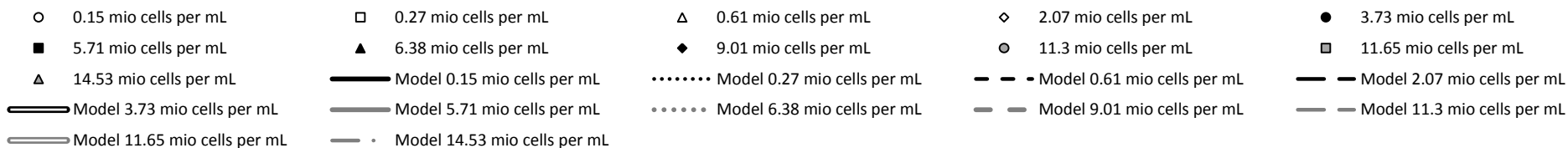
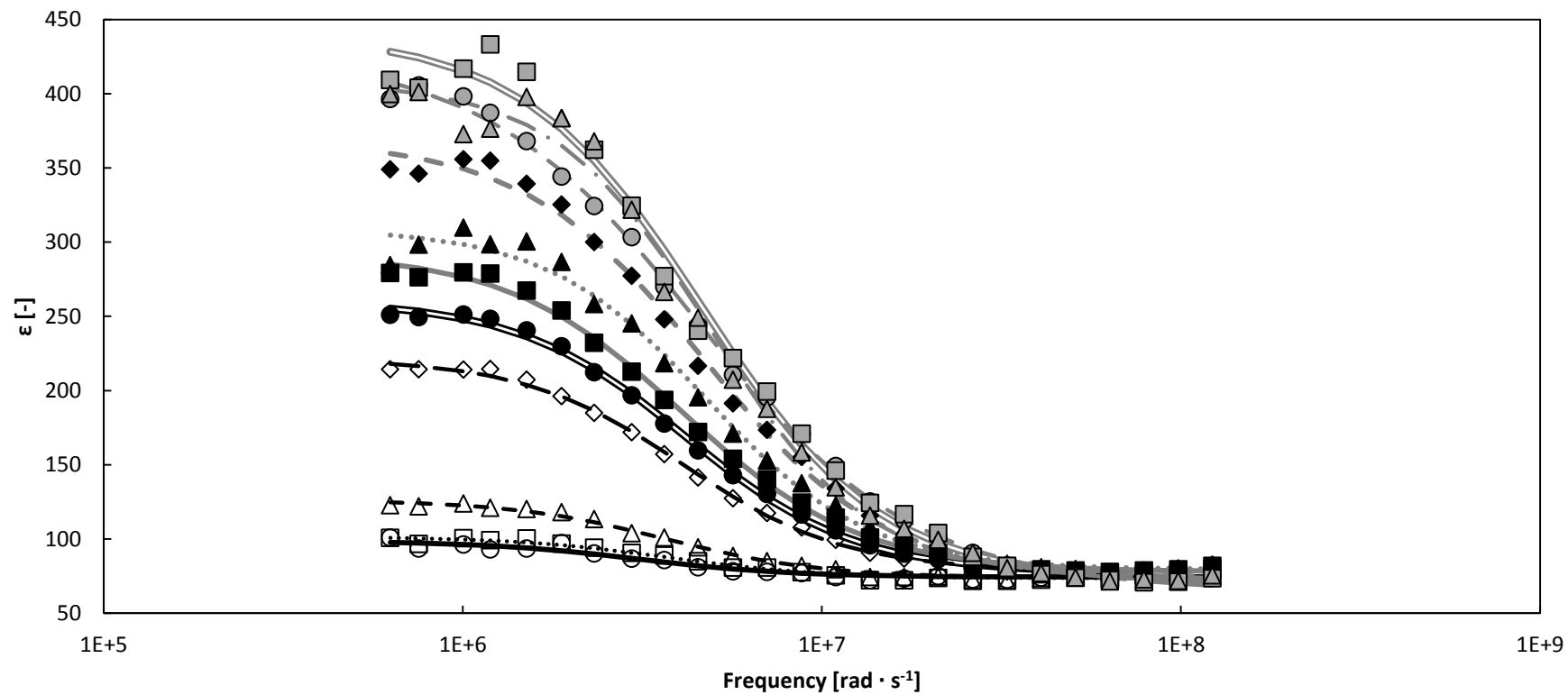


Figure 5.3 Capacitance measurements over the pre-set 25 frequencies performed on different encapsulated cell densities. Each scan was modelled with the Cole-Cole equation and fitted in the LabVIEW VI using the Levenberg-Marquardt algorithm (each density is expressed in (mio) million cells per mL).

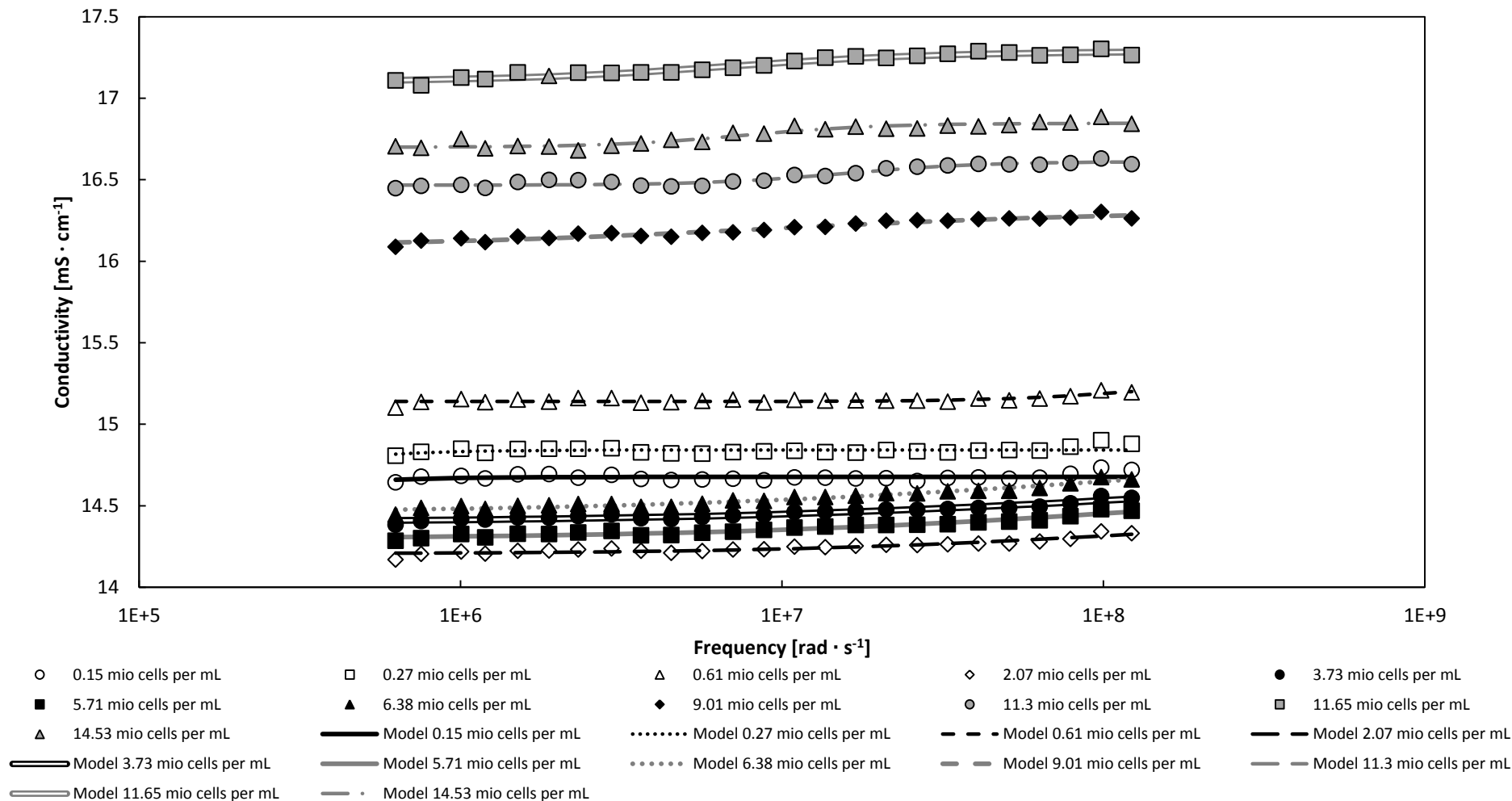


Figure 5.4 Conductivity measurements over the pre-set 25 frequencies performed on different encapsulated cell densities. Each scan was modelled with the adapted Cole-Cole equation and fitted in the LabVIEW VI using the Levenberg-Marquardt algorithm (each density is expressed in (mio) million cells per mL).

As the cell density of the perfusion culture increased, the permittivity difference between high and low frequencies, $\Delta\epsilon$, proportionally increased, as demonstrated in Figure 5.3 and Figure 5.5A. In addition, it can be observed in Figure 5.3 that the permittivity values at high frequencies remained constant throughout the duration of the culture. In contrast, the lowest conductivity values evolved over the culture period, Figure 5.4. The conductivity of the culture increased with the production of waste metabolites such as lactate and NH_4^+ , and with the addition of NaOH to control the pH. A drop in the conductivity values was noticed soon after the perfusion feed was initiated, on day 4, when the cells reached $1.65 \cdot 10^6 \text{ vcells} \cdot \text{mL}^{-1}$. The perfusion feed caused a dilution effect on the lactate and NH_4^+ concentrations, Figure 6.9, and the Na^+ ions and possibly, the structural components of the microcapsules, see Chapter 6.

During the growth phase of the culture (from day 1 to day 12), the cell radius remained constant at $5.8 \pm 0.2 \mu\text{m}$ ($\Phi = 95\%$, standard, $N = 120$), which was confirmed by the stable characteristic frequency ω_c , illustrated in Figure 5.2. This factor of the Cole-Cole equation, which is highly dependent on the cell size distribution, was evaluated at $4.2 \cdot 10^6 \pm 0.3 \cdot 10^6 \text{ rad} \cdot \text{s}^{-1}$ ($\Phi = 95\%$, standard, $N = 11$) throughout the culture.

The parameters and the variables of the Cole-Cole equation and offline VCD and cell radius measurements were then inserted into equations (2.8) and (2.9) to determine the cell membrane surface capacitance C_m and internal conductivity σ_i . These values were evaluated to be at $C_m = 0.02295 \text{ [pF} \cdot \text{cm}^{-2}\text{]}$ and $\sigma_i = 0.6524 \text{ [mS} \cdot \text{cm}^{-1}\text{]}$.

$$\Delta\epsilon = \frac{3N_v \cdot \pi \cdot r^4 \cdot C_m}{\epsilon_0} \quad (5.2)$$

$$\omega_c = \frac{1}{r \cdot C_m \cdot \left(\frac{1}{\sigma_i} + \frac{1}{2\sigma_e} \right)} \quad (5.3)$$

C_m and σ_i values were used in the LabVIEW VI to estimate the number of cells per unit volume and compared to the VCD obtained through the off-line cell counts, Figure 5.5. Since the cell size and viability did not significantly vary throughout the perfusion culture, the $\Delta\epsilon$ and N_v were similarly correlated to the VCD, with a correlation coefficient $R_{\Delta\epsilon} = 0.96$ and $R_{N_v} = 0.98$.

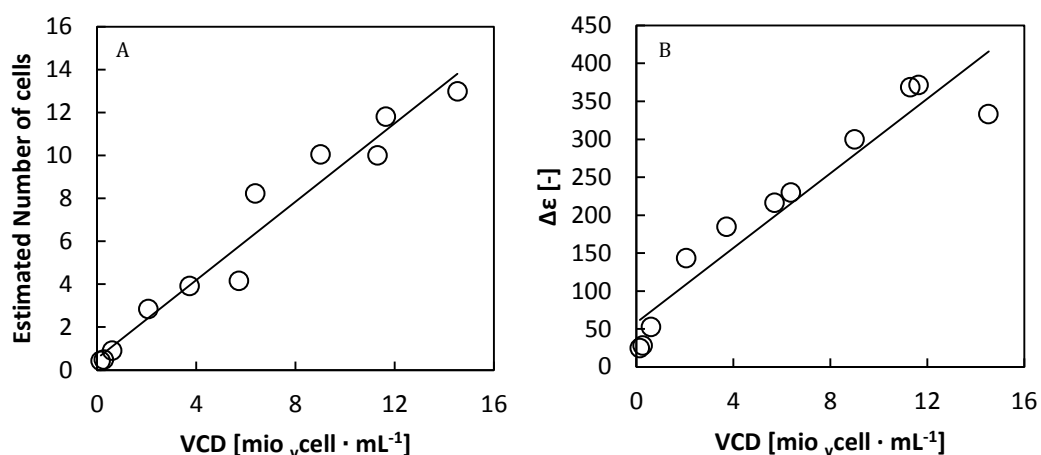


Figure 5.5 Linear correlation between the results of a frequency scan and the offline VCD determination method. A: The number of viable cells per unit volume; B: The permittivity difference $\Delta\epsilon$.

The frequency scans and Cole-Cole modelling were therefore shown to be online methods which could provide accurate information on the viable cell density. However, the method appears not to be accurate at the low cell densities occurring during the first stages of a batch culture. When the culture was inoculated the viable cell density was less than $0.3 \cdot 10^6$ vcells \cdot mL⁻¹. When the cell density is less than $2 \cdot 10^6$ vcells \cdot mL⁻¹, the conductivity measurements between the low and high frequencies are of the order of 0.07 [mS \cdot cm⁻¹]. At these small differences, the scan values are randomly dispersed and fitted by a simple horizontal line Figure 5.4.

5.3.2. Viable cell density and capacitance $C_{580 \text{ kHz}}$ correlation

To use a PAT tool to continuously analyse a process parameter, it must be possible to calibrate the measurements with respect to the process property (Carloni et al., 2009). This work aims to generate and follow the development, in real-time, of high cell density encapsulated cell cultures. It was first necessary to verify the linearity of the relationship between the viable cell density and capacitance measurements, within the lower and upper cell density limits, or in other words in the range of the seeding and expected maximum cell densities.

The biomass monitor offers different frequency settings to continuously assess the capacitance of a culture at a set frequency. The choice of the frequency is made at the frequency that offers the best sensitivity whilst minimising the variations that can be induced by a change in media conductivity, such as the accumulation of metabolic bi-products, base addition, etc. (Carvell and Dowd, 2006b; Noll and Biselli, 1998b). Depending on the cell line and cell radius, the optimal frequency for a CHO cell ranges

between 0.5 and 0.6 MHz. In this work the biomass monitor, was set at 580 kHz ($3.64 \cdot 10^6$ [rad · s⁻¹]) which is slightly below the determined characteristic frequency.

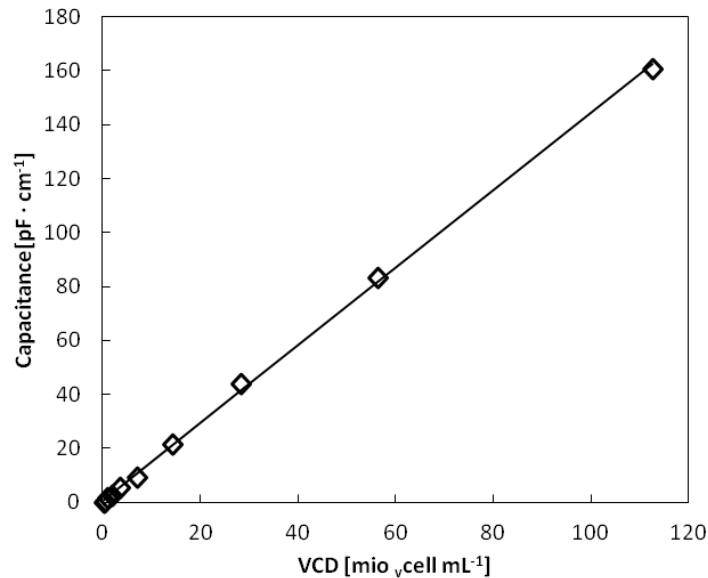


Figure 5.6 Linear correlation between the viable cell density with the capacitance. The correlation coefficient is equal to $R = 0.9996$.

The calibration model was built by measuring the capacitance of ten viable CHO-DP12 suspensions, ranging from $0.2 \cdot 10^6$ to $100 \cdot 10^6$ $v_{cells} \cdot mL^{-1}$. The dielectric signal (and thereby biomass) was set to a zero value using pre-heated media before evaluating the highest cell density suspension. After recording the density of each suspension, the cell suspension was diluted twice with fresh media. The ten data points form a firm linear regression, with a correlation coefficient $R = 0.9996$, Figure 5.6, and Table 5.1.

The calibration model was constructed by measuring the capacitance of one mother cell suspension that was serially diluted using the same pre-heated growth media. The experiment was undertaken within 50 minutes to minimise any possible cellular or suspending media alterations.

The reproducibility of the dielectric measurements can be influenced by the reactor design, the conductivity of the cell culture, the presence of polyelectrolytes in the microcapsules, medium and cell line used (Dabros et al., 2009b). Therefore, calibration models for both suspension and encapsulated cultures were developed Figure 5.7A and Figure 5.7B. Culture samples were removed daily and the viable cells were counted microscopically and compared to the capacitance measurements at 580 kHz. Because the suspension and encapsulated cultures were performed in batch mode, the model was constructed by comparing off-line viable cell counts to the capacitance measurement in the range of $0.3 - 3 \cdot 10^6$ $v_{cells} mL^{-1}$.

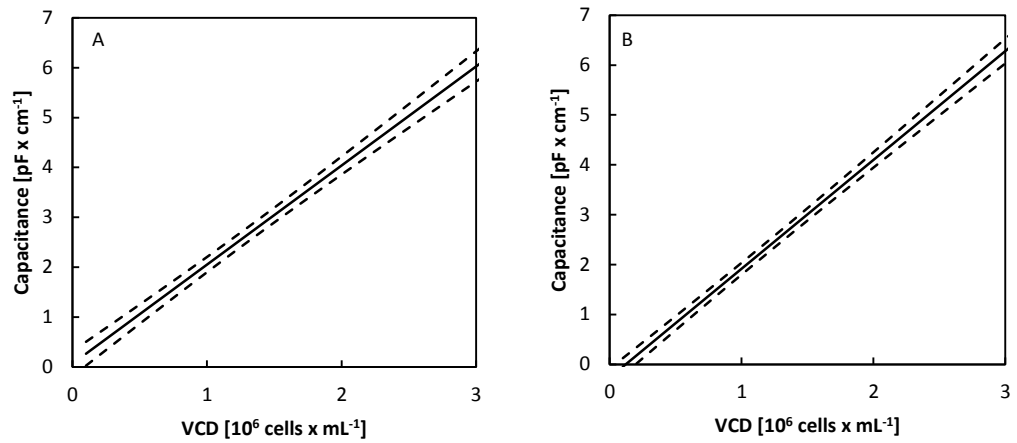


Figure 5.7 Linear regression of on-line capacitance plotted against viable cell density per mL in A: suspension cell cultures; B: in encapsulated cultures (solid line). The area between the dashed lines represents the confidence band ($\phi = 95\%$, $N= 13$ for the suspension cultures and $N= 17$ for encapsulated cultures)

Like the calibration model, the capacitance measurements were shown to be proportional to the viable cell density, for both suspension and encapsulated cultures (Figure 5.7 and Table 5.1). The models were constructed using 13 data points from suspension cultures and 17 from encapsulated cell cultures and show, in both instances, a narrow confidence interval ($\phi=95\%$). The narrow confidence interval suggests that dielectric spectroscopy may indeed be a reliable PAT tool to accurately determine the viable cell density of suspension and encapsulated cell cultures within the tested range. Nevertheless, it is important to note that these calibration models are only applicable as long as the cell size distribution (or the total biovolume), capacitance per surface area C_m and static internal conductivity σ_i remain constant throughout the culture (Opel et al., 2010b).

Table 5.1 Parameters and respective confidence interval ($\alpha=0.05$) for the calibration model ($N=10$), suspension ($N= 13$) and encapsulated cultures ($N=17$) of the linear correlation $y = ax + b$, and correlation coefficient R

Culture type	$a \left[\frac{\text{mL} \cdot \text{pF}}{\text{cells} \cdot \text{cm}} \right]$	$b \left[\frac{\text{pF}}{\text{cm}} \right]$	R [-]
Calibration model	$1.44 \cdot 10^{-6} \pm 2.82 \cdot 10^{-8}$	0.74 ± 1.16	0.9996
Suspension cultures	$1.99 \cdot 10^{-6} \pm 1.99 \cdot 10^{-7}$	$0.066 \pm 3.19 \cdot 10^{-1}$	0.97
Encapsulated cultures	$2.20 \cdot 10^{-6} \pm 1.64 \cdot 10^{-7}$	$-0.26 \pm 2.50 \cdot 10^{-1}$	0.98

As well as showing two linear models, Figure 5.6, Figure 5.7 and Table 5.1 reveal three highly comparable linear correlations which were then used as calibration models to use capacitance data to determine total viable cell density. Indeed the intercept and more importantly the slope (or specific capacitance) of the calibration of the three models indicated in Table 5.1, are of the same order of magnitude. The specific capacitance for the

calibration model ($1.44 \cdot 10^{-6} \text{ pF cm}^{-1} \text{ v}_{\text{cell}}^{-1} \cdot \text{mL}^{-1}$), suspension cultures ($1.99 \cdot 10^{-6} \text{ pF cm}^{-1} \text{ v}_{\text{cell}}^{-1} \cdot \text{mL}^{-1}$) and the determined specific capacitance for the encapsulated cultures ($2.20 \cdot 10^{-6} \text{ pF cm}^{-1} \text{ v}_{\text{cell}}^{-1} \cdot \text{mL}^{-1}$) for the encapsulated cell cultures suggests that the physical proprieties of the cells were similar whether in suspension or entrapped within alginate-poly-L-lysine-alginate microcapsules. The dielectric data is sensitive to the cell size and shape and, as illustrated in Figure 5.11d, the microscopic images of the microcapsules confirm that the cells were spherical in shape.

The limit of detection of encapsulated cells using dielectric spectroscopy was estimated to be $0.26 \cdot 10^6 \text{ cell} \cdot \text{mL}^{-1}$ which is comparable to that reported for CHO cultures elsewhere (Ducommun et al., 2002b; Guan et al., 1998). Both models reported here are in agreement with those reported elsewhere for CHO cell cultures (Ducommun et al., 2002b; Párta et al., n.d.), indicating that the sensitivity of the biomass monitor was not significantly influenced by the presence of the microcapsules and the polyelectrolytes from which they are made.

5.4. The monitoring of batch cultures

Three cell suspension cultures and three encapsulated cultures were carried out in the Minifors bioreactor (Infors HT, Switzerland) using EX-CELL 325 PF culture medium. All cultures were seeded to form a total working volume (WV) of 1200 mL, with an initial cell density of $0.3 \cdot 10^6 \text{ v}_{\text{cells}} \cdot \text{mL}^{-1}$. The culture conditions were monitored and controlled to a set-point of 37 °C and pH 7.2. The pH was controlled by automatic injection of CO₂ to the headspace or by addition of 2M NaOH. Agitation was generated using a marine impeller set at 100 rpm. Air was sparged using mass flow controllers (Books Instrument, USA) into the culture media at 0.005 vvm and the headspace aerated at 0.1 vvm. The viable cell density was monitored using a Biomass monitor (Aber Instruments, UK). The encapsulated cell cultures were prepared following the procedure described in Chapter 3.

The capacitance values were successfully recorded accumulatively in a text file throughout the full culture period. As coded in the created LabVIEW VI, an average of acquired capacitance readings was computed into the estimated viable cell density every 5 minutes, in accordance with the linear calibration model. The data point was then added to the respective time chart, as shown in Figure 5.8. Both on-line and off-line data were in agreement upon the evolution of the viable cell density. The suspension and encapsulated cultures yielded a maximum cell density cell of $3 \cdot 10^6 \text{ v}_{\text{cell}} \text{ mL}^{-1}$. The online data on the other hand gave more comprehensive information, since it was measured continuously. An average data point was saved every 5 minutes, in contrast to the daily off-line cell

counts, executed every 24 hours. By comparison to the 26.8 hour doubling time of the CHO-DP12 cell line used, the 5 minute interval represents only 0.3 % of this doubling time.

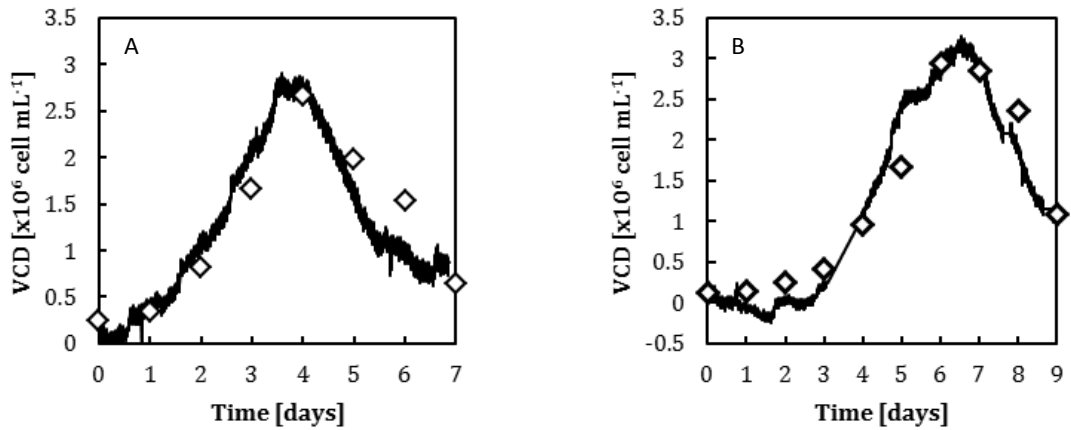


Figure 5.8 Evolution of the viable cell density determined with on-line (—) and off-line (◊) methods for A: cell suspension culture, and B: encapsulated cell culture

The microencapsulated batch cell culture (Figure 5.8B) evolved in a similar way to the suspension culture (Figure 5.8A). The maximum density in the encapsulated culture at the end of the growth phase attained $3.0 \cdot 10^6$ $\text{vcell} \cdot \text{mL}_{\text{WV}}^{-1}$. A short stationary phase was observed between days 6 and 7 followed by a rapid cell death phase, Figure 5.8B.

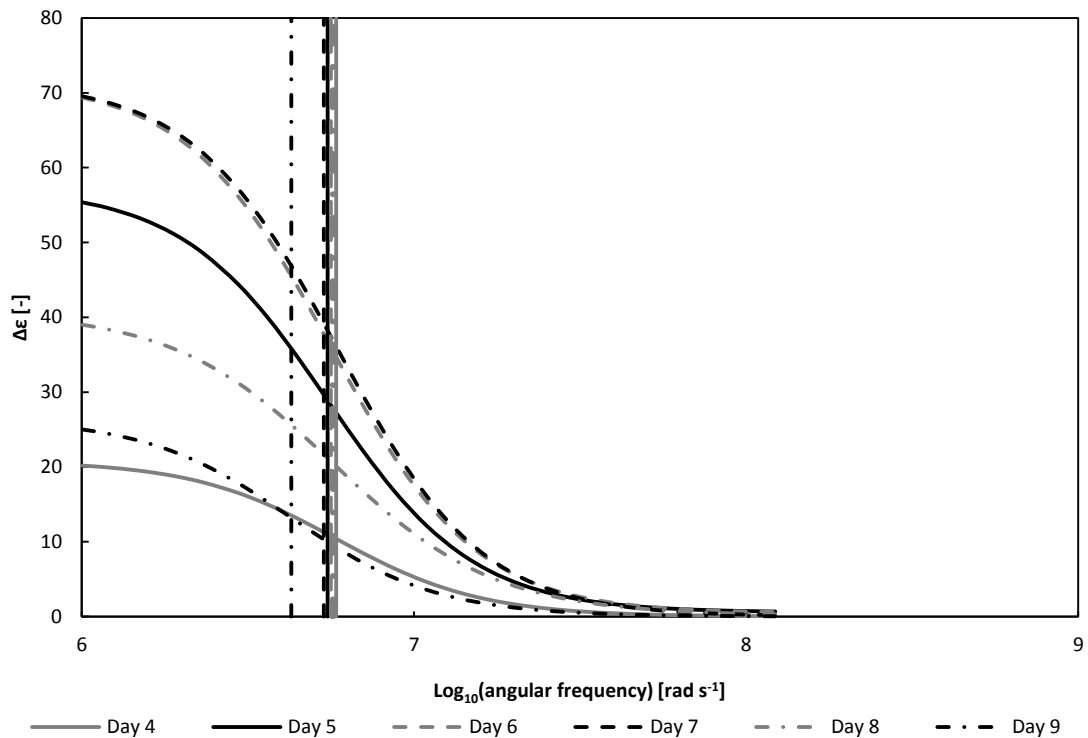


Figure 5.9 Daily frequency scans modelled using the Cole-Cole equation and fitted in LabVIEW VI using the Levenberg-Marquardt algorithm. The vertical lines represent the characteristic angular frequency ω_c

Frequency scans were performed on a daily basis to obtain further information on the growth of the cells at each stage of the cultures. The characteristic frequency ω_c illustrated in Figure 5.9 remained constant throughout the culture until the culture viability was <50%, on day 8. This shows that cell size (or biovolume) remained constant until day 8 and confirms the validity of the model depicted in Figure 5.7 and Table 5.1.

The main difference between encapsulated and suspension cultures appeared to be a slightly lower initial cell density ($0.1 \cdot 10^6 \text{ v}_{\text{cell}} \cdot \text{mL}_{\text{WV}}^{-1}$) accompanied by a lag phase of approximately one day while the cells adapted to growth in the microcapsules. After this period both cultures were observed to grow at similar specific growth rates μ . The growth rates were determined, in both instances, by evaluating the slope of the natural logarithm of the viable cell density plotted against the culture time. From the off-line data μ_{max} was determined to be 0.65 day^{-1} for suspension cultures and 0.64 day^{-1} for encapsulated cultures. These values are very similar to those determined from continuous on-line dielectric measurements (0.60 day^{-1} and 0.65 day^{-1} respectfully). The similarity between the growth rates determined using off-line and on-line methods shows that the dielectric method may be reliably used to determine viable cell density and volume in real-time without the need for culture sampling, dissolution of the microcapsules and laborious off-line cell counting.

Cell viability was dependent on the availability of all substrates. Given the nature of a batch culture, the cells enter death phase when a limiting substrate is depleted or a metabolite accumulates to toxic levels. In this study, glucose and L-glutamine concentrations were measured throughout the culture. It was found in Figure 5.10 that L-glutamine was entirely consumed by day 4 whereas glucose only by day 7. Since growth continued after glutamine depletion, the latter was not considered to be the limiting substrate. However, when glucose was depleted the cells entered a short stationary phase (between day 6 and 7), followed by rapid death phase. In suspension, the cells converted 95 % of the glucose into lactate, whereas the encapsulated cells fermented only 62% of the available glucose, Table 5.2. The ammonia from L-glutamine yield was also reduced by 21% from 0.96 to $0.76 \text{ mmol} \cdot \text{mmol}^{-1}$ when the cells were encapsulated.

These results are in agreement with published data which suggest that when encapsulated, the cells adapt their metabolism to more energetically efficient metabolic pathways, possibly due to a reduction in hydrodynamic stress provided by the protective semi-permeable membrane (Breguet et al., 2007a; Gugerli, 2003b; Verica et al., 2009a).

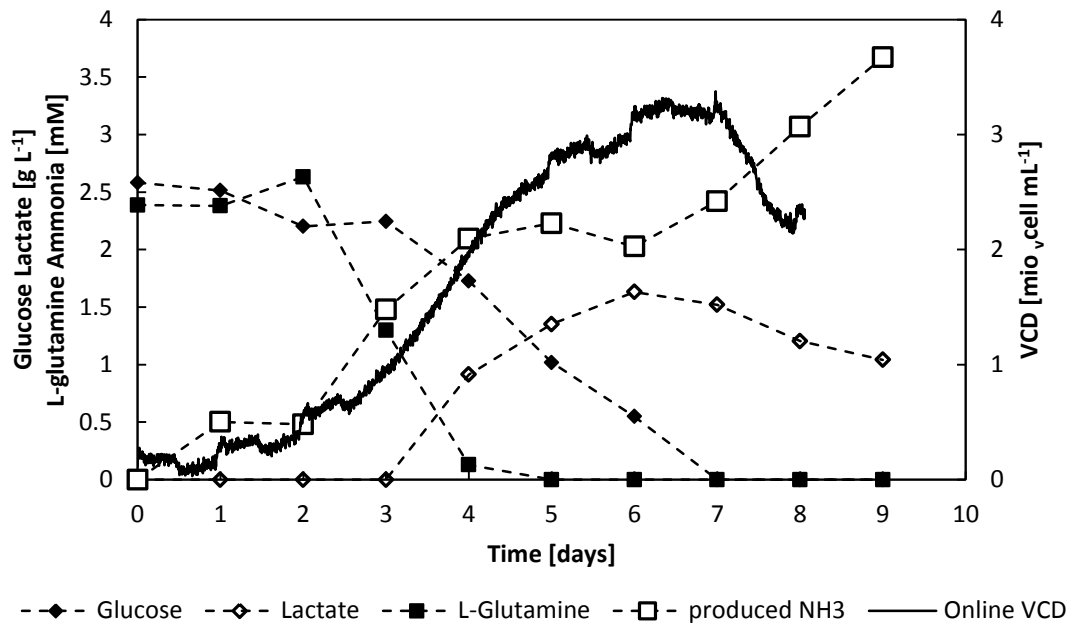


Figure 5.10 Typical evolution of metabolite concentrations during an encapsulated culture. **A:** Glucose and lactate concentrations and viable cell density with respect to the total working volume evolution. Glucose (61.5%) was converted to lactate up until glucose depletion on Day 7. **B:** L-Glutamine and ammonia concentrations. L-glutamine was totally consumed between days 0 and 4. After L-glutamine depletion, the ammonia concentration remained constant until day 7 and then increased once again. The depletion of L-glutamine did not appear to influence cell growth

To evaluate the effect of encapsulation on rIgG₁ production, culture samples were removed from the suspension cultures on a daily basis from day 4 onwards and from day 5 onwards for the encapsulated cultures and the rIgG₁ determined. rIgG₁ was produced at the specific production rate of $3.7 \pm 0.7 \text{ pg} \cdot \text{cell}^{-1} \cdot \text{day}^{-1}$ by suspension cells and of $10.8 \pm 2.9 \text{ pg} \cdot \text{cell}^{-1} \cdot \text{day}^{-1}$ by encapsulated cells representing an increase of 3 fold, Table 5.2. This improved specific productivity has also been observed elsewhere (Breguet et al., 2007a) and once again indicates that a shift in metabolism caused by encapsulation, results in enhanced product formation. To improve the culture protein production further, the viable cell density would have to be increased.

When the APLLA microcapsules were manufactured and transferred into the bioreactor, the cells appeared to be initially homogeneously dispersed within the microcapsules Figure 5.11.a. As the batch culture evolved, the cells appeared to agglomerate and cell clusters began to develop (Figure 5.11. b and c). When the cells reached a maximum total cell density on day 7 the microcapsules did not appear to completely populate the entire core of the microcapsules.

The microcapsules used in this study have a core (available for cell population) radius of $490 \mu\text{m}$ whereas a viable cell was determined to have an average radius of $6.5 \mu\text{m}$. As a result the microcapsules could theoretically be populated by $3.71 \cdot 10^5$ cells per capsule. On Day 7, as portrayed in Figure 5.11. c, the total encapsulated cell density reached a

maximum of $5.19 \cdot 10^3$ cells per capsule, corresponding to only 1.8 % of the theoretical maximum colonisation potential.

Table 5.2 Comparison of the growth kinetics and stoichiometric characteristics between the encapsulated and suspension CHO-DP12 cell cultures

Yield/Rate	Units	Suspension	Encapsulated
μ_{max}	$[day^{-1}]$	0.60	0.64
$Y_{\frac{cells}{gluc}}$	$[v_{cell} \cdot mmol^{-1}]$	$1.51 \cdot 10^8$	$1.91 \cdot 10^8$
$Y_{\frac{cells}{gln}}$	$[v_{cell} \cdot mmol^{-1}]$	$8.48 \cdot 10^8$	$8.53 \cdot 10^8$
$Y_{\frac{Lac}{glc}}$	$[mmol \cdot mmol^{-1}]$	1.90	1.23
$Y_{\frac{NH_3}{gln}}$	$[mmol \cdot mmol^{-1}]$	0.96	0.76
q_{gluc}	$[mmol \cdot v_{cell}^{-1} \cdot day^{-1}]$	$4.03 \cdot 10^{-9}$	$3.36 \cdot 10^{-9}$
q_{gln}	$[mmol \cdot v_{cell}^{-1} \cdot day^{-1}]$	$7.16 \cdot 10^{-10}$	$7.53 \cdot 10^{-10}$
q_{lac}	$[mmol \cdot v_{cell}^{-1} \cdot day^{-1}]$	$7.64 \cdot 10^{-9}$	$4.13 \cdot 10^{-9}$
q_{NH_3}	$[mmol \cdot v_{cell}^{-1} \cdot day^{-1}]$	$6.89 \cdot 10^{-10}$	$5.79 \cdot 10^{-10}$
q_{IGG}	$[pg \cdot v_{cell}^{-1} \cdot day^{-1}]$	3.74	10.76
Max VCD	$[v_{cell}^{-1} \cdot mL^{-1}]$	$2.9 \cdot 10^6$	$*2.8 \cdot 10^6$

* Only Intra-capsular cells are considered

The total number of cells is influenced by substrate and oxygen availability, as well as the volume within the microcapsules available for growth. The latter can be influenced by changing the size of the microcapsules and/or by changing the proportion of microcapsules in the reactor. In the present study the microcapsule volume represented 25% (300 mL) of the culture volume (1200 mL), the total number of cells per microcapsule can be increased simply by reducing the number of capsules in the reactor however, this should have little or no effect on the cell density in the reactor. In order to increase the latter it would be necessary to supply a medium feed to the reactor in the form of fed-batch or perfusion operation.

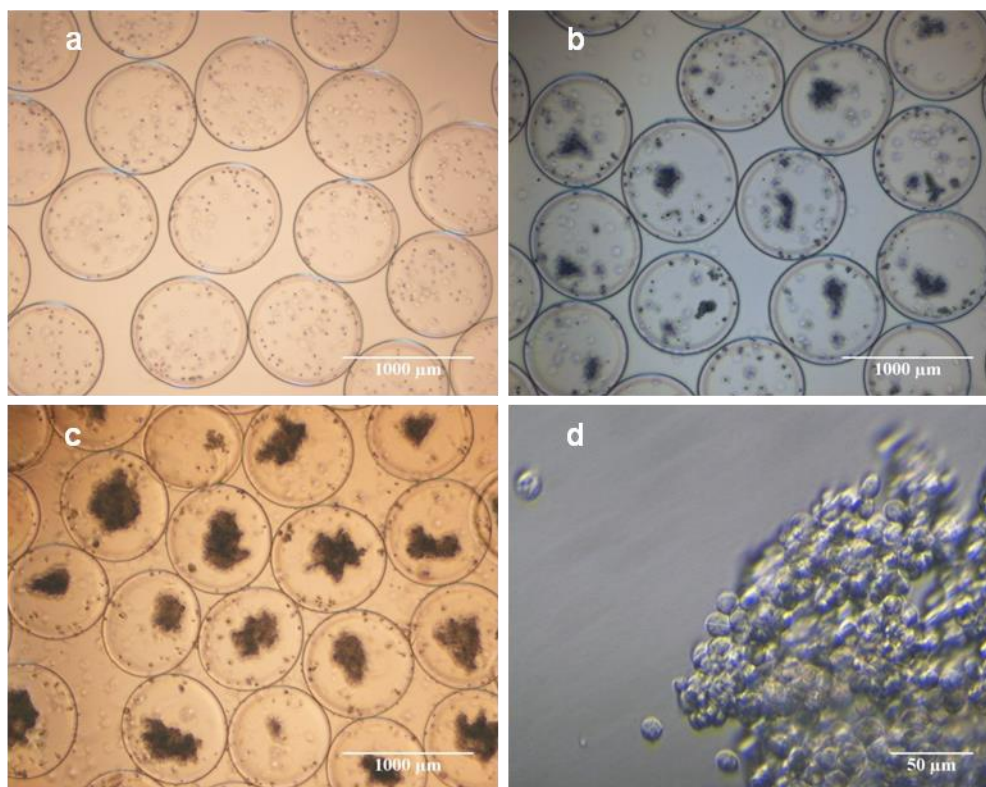


Figure 5.11 Cell growth evolution within microcapsules; a: Day 0: cells were homogeneously dispersed (magnification 40X); b: Day 3, small colonies start to form (magnification 40X); c: Day 7, the average capsule colonisation reached 1.8 % of the total theoretical colonization potential (magnification 40X); d: Day 7, magnification 400 x showed cells forming close contacts with one another to create aggregates

5.5. Outcome and conclusion

Dielectric spectroscopy was shown to be a reliable method to accurately follow cell growth and viability within microcapsules. This method offers the possibility to monitor continuously, on-line with an accurate, linear and fast response. The continuous capacitance measurements were linearly proportional to the viable cell biovolume. The linear regression analysis revealed a narrow confidence interval making dielectric spectroscopy a precise method to monitoring cell growth and viability. In addition, the developed model for the encapsulated cultures was validated by daily frequency scans. Indeed, the characteristic frequency, a cell size dependant parameter, remained constant until the viability dropped below 50%. The limit of detection and limits of quantification of viable encapsulated cell density were comparable to the viable cell density of suspension cultures, showing that the materials of construction of the microcapsules together with the formation of cell aggregates had no effect on the capacitance measurements and proportionality.

The membrane capacitance and the internal conductivity of the CHO-DP12 cells were determined to be $C_m = 0.02295$ [pF · cm⁻²] and $\sigma_i = 0.6524$ [mS · cm⁻¹]. The specific cellular characteristics were obtained by modelling the frequency scans with the Cole-Cole

model. The LabVIEWVI received the capacitance and conductivity and effectively fit the equation within the capacitance values of all measured cell densities and the conductivity readings above $2 \cdot 10^6 \text{ }_{\text{vcell}} \cdot \text{mL}^{-1}$.

Though the capacitance was linearly correlated to the viable cell density, within the $0.2 - 100 \cdot 10^6 \text{ }_{\text{vcell}} \cdot \text{mL}^{-1}$ range, providing the cell volume did not vary, only 1.8 % of the total microcapsules core was colonised. The batch culture cell growth appeared to be inhibited by the complete uptake of glucose. These batch cultures were primarily a stepping stone to show the potential of dielectric spectroscopy to follow growth and viability, before optimising the cultures and microcapsule colonisation.

Based on the results of the batch cultures, it is suggested to use dielectric spectroscopy to monitor the growth of the cells whilst providing a nutrient feed to avoid nutrient depletion and to control medium feed rates in fed-batch and/ or perfusion cultures, in which case 90-100% colonisation should be achievable, resulting in cell densities greater than $10^8 \text{ }_{\text{vcell}} \cdot \text{mL}^{-1}_{\text{wv}}$.

Dielectric spectroscopy monitors one physical aspect of the cell population in a culture. A cell can only act as a microcapacitor if the cell membrane is not ruptured. Yet, it provides no information on the biochemical composition of a culture, or the cell metabolic activity. For this reason it is also necessary to complement the monitoring method with an orthogonal one such as FTIR spectroscopy or biocalorimetry.

Chapter 6 Application of biocalorimetry combined with dielectric spectroscopy for the monitoring of microencapsulated CHO perfusion cultures

Summary: The purpose of this study was to introduce biocalorimetry as a monitoring method combined with dielectric spectroscopy to follow cell development in microencapsulated bench-scale perfusion cultures. A feasibility study was first undertaken where a 25% v/v microencapsulated perfusion culture would reach a maximum cell density of $139 \cdot 10^6 \text{ } \nu\text{cells} \cdot \text{mL}_{\text{WV}}^{-1}$. Based on the specific heat flow rate of $20 \text{ pW} \cdot \text{cell}^{-1}$, such perfusion cultures of 1.4 L culture could generate heat fluxes above $10 \text{ W} \cdot \text{L}^{-1}$, a value which is 200-fold higher than the eRC1 (reaction calorimeter) heat signal resolution. The method validation showed that the method has a limit of detection greater than $8.86 \cdot 10^6 \text{ } \nu\text{cells} \cdot \text{mL}_{\text{WV}}^{-1}$ and could only provide accurate and precise viable cell quantification when the cell densities exceed $26.88 \cdot 10^6 \text{ } \nu\text{cell} \cdot \text{mL}_{\text{WV}}^{-1}$. An encapsulated perfusion culture, monitored by biocalorimetry combined with dielectric spectroscopy, achieved a maximum cell density of $15 \cdot 10^6 \text{ } \nu\text{cell} \cdot \text{mL}_{\text{WV}}^{-1}$. The correlation between viable cell density measurement, determined using off-line microscopy analysis, and continuous capacitance readings was very good. The heat flux signal provides accurate information after day 5 of the culture, when the cell density is greater than $4 \cdot 10^6 \text{ } \nu\text{cell} \cdot \text{mL}_{\text{WV}}^{-1}$. The calorimetry signal indicated a reduction in the growth rate after day 10 with a stabilisation in the signal. However, further advances in microcapsule stability in perfusion culture are necessary, since a high level of cell loss was caused by microcapsules rupturing followed by a wash-out of the released cells.

Keywords: Biocalorimetry, Dielectric spectroscopy, Perfusion culture, High cell density cultures, Method validation

¹Sections of this chapter have been published in Processes: Cole HE, Demont A and Marison IW-The Application of Dielectric Spectroscopy and Biocalorimetry for the Monitoring of Biomass in Immobilized Mammalian Cell Cultures

6.1. Introduction

Batch cultures are usually limited by the depletion of the limiting substrate. Though batch and fed-batch cultures are traditionally preferred culture modes, perfusions cultures are gaining importance for the commercial production of recombinant therapeutics (Ozturk and Kompala, 2005b). In 2003, 8 commercially available products were manufactured using perfusion systems, with this number increasing to 12 recombinant therapeutics, according to an article published in January 2013 (Pollock et al., 2013).

Perfusion cultures involve continuously supplying the culture with fresh culture media whilst continuously removing the spent media at an identical rate, ensuring the working volume remains constant. This culture type has the advantage to obtain high cell densities whilst continuously supplying the cells with all the essential nutrients and removing the waste by-products. The cells are retained within the reactor by a cell separating device such as a spin filter, a cross flow filter, hydrocyclones or acoustic cell settlers, Figure 6.1A.

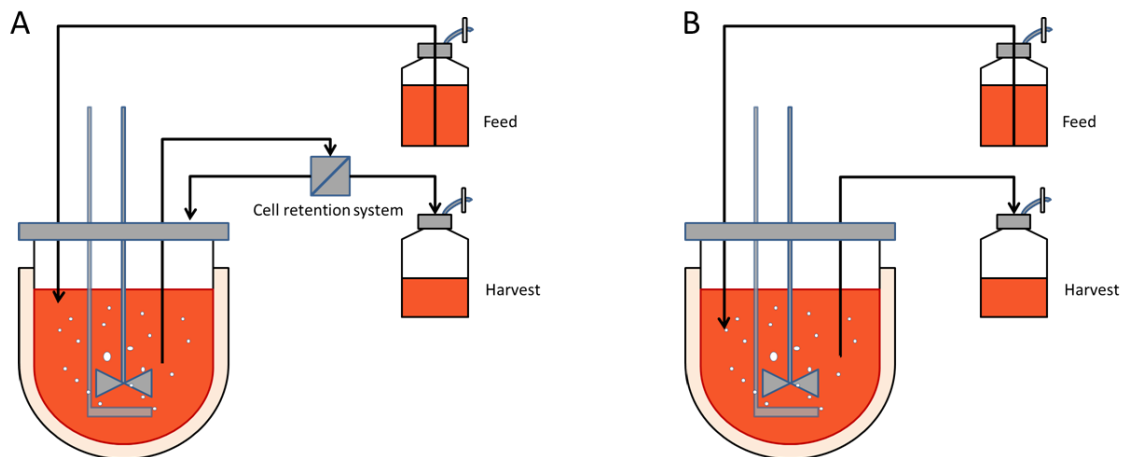


Figure 6.1. Diagram of a perfusion culture setup. (A) Schematic representation of a perfusion culture for suspension cells in a stirred tank reactor. A cell retention system, such as a microfilter, is necessary to separate the cells from spent media. (B) Schematic representation of a perfusion culture for immobilized cells. The microcarriers or microcapsules are sufficiently large to be retained within the vessel by a wire mesh

Perfusion cultures represent other advantages in comparison to batch or fed-batch cultures. First, the downtime period is a much smaller portion of the overall production cycle. It has been reported that perfusion cultures can last up to 220 days, depending on the used cell retention system (Ozturk and Kompala, 2005b; Voisard et al., 2003), in contrast to 1-15 days encountered in batch and fed-batch modes. Secondly, mammalian cells, by contrast to bacterial cells, have a long doubling time. It is therefore more efficient to retain the biomass and reach high cell densities than to build-up the required biomass in repeated batches to manufacture commercial amounts of the target product (Ozturk and Kompala, 2005b). Another advantage that is offered by perfusion cultures would be continuous product removal. Mammalian cells secrete the recombinant protein into the

medium. Some products are labile and after long periods of time degrade. Perfusion cultures allow the continuous harvest of the target protein, but also to manufacture the protein in a steady state environment, which consequently maintain the glycosylation profile and quality consistent (Yang et al., 2014)

Nevertheless, cell separators represent an added cost, can gradually foul or are difficult to scale- up. On the other hand microencapsulated cultures do not require sophisticated equipment to retain the cells within the vessel. A simple mesh is sufficient to extract the spent media as represented in Figure 6.1B, (Breguet et al., 2007b).

This chapter seeks to fully colonise the microcapsules using a perfusion feed, whilst monitoring the cell physiology using dielectric spectroscopy in combination with monitoring the cell metabolic activity. First, based on the kinetics presented in chapter 5, and microcapsule and cell measurements, the culture time and maximum viable cells are predicted. The predicted cell density evolution is computed into both capacitance and heat flow rates. Next, a feasibility study to use the eRC1(Mettler Toledo, USA), a bench scale calorimeter to follow the cells' metabolic activity was undertaken. Then the method was validated using the results from the perfusion cultures performed in the eRC1. The reactor was inoculated following the methods presented in Chapter 3, and the cells were then fed at a constant rate as described below in subsection 6.5.1.

Table 6.1 Equations used to evaluate the evolution of the biomass to substrate and product to biomass yields from day to day depending on the perfusion culture stage Nomenclature: $Y_{X/S}$ = Biomass to substrate yield, $Y_{P/X}$ = Product to biomass yield, X viable cell density, S = substrate concentration culture, S_f = substrate concentration in the feed, P = product concentration, D = Dilution rate, μ = growth rate, and t = time

Batch phase	Perfusion phase non-steady-state	Perfusion phase steady-state
$Y_{X/S} = \frac{\Delta X}{\Delta S}$ (6.1)	$Y_{X/S} = \frac{(1 - e^{-Dt}) \cdot X(t) \cdot \frac{\mu_{max}}{D} - (X(t) - X_0) \cdot e^{-Dt}}{S(t) - S_f}$ (6.2)	$Y_{X/S} = \frac{\mu X}{D(S_f - S(t))}$ (6.3)
$Y_{P/X} = \frac{\Delta P}{\Delta X}$ (6.4)	$Y_{P/X} = \frac{P(t)}{(1 - e^{-Dt}) \cdot X(t) \cdot \frac{\mu_{max}}{D} - (X(t) - X_0) \cdot e^{-Dt}}$ (6.5)	$Y_{P/X} = \frac{DP}{\mu X}$ (6.6)

The online capacitance and heat flow rates are compared to the offline viable cell density determined by microscopy. Additionally, changes in the CHO-DP12 cell metabolism, if any, was examined by calculating the yields and kinetics and compared with the calorimetric signal. The perfusion culture was divided into three phases: batch phase, perfusion non-steady state, which is the microcapsule packing stage and perfusion at steady state, being the cell maintenance phase. The kinetic study applied the equations (6.1) to (6.6) presented in Table 6.1, according to the culture phase (Hernández et al., 2009).

It is the first time, to my knowledge, that CHO cell cultures are monitored using bench-scale calorimeter in combination to dielectric spectroscopy. Though this work was only done at bench scale, it also shows the potential of the monitoring method to be used at larger scale, such as in industrial production processes.

6.2. Culture predictions and applicability of bench scale biocalorimetry

In chapter 5, microencapsulated batch cultures demonstrated that the cells developed well, but populated only 1.8 % of the microcapsule internal core. The online dielectric monitoring and the offline results suggest that the cell growth and viability were not restricted by the available space, but inhibited by the exhaustion of glucose in the medium.

For microcapsule stability optimisation, and for nutrient distribution to the cells, the cell/alginate suspension was extruded using a 200 μm \emptyset nozzle. As a result, the average microcapsule radius is reduced from 490 to 260 μm . The membrane thickness of the microcapsule, is measured to be 18 μm by confocal microscopy, Figure 6.2, and thus the average internal volume represents $4.71 \cdot 10^7 \mu\text{m}^3$. The cell volume being $115 \mu\text{m}^3$, (radius = 6.5 μm), would entail the microcapsules having a maximum colonisation potential of $6.40 \cdot 10^4 \text{ cells} \cdot \text{capsule}^{-1}$.

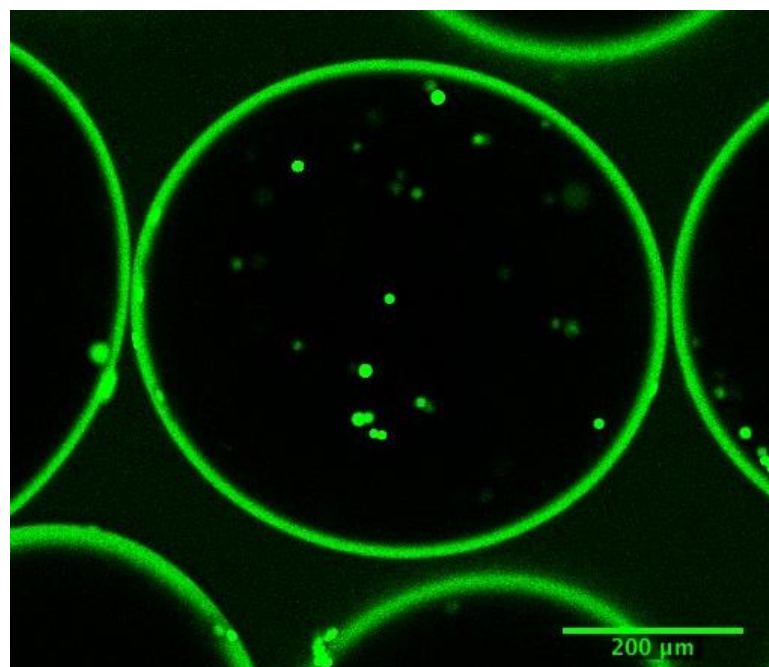


Figure 6.2 Confocal image of calcium-alginate poly-L-lysine-alginate microcapsules and membranes, on Day 0, immediately after inoculation. The average microcapsule radius is 260 μm and the membrane, 18 μm . The stained cells fluoresce green if viable, or red if dead.

The work involved monitoring microencapsulated cell densities in approximately 25 % (v/v) microcapsule cultures. Therefore, a culture, without any inhibitory factors, would be expected to generate cell densities up to $139 \cdot 10^6 \text{ cells} \cdot \text{mL}_{\text{WV}}^{-1}$. Providing the cells

grow constantly at 0.62 days^{-1} , without a lag phase, the full microcapsules' core colonisation should be achieved after 11.3 days. Based on the specific capacitance found previously in chapter 5, such densities would have a capacitance reading of $200.1 \text{ pF} \cdot \text{cm}^{-1}$, as illustrated in Figure 6.3 A. It is expected that once the maximum cell density is achieved, and the metabolites are present in suitable concentrations, that the capacitance would remain stable (Guan et al., 1998).

In addition to the continuous capacitance readings, the heat produced by the cells will be monitored by the eRC1 calorimeter. In the literature, it has been reported that mammalian cells produce very little heat in contrast to microbial cells (García-Payo et al., 2002; Maskow and Paufler, n.d.). More specifically, the specific heat flow rate of the CHO 320 cell line was evaluated at its peak at 20 pW cell^{-1} (Guan et al., 1998). Consequently, it is expected that the heat flow rate would increase at the same rate as the cells up to $2.8 \text{ W} \cdot \text{L}^{-1}$. Once the cells have no longer any free space to replicate, the cell growth should become inhibited. As the heat flow rate is dependent upon the growth rate, it is forecast for the heat signal to fall and stabilise at inferior lower heat flow rate, Figure 6.3 B, (Schuler et al., 2012; Sivaprakasam et al., 2007).

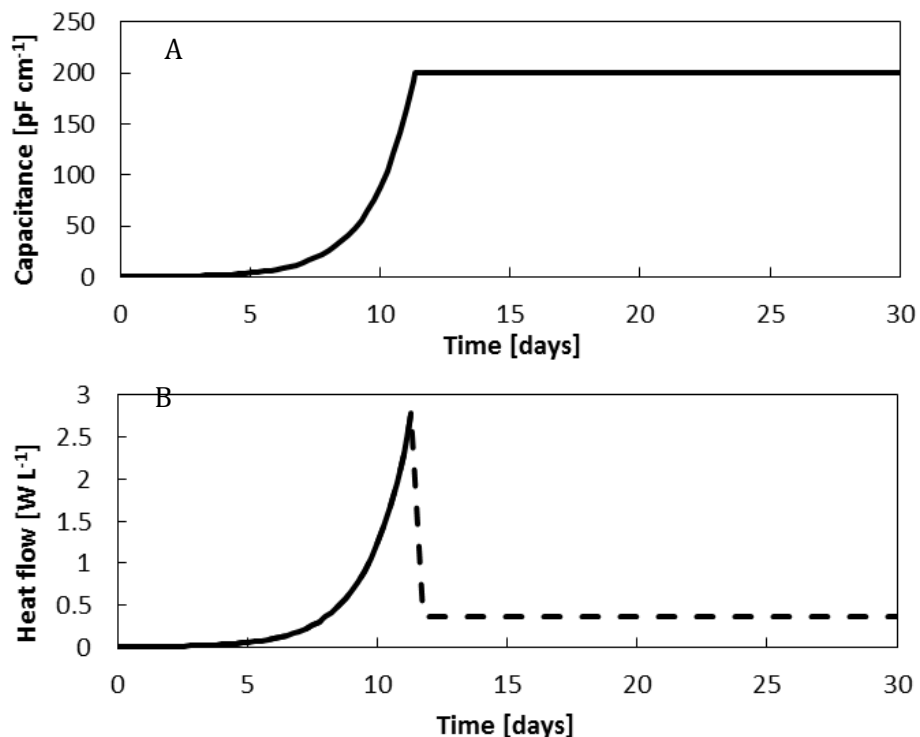


Figure 6.3 Capacitance (A) and heat flow (B) predictions throughout the exponential phase, assuming the cells duplicate at the maximum growth rate $\mu_{\max} = 0.64 \text{ day}^{-1}$, and the stationary phase, when the full microcapsule colonisation potential is achieved.

The eRC1 calorimeter, used during this work, has a resolution reported resolution of $50 \text{ mW} \cdot \text{L}^{-1}$. This means that, for a 1.4 L CHO culture, the Limit of blank (LOB), or the maximum cell density that was still considered as a blank sample, could not exceed $3.5 \cdot 10^6 \text{ cell} \cdot \text{mL}^{-1}$. The lowest measurable cell density, or the Limit of detection (LOD)

was estimated at approximately $11.6 \cdot 10^6 \text{ }_{\text{cell}} \cdot \text{mL}^{-1}$. Therefore, the monitoring method is not sufficiently sensitive to monitor batch cultures. However, biocalorimetry has a promising potential to monitor the biomass development stage of microencapsulated CHO cell perfusion cultures that are projected to exceed these densities.

6.3. eRC1 installation for perfusion culture operation

Perfusion cultures involve feeding cells at the same rate as removing the spent medium whilst retaining all, or a portion, of the cells within the culture. In addition to the dielectric, pH and eRC1 calorimeter probes, air inlets and outlet, sampling and base control ports, a feed inlet and outlet were connected. To the feed outlet, a tube long enough to permit the spent media removal, with an attached 200 μm pore size wire mesh, was inserted. Because the microcapsules are approximately 480 μm large, only extra-capsular cells and microcapsule debris would be washed out.

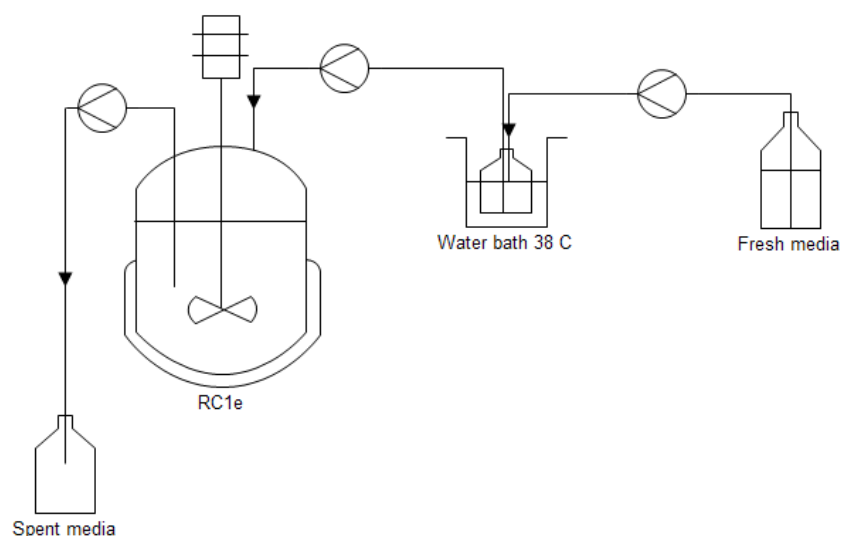


Figure 6.4 Perfusion culture equipment setup. The fresh media is pumped to a smaller bottle to preheat the feed before being supplied to the cells. At the same rate, spent medium is removed and collected in a third bottle. It must be noted that the set-up only has one peristaltic pump.

The fresh feed bottle is placed on a balance (Mettler Toledo, USA), and the mass of added feed is acquired in the LabVIEW VI. The medium is pumped into a smaller 200 mL hermetically sealed Duran® bottle. This bottle is placed into a 38 °C water bath to reduce the temperature difference between that of the reactor and of the feed, Figure 6.4. To ensure the reactor volume remains constantly at 1400 mL, and therefore, that all feed and spent media flows are identical, one multichannel IPC peristaltic pump (ISMATEC, Germany) was used. The feed balance is then connected to the NI-9870 hardware module and the data was acquired within the designed LabVIEW VI. This offered the possibility to verify in real-time the feed rate from the feed bottle to the pre-heating bottle, from the

pre-heating bottle to the reactor and from the reactor to the waste collection bottle, Figure 6.4. The perfusion feed was manually initiated when the cells reached the desired density and the culture perfused continuously at a constant rate, see section 6.5.1.

6.4. Validation of biocalorimetry as monitoring method

The eRC1 calorimeter is operated in isothermal mode to maintain the temperature of the cell suspension constant throughout the culture time. To ensure the reactor remains at the set-point, the calorimeter adapts the temperature of the silicone oil that flows throughout the vessel jacket at a rate of $2 \text{ L} \cdot \text{s}^{-1}$. As the culture of an exothermic strain progresses, the heat of reaction increases, requiring a reduction in the jacket's temperature (Marison et al., 1998).

In addition to the heat of reaction q_r influencing the suspension temperature, other factors are to be taken into account (Voisard et al., 2002a). The accumulated heat in the reactor q_{acr} is dependent upon q_s the heat induced by stirring, q_g which includes the sensible heat lost to the gas stream and a heat loss due to evaporation, q_e the heat loss to the environment, q_f the heat flow caused by addition of a substrate or medium to the culture, q_a the addition and dissolution of either an acid and/or a base for the maintenance of a constant pH, q_{CO_2} the heat flow caused by CO_2 evaporation and q_c the heat emitted by the calibration heater. The heat flow q_j of the jacket and the accumulated heat within the jacket are important factors and play an important role in controlling the vessel temperature, equation (6.7).

$$q_{acr} = q_r - q_j + q_s - q_g - q_e - q_f - q_a - q_{CO_2} + q_c - q_{acj} \quad (6.7)$$

Because the bench scale calorimeter was to be used for monitoring mammalian cell metabolic activity, all the heat flows other than the heat of reaction, must be as constant as possible, or otherwise punctual. Subsequently, the heat of reaction can be determined subtracting the baseline heat q_b as described in equation (6.8).

$$q_r = q_{acr} - q_b = U_A \cdot (T_r - T_j) - U_{A,b} \cdot (T_{r,b} - T_{j,b}) \quad (6.8)$$

6.4.1. Signal resolution

The heat flow baseline was analysed by inserting all the probes in the correct ports, and having all the sampling and feed inlet and outlet ports connected, in the same configuration as if undertaking a culture. Probes and ports are heat bridges and facilitate heat loss (García-Payo et al., 2002). Axial mixing was ensured using a pitched blade disc turbine impeller at 100 rpm. Aeration of the headspace was set at 0.1 vvm and was sparged in parallel at 0.01 vvm using a mass flow controller (Brooks instruments, UK).

Unlike the Minifors bioreactor setup, the pH was maintained at 7.2 by a continuous CO₂ headspace enrichment initially set at 5 %. As the culture pH stabilises and requires less acidification of the suspension, the enrichment was reduced manually, step-wise, and then switched off, to avoid unnecessary supplementation of NaOH 2M. The alkali addition to maintain the pH at 7.2, was executed by the pH controller (Bioengineering, Switzerland). As it was desired to have punctual base addition, the controller was fixed at pH = 7.2 ± 0.2, T_{ON}/T_{OFF} potentiometers, controlling opening or closing times are set to obtain punctual addition, that would translate to a peak in the signal. The reactor was filled with 1400 mL deionised water, the temperature of the reactor was fixed to 37 °C.

At this scale, the surface area to volume ratio is high, meaning the heat loss to the environment is significantly important. The heat loss to the environment is dependent upon the ambient temperature, as demonstrated by the heat loss to the environment balance, Equation (6.9). If the temperature of the environment fluctuates, the temperature of the jacket needs to respond accordingly to maintain the temperature of the reactor constant (Janssen et al., 2005; Schubert et al., 2007; Voisard et al., 2002a). Therefore, to avoid fluctuations in the baseline signal, the thermostat of the laboratory was kept constant, throughout the different experiments. The calorimeter was allowed to run for a period of three days, as illustrated in Figure 6.5.

$$q_e = U_e \cdot A_E \cdot (T_r - T_{amb}) \quad (6.9)$$

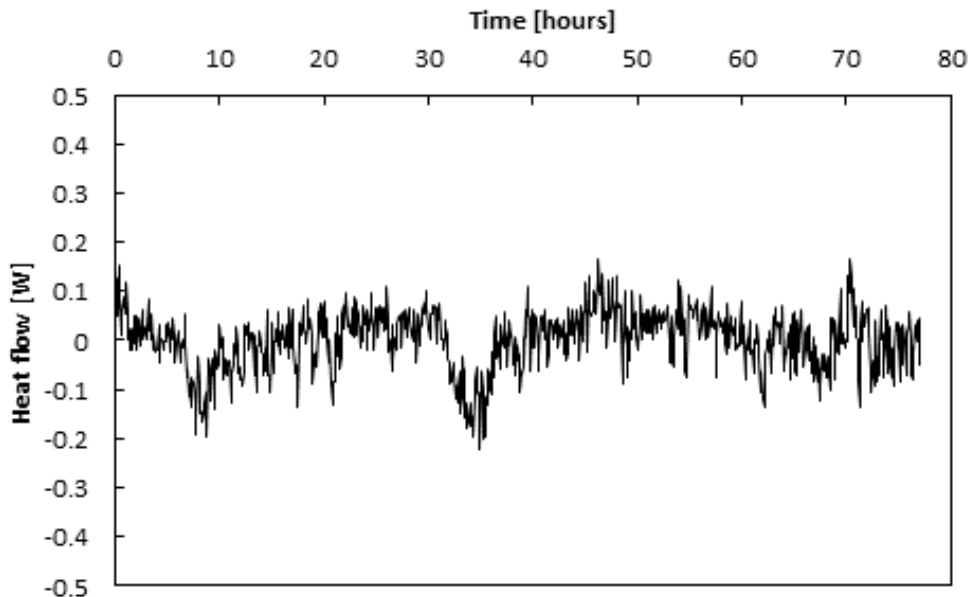


Figure 6.5 Heat flow baseline measurements over a three day period. The standard deviation is evaluated at 0.061 W.

A total of 925 data points were recorded over 3.2 days. The standard deviation was evaluated at 0.061 W, or 43.3 W · L⁻¹ and is comparable to the reported calorimeter resolution, (Marison et al., 1998). The heat transfer coefficient U_A was determined

automatically using the iControl software heat calibration function prior to start the baseline analysis. (Mettler Toledo, USA). This value was found to be to $U_A = 6.57 \text{ W} \cdot \text{K}^{-1}$.

6.4.2. Influence of the feed on the signal

According to equation (6.7), the heat flow measured during a culture is likely to alter with the feed rate, (Voisard et al., 2002b). To check the influence of the feed rate and possible relationship with the heat flow rate, and ulteriorly the stability of the perfusion system described above in Section 6.3, the feed bottles were filled with deionised water, connected as demonstrated in Figure 6.4, and different rates were tested. For each evaluated feed rate, at least 220 data points were acquired within the LabVIEW VI.

Six different rates were tested, whilst keeping all the other settings identical throughout the whole experiment. The assessed feed rate ranges were selected between the lowest pump speed setting and the highest feasible rate with the available laboratory equipment.

It was found that the feed rate reduced the measured heat flow rate. With the current setup, the calorimeter had to compensate a heat reduction, caused by the inflow of feed, by increasing the jacket temperature. To be more specific, the average heat flow, within the tested range and equipment installation, is linearly correlated to the feed rate, as depicted in Figure 6.6. The correlation coefficient is equal to $R = -0.995$, and relationship between the two rates is characterised by the linear regression slope $a = -0.438 \text{ W} \cdot \text{mL} \cdot \text{day}^{-1}$. Though it was planned to feed at a steady rate, these findings may become relevant when designing a controlled feed rate, based upon the cell nutrient requirements.

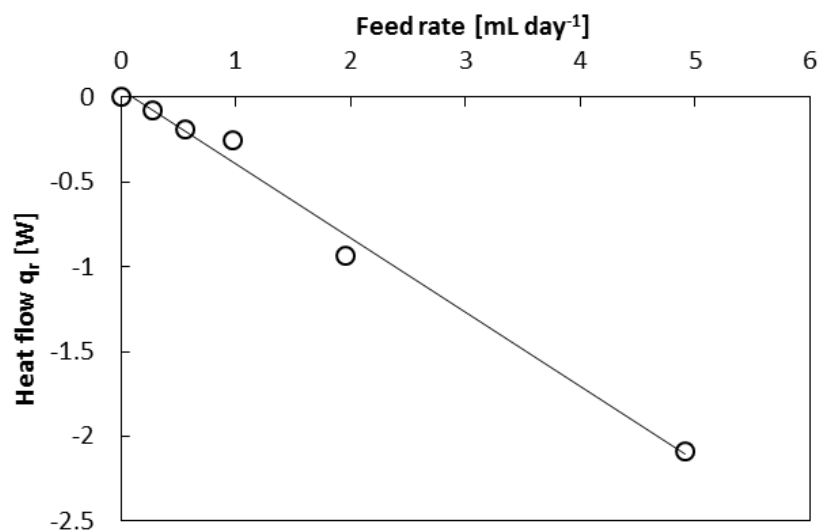


Figure 6.6 Linear relationship between the measured heat flow rate and the tested feed rates ranging from 0.276 to 5 L·day⁻¹

Moreover, the standard deviation, did not seem to significantly vary with the different feed rates (average standard deviation = ± 0.054 W). The outcome of the experiment shows that the feed rate will shift the baseline, once the feed is initiated, but should not have a negative impact upon the monitoring method sensitivity.

6.4.3. Method validation for CHO cell cultures

In section 6.2, the LOB and LOD were estimated at $3.5 \cdot 10^6$ $v_{\text{cell}} \cdot \text{mL}^{-1}$ and $11.55 \cdot 10^6$ $v_{\text{cell}} \cdot \text{mL}^{-1}$ respectively for a 1.4 L culture. These values were based on the specific heat flow rate of a CHO 320 cell line, reported in the literature, and on the biocalorimeter resolution. The perfusion cultures undertaken during this work were continuously monitored by calorimetry and dielectric spectroscopy, Figure 6.8. The data points of the heat flow signal were compared to the offline cell densities determined by microscopy to verify the validity of calorimetry as a CHO cell culture monitoring method.

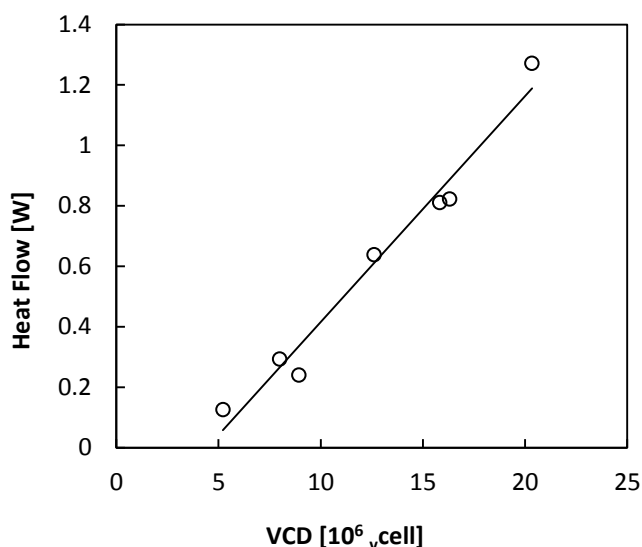


Figure 6.7 Metabolic heat flow rate and viable cell density are linearly correlated. The linear regression is constructed with a slope $a = 74.77 \cdot 10^{-11} \text{ W} \cdot \text{cell}^{-1}$ and a correlation coefficient of $R = 0.99$.

The heat signal plotted against the cell density displayed a linear relationship which was modelled by linear regression. The data points were found to be linearly correlated with a coefficient $R = 0.99$, Figure 6.7. The slope of the linear regression, corresponding to the specific cellular heat flow is estimated at $74.77 \pm 5.66 \text{ pW} \cdot \text{cell}^{-1}$, Table 6.2.

Table 6.2 Monitoring encapsulated CHO-DP12 cell cultures method validation

Specific cellular heat flow rate	$74.77 \pm 5.66 \text{ pW} \cdot \text{cell}^{-1}$
Standard deviation of the ordinate	0.201 W
Limit of blank	$1.33 \cdot 10^6 v_{\text{cell}} \cdot \text{mL}^{-1}$
Limit of detection	$8.87 \cdot 10^6 v_{\text{cell}} \cdot \text{mL}^{-1}$
Limit of quantification	$26.88 \cdot 10^6 v_{\text{cell}} \cdot \text{mL}^{-1}$

From the linear regression analysis, the LOB, LOD and LOQ were established, Table 6.2. The LOB, LOD and Limit of quantification (LOQ) were calculated following the ICH Harmonised Tripartite Guideline's "Validation of Analytical Procedures: Text and Methodology Q2(R1)" emitted in November 2005. From the linear regression, the limit of the blank is evaluated at $1.33 \cdot 10^6 \text{ }_{\text{vcell}} \cdot \text{mL}^{-1}$ and the lowest possible cell density to be properly detected is $8.87 \cdot 10^6 \text{ }_{\text{vcell}} \cdot \text{mL}^{-1}$. Cell densities above $26.88 \cdot 10^6 \text{ }_{\text{vcell}} \cdot \text{mL}^{-1}$, according to the ICH method should be reliably quantified.

These findings are comparable to the predicted method limits presented in Section 6.2. Both the predicted limit of detection, evaluated at $11.55 \cdot 10^6 \text{ }_{\text{vcell}} \cdot \text{mL}^{-1}$, and the one based on the calibration model $8.87 \cdot 10^6 \text{ }_{\text{vcell}} \cdot \text{mL}^{-1}$ are of the same magnitude, which is 30% inferior to the predicted LOD. Nevertheless, this confirms the previous conclusion, that bench scale calorimetry using the eRC1 is not a sensitive enough method to monitor 1.4 L CHO-DP12 suspension cultures, but has a strong potential to monitor microencapsulated perfusion cultures. These cultures, with 25 % (v/v) microcapsule are expected to reach densities above $10^8 \text{ }_{\text{vcell}} \cdot \text{mL}^{-1}$ and according to the specific heat flow rate, should generate heat flows above $10 \text{ W} \cdot \text{L}^{-1}$.

6.5. Online monitoring of perfusion cultures

6.5.1. Perfusion method

The microcapsules were manufactured following the method described in Chapter 3. To improve the microcapsule stability, the EX-CELL CHO DHFR (Sigma Aldrich, USA) basal and feed media were supplemented with 13 mM CaCl_2 . In addition, with the 2.5 M NaOH addition for base control, a 125 mM CaCl_2 solution was supplemented in parallel, to keep the $\text{Ca}^{2+}:\text{Na}^+$ ratio constant.

After inoculation, the cells were allowed to develop to $2 \cdot 10^6 \text{ }_{\text{vcell}} \cdot \text{mL}^{-1}$ in batch mode. When the cells reach that benchmarked density, the perfusion feed was manually initiated. The feed rate was set at a dilution rate $D = 2 \cdot \mu_{max}$, to avoid early nutrient depletion, extracapsular cell wash-out as well as an important accumulation of waste metabolic by-products. This meant that over a 24 hour period, 1.7 L of feed was supplied to the culture, and 1.7 L of spent media containing extracapsular cells and microcapsule debris was removed.

The EX-CELL CHO DHFR medium (Sigma Aldrich, USA), is composed of approximately $6 \text{ g} \cdot \text{L}^{-1}$ glucose and was supplemented with 4 mM L-glutamine. The total daily glucose and L-glutamine requirements were calculated using equation (6.10), where S is the substrate expressed in [g], q_s , the specific substrate uptake rate in $[\text{g} \cdot \text{cell}^{-1} \cdot \text{day}^{-1}]$, X the

total number of viable cells in the culture and t the time in days. If the required glucose or L-glutamine exceeds the concentration readily available in the medium, the feed was supplemented with additional D-glucose and L-glutamine. The freshly prepared feed bottle is placed on the feed balance to monitor and ensure that the feed rate remains constant. On the other extremity of the perfusion system, the 5L recuperation bottle was visually inspected before sampling. The recuperated spent media turbidity is a valuable preliminary indicator upon the microencapsulated cell culture's evolution and the microcapsule stability.

$$S = q_s \cdot (X * e^{\mu \cdot t}) \cdot t \quad (6.10)$$

6.5.2. *Perfusion cultures cell density and metabolite analysis*

The perfusion culture was operated in two distinct phases: the batch and the perfusion phase. The batch phase lasted 4 days, until the viable cell density reached $1.7 \cdot 10^6 \text{ vcell} \cdot \text{mL}^{-1}$. The feed perfused at $1.7 \text{ L} \cdot \text{day}^{-1}$ for duration of 8 days, and ended 12 days after inoculation. A maximum cell density of $15 \cdot 10^6 \text{ vcell} \cdot \text{mL}^{-1}$ was achieved; a 5-fold augmentation of the viable cell density yielded from batch cultures, (see chapter 5). The viability remained above 80% throughout, yet the fall in the viable cell density on day 12 was caused by loss of microcapsule stability. The released cells from the ruptured microcapsules were then washed out with the media outflow.

The viable cell density was estimated using three different methods: offline by counting cells under the microscope, by continuous real-time dielectric measurements and the continuous real-time calorimetry measurements. The continuous capacitance measurements were computed into the viable cell using the model proposed in Chapter 5, and the heat flow rate using the calibration model proposed in sub-section 6.4.3. The viable cell density assessed by the three monitoring methods throughout the full culture time is displayed in Figure 6.8.

As expected, and previously demonstrated, the cell density determined by dielectric spectroscopy and microscopy correlate well, from the beginning of the culture. On the other hand, the heat flow rate measurements did not provide accurate information before day 6, when the cell density was greater than $4 \cdot 10^6 \text{ vcell} \cdot \text{mL}^{-1}$.

The heat signal between day 0 and day 3 had greater variations than the remainder of the culture time. The headspace was enriched with initially 5% CO₂ to stabilise the pH between 7.2 and 7.4. With the progression of the culture and the accumulation of lactate, Figure 6.9, the culture started to acidify. To avoid unnecessary addition of NaOH, the CO₂ enrichment was punctually diminished, once a day, when sampling. This was undertaken to avoid unnecessary NaOH addition to the culture and calorimetric signal interference. The

step-wise reduction off CO₂ has subsequently an effect on the heat signal. Indeed, the dissolution of CO₂ into water has an enthalpy of -461.4 kJ · kg⁻¹ or -20.3 kJ · mol⁻¹ (Han et al., 2010; Voisard et al., 2002b).

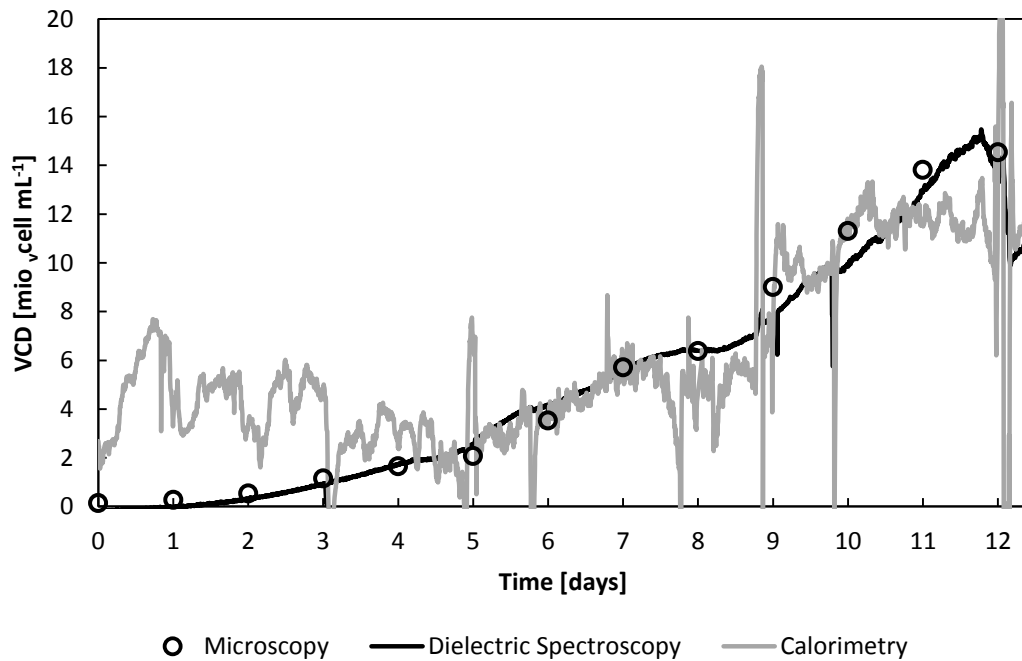


Figure 6.8 The viable cell density evolution throughout the whole culture time estimated by offline cell counts, dielectric spectroscopy and calorimetry. The peaks in the viable cell density signal determined by calorimetry were caused by sampling.

Moreover, it appears that there was a shift of metabolism after day 10. The heat flow rate evolved in the same manner as the offline cell counts and online capacitance data. But after day 10, the heat flow rate stabilises at 0.8 W (or at $11 \cdot 10^6$ $\nu_{\text{cell}} \cdot \text{mL}^{-1}$). The heat flow rate is highly dependent on the cellular growth rate (Biener et al., 2012). This stabilisation of the heat flow rate signal may be explained by the observed reduction of the microencapsulated cell growth rate by 50% from 0.62 day^{-1} to 0.29 day^{-1} .

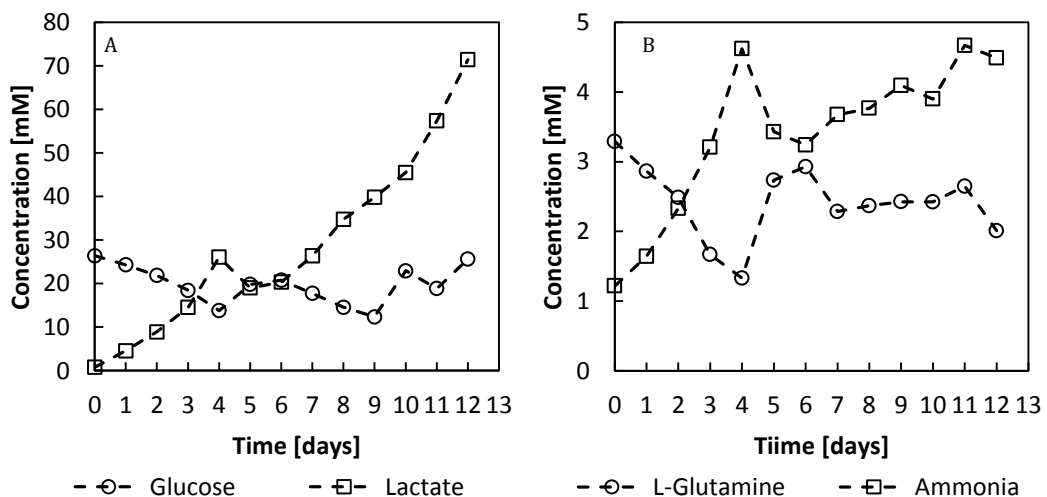


Figure 6.9 Metabolite concentration during the batch and perfusion phases of the culture. The perfusion phase is initiated on day 4 with a feed rate of $1.7 \text{ L} \cdot \text{days}^{-1}$.

The heat flow stabilisation after day 10 would also suggest a change in the cell metabolism. The offline metabolite quantification revealed that during the batch phase, glucose and L-glutamine were consumed in a similar manner to the previous batch cultures presented in Chapter 5, at $4.86 \cdot 10^{-9} \text{ mmol} \cdot \text{cell}^{-1} \cdot \text{day}^{-1}$ and $7.18 \cdot 10^{-10} \text{ mmol} \cdot \text{cell}^{-1} \cdot \text{day}^{-1}$. As a result lactate was produced at $4.83 \cdot 10^{-9} \text{ mmol} \cdot \text{cell}^{-1} \cdot \text{day}^{-1}$ and ammonia $1.33 \cdot 10^{-9} \text{ mmol} \cdot \text{cell}^{-1} \cdot \text{day}^{-1}$. The substrate to biomass yields were determined during the batch phase to be $Y_{X/glc} = 1.28 \cdot 10^8 \text{ cells} \cdot \text{mmol}^{-1}$ and $Y_{X/gln} = 8.66 \cdot 10^8 \text{ cells} \cdot \text{mmol}^{-1}$, and remained constant throughout the perfusion phase, Figure 6.10. In addition, the product to biomass yields did not change either and were evaluated at $Y_{Lac/X} = 1.18 \cdot 10^{-8} \text{ mmol} \cdot \text{cell}^{-1}$ and $Y_{NH_3/X} = 2.09 \cdot 10^{-9} \text{ mmol} \cdot \text{cell}^{-1}$. Thus, since the substrate to biomass yield and product to biomass yields remained constant throughout the culture, this would indicate that no shift in the catabolic pathways occurred.

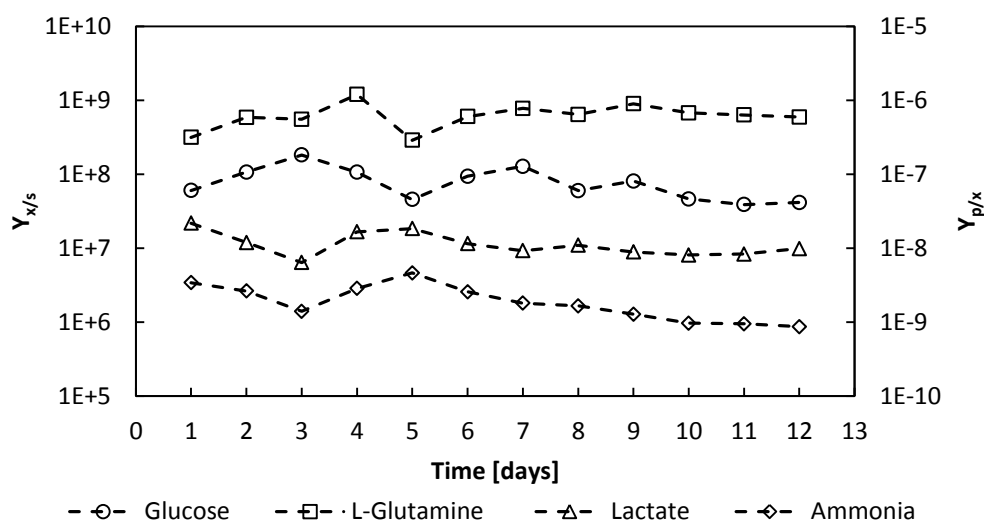


Figure 6.10 Evolution of glucose and L-glutamine to number of cells yields $Y_{X/s}$, and the produced lactate and ammonia to cells yields, $Y_{p/x}$, over the whole culture period, expressed in $[\text{cells} \cdot \text{mmol}^{-1}]$ and $[\text{mmol} \cdot \text{cell}^{-1}]$ respectively.

The perfusion feed, initiated on day 4, provided the cells with sufficient glucose and L-glutamine for optimal growth, and these nutrients did not become limiting, Figure 6.9. The perfusion feed and continuous removal of medium reduced the accumulation of metabolic by-products, which may have important undesirable cell growth inhibition effects and change the protein glycosylation profile. After day 10, whilst the the cell growth rate drops to 0.29 day^{-1} , the lactate concentration was found to have surpassed 40 mM and accumulated up to 70 mM by the end of the culture (day 13). In the following chapter, Chapter 7, the influence of lactate on the cell growth of the CHO-DP12 cell line is discussed. It seems that these concentrations of lactate reduces the rate of cellular development.

Finally, the CHO-DP12 12 cells produced the recombinant IgG₁ protein at rate of 25.52 pg · cell⁻¹ · day⁻¹. The perfusion culture generated at total of 2.4 g of IgG₁, Figure 6.11, which is 39.7-fold the amount synthesised in a batch culture.

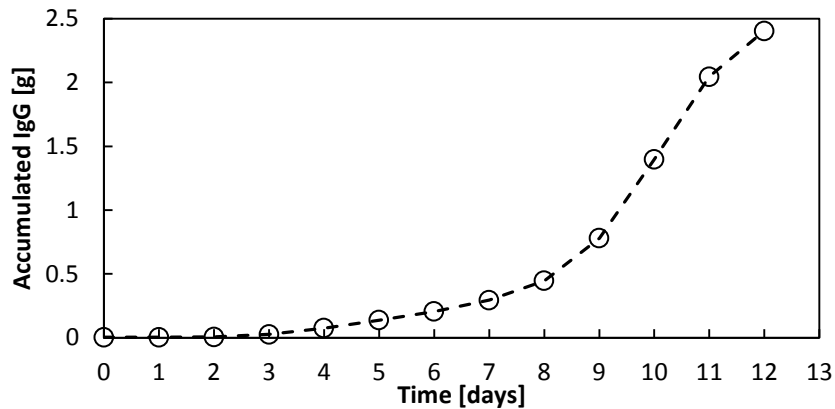


Figure 6.11 Accumulated recombinant IgG₁ manufactured in an encapsulated perfusion culture. After 12 days, 2.4 g of IgG₁ was produced by $14.5 \cdot 10^6$ cells · mL⁻¹ in a 1.4L culture.

6.5.3. Microcapsule colonisation and limitations

Though 350 mL of alginate-cell suspension was extruded, the culture was initially composed of a microcapsule to working volume ratio of 0.6 [-] (v/v). The unexpectedly high ratio was explained by an important microcapsule swelling during the citrate washing step and media wash and transfer. The average microcapsule radius on day 0 was evaluated at 300 μm and increased to 320 μm. From Day 2 onwards, the microcapsule radius dropped and stabilised at 240 μm, as shown in Figure 6.12A. In parallel, the mechanical resistance followed a similar pattern. The microcapsule mechanical resistance initiated at 0.94 g · capsule⁻¹. From day 2 to day 5, the mechanical resistance dropped and stabilised at 0.75 g · capsule⁻¹. On day 6, the mechanical resistance was evaluated at 0.02 g · capsule⁻¹, meaning the microcapsules lost 78% of their initial mechanical resistance. At this stage of the culture, 46% of the microcapsules ruptured, and the microcapsule debris and extracapsular cells were washed out with the feed, Figure 6.12B.

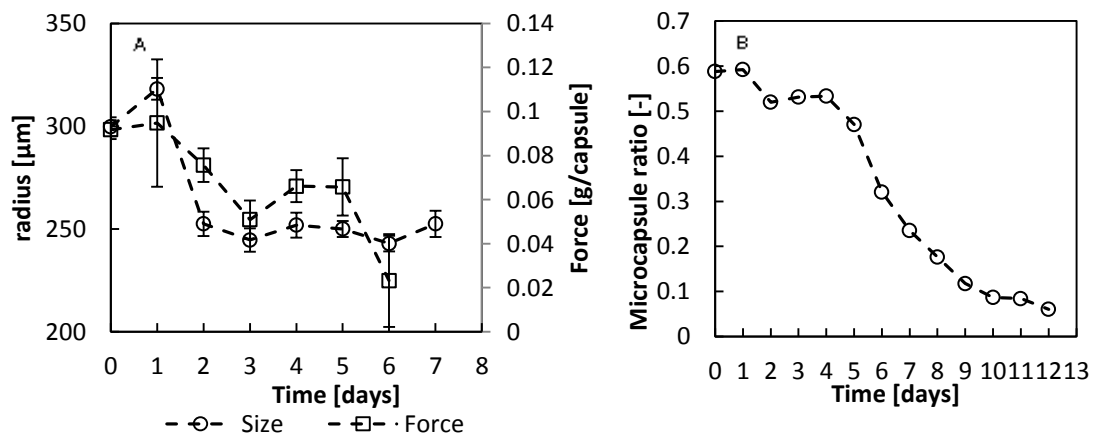


Figure 6.12 Typical microcapsule structural proprieties (A) and microcapsule to working volume ratio (B) development throughout a perfusion culture

Though most of the microcapsules rapidly disintegrated, the perfusion culture was allowed to carry on until the capacitance readings and off line viable cell density values began to fall. Another factor that could have had an impact upon the cell growth rate, aside from the presence of lactate in high concentration, could have been a lack of available space within the microcapsules. It was visually observed on day 12, that the microcapsules appeared to be almost fully packed with cells, Figure 6.13. However, the microcapsules contained an average of $1.71 \cdot 10^4$ cells · capsule⁻¹, which only represented 43.6 % of the microcapsule full potential. Had there been no microcapsule loss, the culture containing 58% microcapsules to working volume (Figure 6.12B), could have potentially achieved the predicted $139 \cdot 10^6$ vcells · mL_{WV}⁻¹ target.

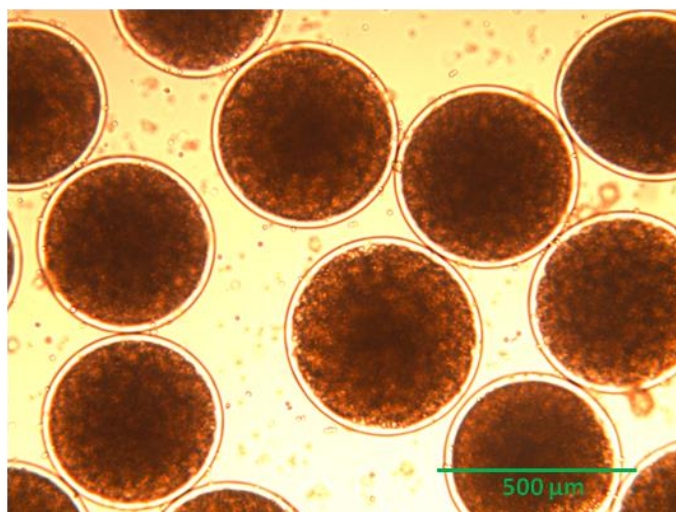


Figure 6.13 Photograph of the remaining intact microcapsules on day 12 suggesting near to full packing has been reached

Calcium-alginate-poly-L-lysine-alginate microcapsules are constructed using poly electrolytes that form the microcapsules through electrostatic interactions (Breguet et al., 2007c; Orive et al., 2004a; Thu et al., 1996a). These interactions are not strong chemical bonds, but are ensured by an equilibrium. It is thought that the perfusion feed caused a destabilisation of the equilibrium and diluted the essential calcium cations and poly-L-lysine polycations with the continuous outflow of spent medium.

6.6. Conclusion and outlook

The perfusion culture yielded a viable cell density of $15 \cdot 10^6$ vcells · mL_{WV}⁻¹, a 5-fold higher density in comparison to batch cultures. The microcapsules contained an average of $1.34 \cdot 10^4$ cells · capsule⁻¹, representing 43.6% of the microcapsule internal volume being filled. The cell development was monitored online by dielectric spectroscopy and biocalorimetry. Both capacitance and heat flow rate measurements were computed into the viable cell density using the calibration models and compared to the viable cell density

determined by offline cell counts, counted under the microscope. The capacitance followed the cell growth reliably, from the culture inoculation through to the decline phase. The heat signal also provided accurate information upon the culture development from day 6 onwards, from $4 \cdot 10^6$ $\nu_{cells} \cdot mL_{WV}^{-1}$. Between day 6 and day 10, the cells grew at a rate of 0.62 day^{-1} . Although no apparent change in the analysed substrates and products to biomass yields was observed, after day 10, the growth rate fell to 0.29 day^{-1} . This resulted in a stabilisation of the heat signal, though the capacitance and offline cell counts continued increasing at a lower rate.

Reaction calorimetry can follow cellular activity of high cell densities but can precisely quantify the number of cells per unit volume only above $26.88 \cdot 10^6$ $\nu_{cells} \cdot mL_{WV}^{-1}$. Higher cell densities are theoretically achievable, but further microcapsule stabilisation studies must be undertaken to avoid capsule breakage and associated cell loss.

Additionally, this study is a stepping stone towards using continuous heat flow rate measurements to evaluate in real-time cell activity at industrial scale. This work involved growing cells in a working volume of 1.4 L. At this scale, the surface area to volume ratio is high, consequently, the heat losses to the environment are significantly (Marks, 2003; Voisard et al., 2002a). However, large reactors e.g., 12.5 m^3 have a much lower surface area to volume ratio, meaning that the heat loss is much smaller. Therefore, a larger difference between T_r and T_j is necessary to maintain the CHO culture at the set reactor temperature, (Doran, 1995c; Nienow, 2006)[32,33] and accurate heat flow measurements can be made.

The perfusion culture feed mode allowed the cells to multiply without being space restricted. Indeed this work proved that the microcapsule internal volume can be filled above the 1.8% colonisation of batch cultures. Yet, at this stage, the microcapsules cannot withhold the important feed in-and outflows, and a different feed strategy needs to be investigated. Fed-batch mode involves adding the feed only, and no spent media is removed. Thus, poly-L-lysine (or other microcapsule components) would not be removed from the culture. In the following chapter, it is proposed to feed the cells using the fed-batch mode, and to control the feed inflow rate according to the acquired online data in LabVIEW.

Chapter 7 Design of a simple feed control based on capacitance data in microencapsulated fed-batch cultures

Summary: This chapter investigates the possibility of using the viable cell density estimated online by dielectric spectroscopy to adjust the feed rate. This would provide the cells with an amount of glucose and L-glutamine equivalent to the cells glucose and L-glutamine consumption requirements. A feed controlled fed-batch culture was designed and implemented in LabVIEW. A preliminary culture was undertaken with the aim to fill the microcapsules to the maximum, to test the functionality of the feed control VI and to show any limitations, if any. 11 mL of feed was supplied to the culture over 1.1 days and the cells only grew to $3 \cdot 10^6 \nu_{\text{cell}} \cdot \text{mL}_{\text{WV}}^{-1}$. Product inhibition, more specifically, lactate inhibition was suggested as being responsible for the low cell titre. This was confirmed by an experiment which showed the growth rate was reduced by 50% when cells were incubated in 50 mM lactate, in shake flask culture, without pH control. To extend the feeding period, a second culture was designed and performed with a lower initial glucose concentration. The dielectric controlled feed lasted 2.5 days, enabling to verify the stabilisation of the glucose and L-glutamine concentrations which did not reach depletion or accumulated to high levels. The cultures showed the feed rate was dictated in both instances by the growth rate and the viable cell density evaluated by real-time capacitance measurements, proving the successful potential of the feed strategy.

Keywords: Fed-batch; Monitoring and Control; LabVIEW; Feed Control; Product inhibition; CHO cells Metabolism

7.1. Introduction

In Chapter 6, it was shown that, while perfusion cultures provided a suitable environment for good cell development, that microcapsules could not withstand the dilution effects of the feed strategy. Perfusion cultures are usually the preferred system for microencapsulated cell cultures, and cell retention is eased by the presence of the microcapsules, entrapping the cells. But after 2 to 3 days of feeding the cells, a 50% loss of microcapsules occurred due to microcapsule rupture, see Chapter 6. In order to pursue the aim of achieving high cell density microencapsulated cells cultures, and to avoid the removal of spent medium, the cultures were then operated in fed batch. A controlled feeding strategy was investigated and developed in section 7.2.

Fed-batch cultures are often viewed as a variations of batch or repeated batch cultures (Liangzhi Xie and Weichang Zhou, 2005). The principle advantage of fed-batch cultures is reported to be the high product titres that can be attained. Fed-batch operations have been reported to attained with final recombinant protein product concentrations $>5 \text{ g} \cdot \text{L}^{-1}$ with cell densities reaching $50 \cdot 10^6 \text{ cells} \cdot \text{mL}_{\text{WV}}^{-1}$ (Cacciuttolo, 2007; Pollock et al., 2013). Companies frequently use fed-batch cultures due to ease of operation, relative ease of process development time and validation, can be carried out with most reactor configurations, with high productivity and reduced risk of contamination compared to perfusion cultures (Altamirano et al., 2004; Cacciuttolo, 2007; Kuwae et al., 2005; Luellau and Fenge, 2005). In some cases, such as the production of certain viral vaccines, perfusion operation cannot be used. An example is the influenza vaccines which are required seasonally and in high quantities over a short period of time. In this case fed-batch operation is reported to be the most efficient way to produce the required commercial amounts (Meghrous et al., 2009).

The feed to a fed-batch culture can be either a constant rate or an exponential rate, which enables a constant specific growth rate. The success of a fed-batch culture is principally dependent on the availability of the essential nutrients. However, rapid changes in osmolarity and/or metabolic waste by-product accumulation may result in undesired inhibitory effects (Altamirano et al., 2004; Liangzhi Xie and Weichang Zhou, 2005; Xie and Wang, 1997). The feed strategy, in which the medium feed rate is controlled by the cell development and/or the nutrient demand of the culture, requires a continuous on-line or rapid at-line, method for the determination of substrate concentration and cell concentration/viability.

In this chapter, a feed control strategy was first designed and implemented in LabVIEW VI. Two different fed-batch cultures were undertaken, with two different growth medium containing different glucose concentrations. After undertaking preliminary cultures, it was

demonstrated that after 26.4 hours of operation, an abrupt reduction in growth rate leading to a stabilisation of the viable cell density, caused the feed to stop. It was therefore hypothesized that a metabolic by-product may have accumulated to cell growth inhibitory levels. Since there are reports in the literature (Cruz et al., 2000; Lao and Toth, 1997; Liangzhi Xie and Weichang Zhou, 2005) which suggest that the accumulation of lactate may be responsible for growth inhibition in CHO cell cultures, the effects of lactate on cell growth was studied. Consequently, after verifying this hypothesis, and to prove that capacitance measurements can be used to control a feed rate, the culture medium was replaced with one containing a lower basal glucose concentration. This allows the feed to be initiated at an earlier stage and thus to prolong the feeding period by an additional 24 hours. In this way the concept of feeding the microencapsulated cells, with the feed strategy based on dielectric spectroscopy as the continuous, real-time cell density monitoring method, was demonstrated.

7.2. Control strategy

7.2.1. Control strategy design

The aim of the feeding strategy is to provide the cells with sufficient D-glucose and L-glutamine for the cells to grow and reach high cell density microencapsulated cultures. The aim was to operate the culture in batch mode until 50% of the available D-glucose and L-glutamine had been consumed. At that point, fed-batch operation would be initiated, supplying the cells with just enough substrates to keep the glucose and glutamine concentrations at a constant level and to maintain the growth rate at a maximum. This goal could be achieved by either manually injecting the necessary volume of feed at set time intervals or automatically, by designing a simple feed control system.

An automatic feed control system is generally constructed with 3 to 4 distinct phases (Mark Riley, 2005). First, one or more process variables is/are measured on-line or at-line. Second, if different variables are measured, the data are reconciliated. Data reconciliation is an important step as it attempts to reduce any possible errors that may occur by statistically evaluating the measurement consistency (Dabros et al., 2009a). Third, the measured culture variable(s) is/are compared with the set-point. Fourth, based on the measurement set-point and the PID gain coefficients, if any, a decision is made and put into action to rectify the process variable.

When designing a monitoring and control system, different process considerations must be kept in mind. The process development speed and reaction to any process alterations are important factors in process control. Animal cells such as CHO have doubling times of 16 to 24 hours, whereas many microbial cells have doubling times less

than an hour. Consequently, the response time to a change in the culture environment is usually much slower for animal cells than for microbial processes. Therefore, the choice of sensor, the timing of each measurement cycle, data acquisition time and strategy and response amplitude and timing are all to be considered (Carloni et al., 2009; Mark Riley, 2005).

A control system can be established in either an open-loop or a closed-loop system. Open-loops rely on a model that predicts the outcome of a process without taking into account any unexpected changes or disturbances that may occur during the process. This control system, though easy to design, is difficult to apply to biological processes since they are complex and a slight change in one variable may cause significant changes to the forecast process evolution. On the other hand, closed loops are dependent on mathematical models between input(s) and output(s) and feedback information is used to adapt the amplitude of the input as a function of any unpredicted changes in the output of the system (Mark Riley, 2005).

In this work, the aim was to automatically provide the cells with sufficient quantities of D-glucose and L-glutamine, in a continuous manner, to counteract the consumption of these two substrates. A feed forward strategy was created to control a feed rate according to equation (7.1), adapted from the model applied in a previous work (Dabros et al., 2010). The necessary feed rate at time (t) was dependant on both the measured viable cell density and the determined growth rate evaluated over time (t) and t_{t-4} hours. Both the viable cell density and growth rate were estimated online by real-time dielectric spectroscopy, and the feed rate determined and generated in an adapted version of the previously designed VI.

$$F(t) = X \cdot V \cdot \frac{\mu}{Y_{x/s} \cdot S_f} \quad (7.1)$$

7.2.2. Implementation in LabVIEW

A peristaltic pump (IPS, ISMATEC, Germany) was wired to a NI-9263 module, which was inserted next to the other modules (NI-9215 and NI-9870) onto the NI-9014 chassis (National Instruments, USA). This NI-9263 module enabled continuous output of an analogue signal within the ± 10 V range. At the other extremity, the cable was connected to an analogue interface, to the speed and the ground pins. As the voltage increased, the rotation of the rollers speeded-up and increased the flow rate of the solution.

As discussed in Chapter 4, LabVIEW is reputed for its graphic coding platform which offers many possibilities for tailoring automated software to monitor and control specific processes. The graphical language not only allows parallel programming, but also to insert new needed features. For the work undertaken for this chapter of the thesis, the rate at

which the feed medium flows was dependent on the viable cell density and the cell growth rate based on measurements of dielectric spectroscopy. The control feature was added to the previously elaborated Main DAq LabVIEW VI (Virtual Instrument), and renamed Main DAq FED-batch, as shown diagrammatically in the flow chart, Figure 7.1. The data acquisition runs were carried out in a similar manner to the previous VI, however, whilst the averaged data point was inserted into the respective time chart and saved in the DAq text file, a parallel task execution stream was created. First, the natural logarithm of the capacitance average data point multiplied by the reactor volume was calculated, and inserted into a 2-D array with the culture time, and was then saved into a buffer file, Figure 7.3A.

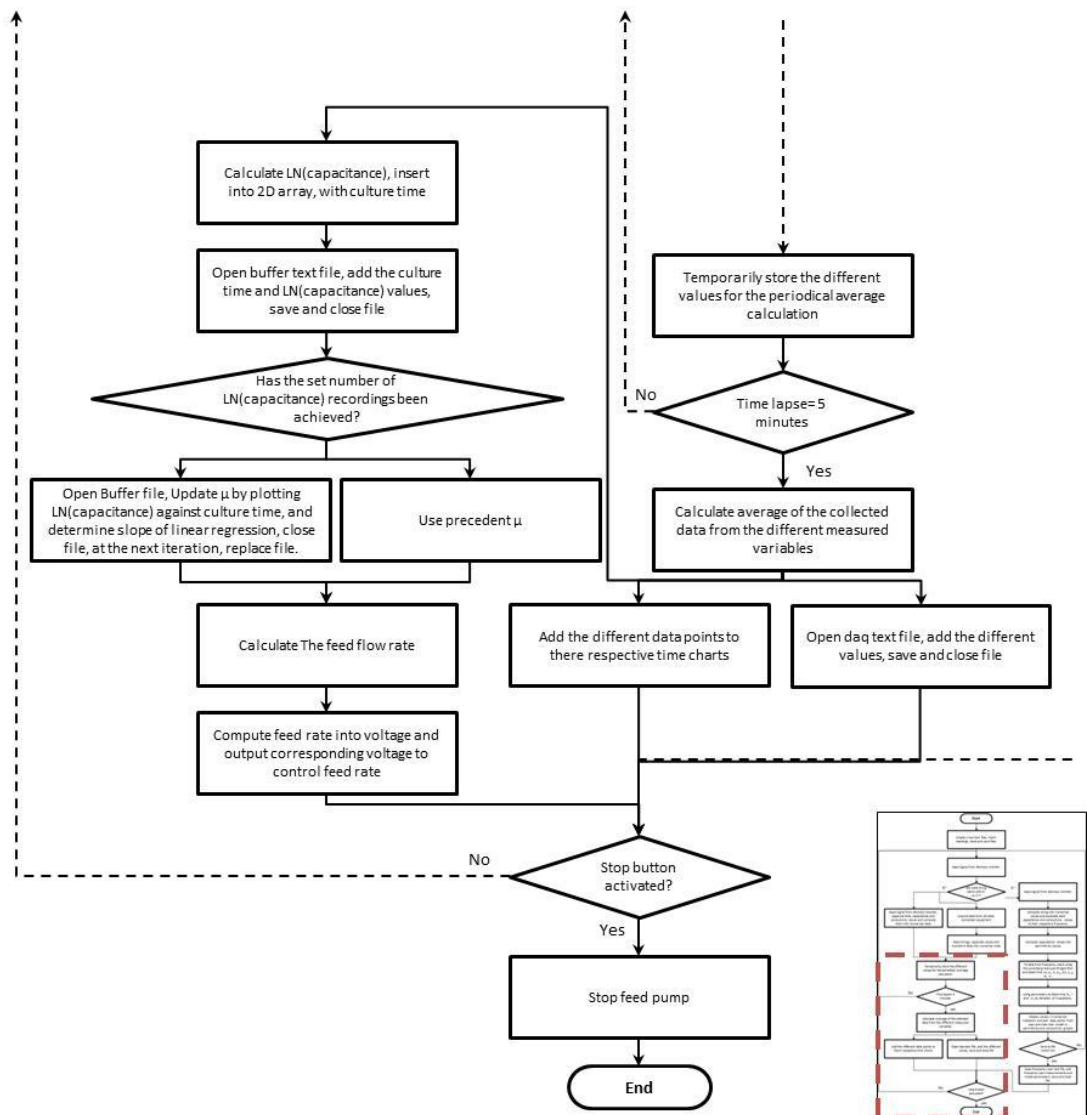


Figure 7.1 Flow chart of the feed control feature inserted within the previously designed LabVIEW VI (Small box, right corner. The red box displays the location where the new code is inserted)

After a set amount of time, the growth rate was calculated by performing a regression analysis and determining the slope between the natural logarithm of the capacitance values against the culture time. The operator can programme the frequency and length of

time (and amount of data points) to calculate the growth rate. For this work, the CHO-DP12 cells we shown to have a doubling time of 1.12 days. It was therefore decided to evaluate the growth rate over a 4 hour period as this time cycle procured 48 capacitance measurements, enough to ensure an accurate growth rate evaluation, whilst rapidly detecting and reacting to any possible changes. After a cycle, the buffer file was replaced by a new one. The number of iterations of the while loop in the main data acquisition was automatically counted in LabVIEW. The number of iterations was divided by the pre-set number of iterations defined by the operator (Period pump control in minutes, divided by data acquisition time; example: $\frac{4 \text{ hours} \cdot 60 \text{ minutes/hour}}{5 \text{ minutes/cycle}} = 48 \text{ cycles}$). When the number of cycles, subtracted by the remainder is equal to 1, the growth rate was calculated, and when equal to 0, the buffer file was renewed, Figure 7.3A.

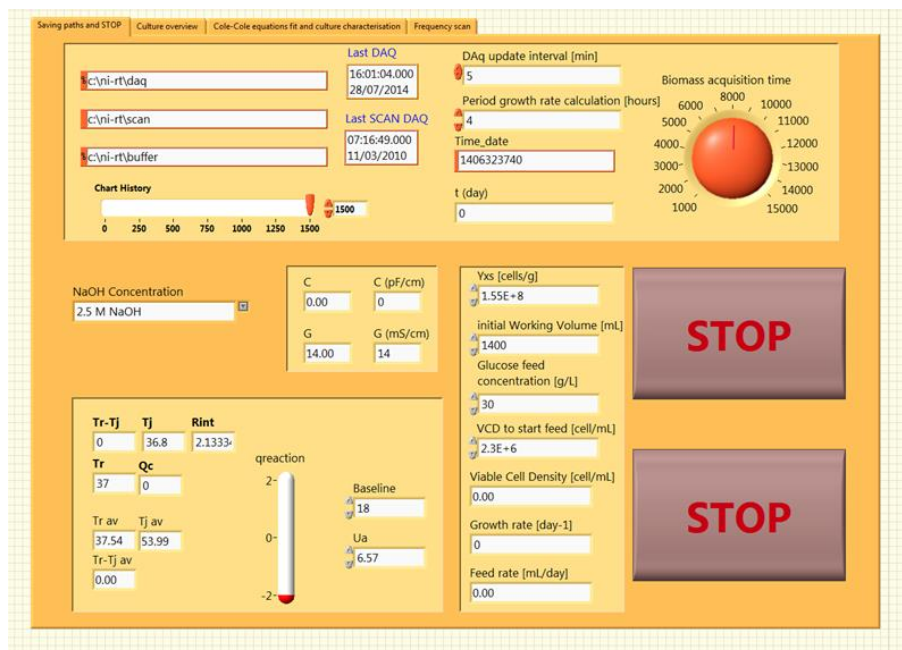


Figure 7.2 Front panel of the Main DAQ FEDBatch VI with added culture parameters that allowed the transfer of the VI to monitor and control various types of fed-batch cultures.

The following step involved determining the feed rate using equation (7.1) and as illustrated in Figure 7.3A and Figure 7.3B. The capacitance was used to calculate the viable cell density using the previously estimated specific capacitance. To allow the cells to develop first as a batch in the first phase of the culture, the code for equation (7.1) was placed within a case structure. The feed would not start before the cell density exceeded a pre-determined density (for example $2.5 \cdot 10^6 \text{ } v_{\text{cell}} \cdot \text{mL}_{\text{WV}}^{-1}$). This value, along with the cell to glucose yield, $Y_{\text{cell}/\text{glc}}$, the initial working volume and the glucose feed concentration, were inserted into their respective numeric control boxes, Figure 7.2. Once the cell density was superior to the pre-set value, the feed could commence. The feed rate was then computed into volts and the voltage output was continuously emitted through the NI-9263 module to the peristaltic pump.

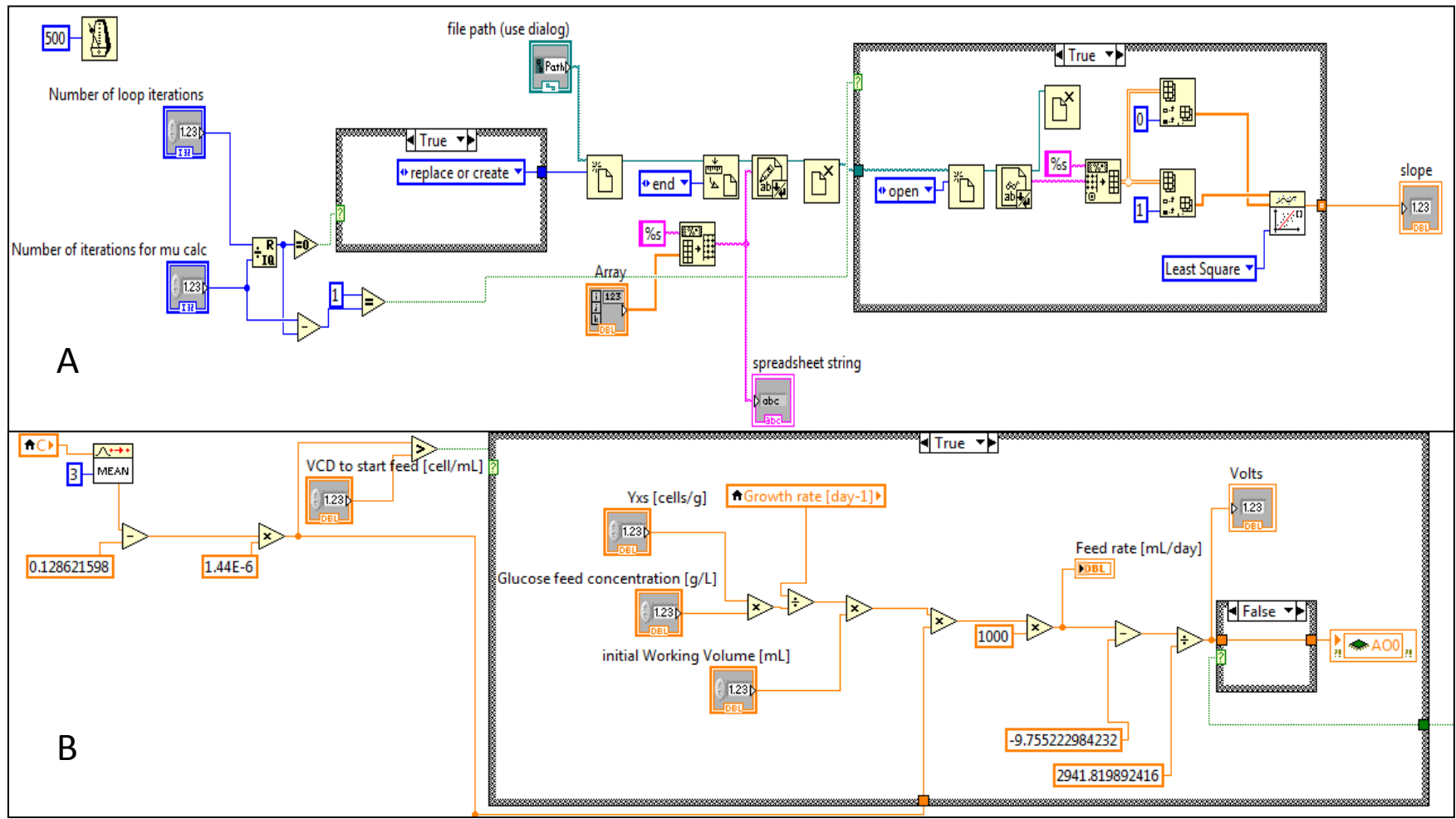


Figure 7.3 LabVIEW code for creating or replacing the buffer file, saving the 2-D array and calculating the growth rate (A). Below in B, is the implementation of equation (7.1), in a case structure to allow the operator to decide when to start the feed.

7.3. Preliminary fed-batch results

7.3.1. Culture method and simulation

The new feed control function added to the previously designed LabVIEW VI was tested by electronically simulating an exponential cell growth. A supplementary VI was temporarily added. This VI was constructed using the exponential cell growth equation, equation (7.7), within a While-Loop. Each cycle was counted and considered as the culture time variable t . Both cell growth and feed rate were recorded and compared to verify the functionality of the feed control VI.

In parallel, a Microsoft Excel spreadsheet was prepared by predicting the evolution of the different measured culture variables such as the cell density per microcapsule volume unit and per working volume unit, glucose and L-glutamine concentrations, reactor volume, waste product concentrations and recombinant IgG₁, Figure 7.4. For the preliminary culture, it was decided to feed the cells in order to fully colonise the microcapsules without exceeding the reactor volume. The first culture also had the purpose of checking the good operation of the controlled feed. When producing the microencapsulated CHO-DP12 fed-batch culture simulation model, it was hypothesised that the cell density would only expand exponentially, without a lag phase, growth inhibition or experiencing a reduction in the growth rate, until the microcapsules were fully colonised. The culture would be initiated within a working volume of 1.4 L, and starting with a cell density of $0.125 \cdot 10^6 \text{ } \nu_{\text{cell}} \cdot \text{mL}_{\text{WV}}^{-1}$ (or $0.5 \cdot 10^6 \text{ } \nu_{\text{cell}} \cdot \text{mL}_{\text{capsule}}^{-1}$) in the EXCELL CHO DHFR^r medium (Sigma Aldrich, USA). Based on the CHO-DP12 cell growth kinetics and yields, the culture should last 9 days.

The culture was allowed to develop under batch conditions until the cells had grown to $2.5 \cdot 10^6 \text{ } \nu_{\text{cell}} \cdot \text{mL}_{\text{WV}}^{-1}$, when theoretically 80% of the available glucose had been consumed. At this point, the culture was switched to fed-batch mode. The feed medium, (EXCELL CHO DHFR^r medium), initially containing 31 mM, was supplemented with an additional 1 M D-glucose monohydrate (Sigma Aldrich, USA) and 130 mM Na-L-glutamine (Sigma Aldrich, USA). The feed rate would be controlled in such a way to stabilise the two limiting measured substrate concentrations, Figure 7.4B. By day 9, when the microcapsules were completely colonised, 390 mL of feed would have been added, bringing the total volume to 1.8 L (nor the addition of the NaOH and CaCl₂ or the water evaporation have been taken into account). Furthermore, it was also estimated that the recombinant IgG₁ could be found at concentrations $>500 \text{ mg} \cdot \text{L}^{-1}$, providing the cells synthesised the recombinant protein at a constant rate of $11 \text{ pg} \cdot \text{cell}^{-1}$. As a result of the

CHO cell metabolic activity, lactate and ammonia would be produced and reach 590 mM and 32 mM, respectively. It should be noted that it has been reported that such high lactate concentration could have important cell growth inhibitory effects (Cruz et al., 2000).

Table 7.1 Equations used to simulate the potential evolution of the different measured variables of a fed-batch culture, in figures Figure 7.4 and Figure 7.10. Nomenclature: F = Feed rate, V = volume, V_0 = volume at t_0 , V_{WV} = working volume, X viable cell density (VCD), q_s = substrate consumption rate, S = substrate concentration culture, S_f = substrate concentration in the feed, P = product concentration, P_0 = product at t_0 , q_p = product production rate and t = time

Variables	Batch phase	Fed-batch phase
Feed rate	$F = 0$ (7.2)	$F = \frac{q_s \cdot X \cdot V}{S_f}$ (7.3)
Volume	$V = constant$ (7.4)	$V = \Delta t \cdot F + V_0$ (7.5)
VCD	$X = X_0 \cdot e^{\mu \cdot \Delta t}$ (7.6)	$X = \frac{X_0 \cdot e^{\mu \cdot \Delta t} \cdot V_0}{V_{WV}}$ (7.7)
Substrate	$S = S_0 - q_s \cdot X \cdot \Delta t$ (7.8)	$S = S_0 - \frac{[(S_f \cdot F) - (q_s \cdot X \cdot V_0)] \cdot \Delta t}{V_{WV}}$ (7.9)
Product	$P = P_0 + q_p \cdot X \cdot \Delta t$ (7.10)	$P = P_0 + \frac{X \cdot V \cdot q_p \cdot \Delta t}{V_{WV}}$ (7.11)

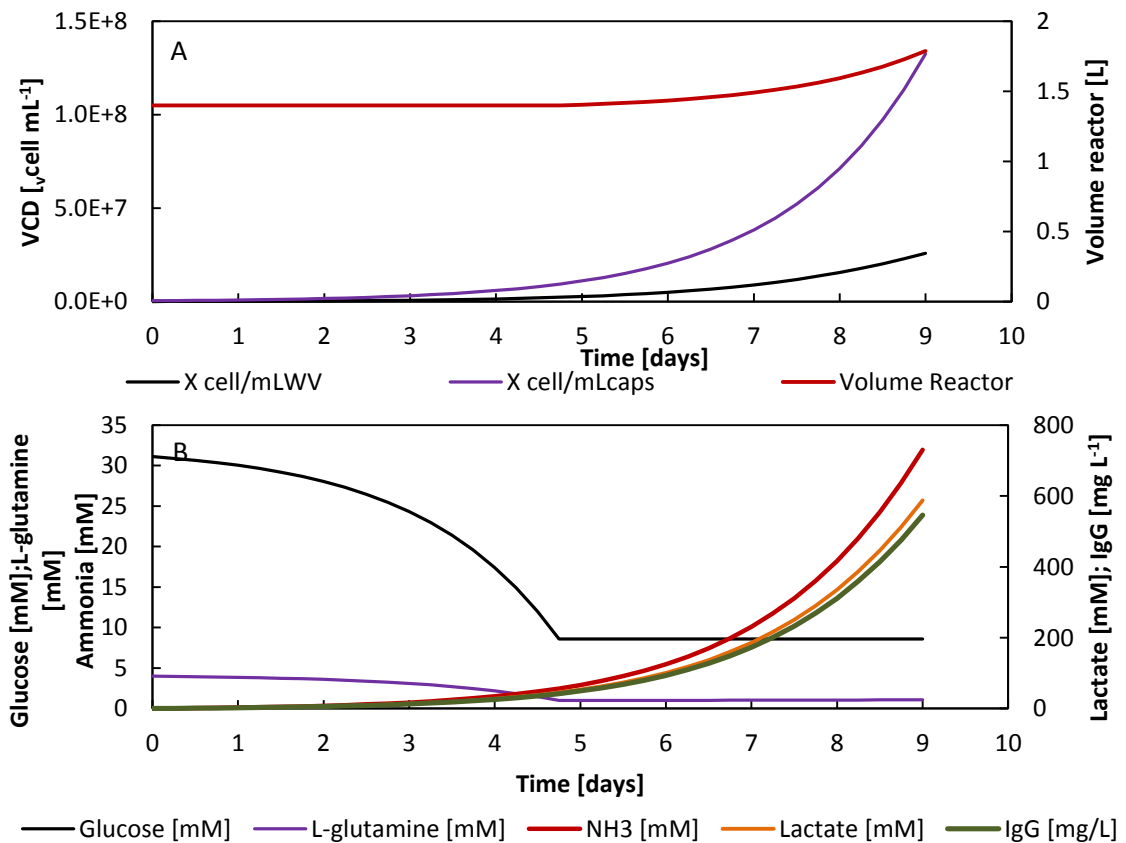


Figure 7.4 Predicted evolution of the culture variables throughout the microcapsule colonisation period, from inoculation to full microcapsule colonisation. The model was constructed admitting that no lag phase or growth inhibition could be observed and using equations (7.3) to (7.11) in Table 7.1.

The eRC1 was equipped in the same manner as for the perfusion culture, except for the feed outlet which was removed. The pH control and gassing were undertaken in the same manner as for the previous cultures.

7.3.2. Results

The first feed controlled fed-batch culture lasted 9 days. The viable cell density was evaluated continuously by dielectric spectroscopy in real-time and daily by off-line cell counts under the microscope. Again, the correlation between both methods was very high throughout the duration of the culture, Figure 7.5A. The cells underwent a two day lag phase, causing a two day delay in the culture from the predicted model. After day 2, the cells then grew exponentially at a growth rate of 0.55 day^{-1} .

It was decided the feed would start when the cell density had reached $2.5 \cdot 10^6 \text{ } \nu\text{cell} \cdot \text{mL}_{WV}^{-1}$, as planned after 6.9 days, whilst taking into account the two day shift caused by the lag phase. When the dielectric signal received and computed into viable cell density in LabVIEW reached the $2.5 \cdot 10^6 \text{ } \nu\text{cell} \cdot \text{mL}_{WV}^{-1}$ benchmark, the VI triggered the commencement of the calculation of the necessary feed rate and output voltage, Figure 7.5B. 11.3 mL of feed was added to the culture between days 6.9 and 8.

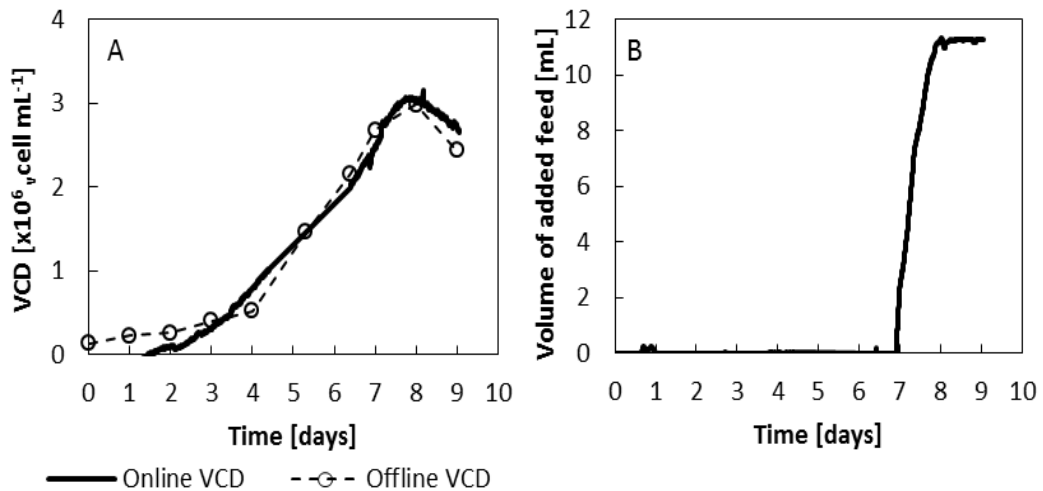


Figure 7.5 Evolution of the cell density and supplementation of feed throughout the whole fed-batch culture. A: Development of the viable cell density estimated by dielectric spectroscopy and off line microscopic cell counts; B: Volume of feed medium added to the culture during the fed-batch phase

During the feeding period, the growth started to gradually reduce and stabilised by day 8, at a maximum cell density of $3 \cdot 10^6 \text{ } \nu\text{cell} \cdot \text{mL}_{WV}^{-1}$, a cell density comparable to that obtained in batch cultures. The feed rate to apply was directly calculated in LAbVIEW using equation (7.1), and therefore was dependent on both viable cell density estimated at time t and the growth rate, calculated between time t and t_{t-4} hours. As the growth gradually diminished until it was below zero, the feed consequently stopped, Figure 7.6.

Therefore, it can be seen that the implemented feed strategy was highly dependent upon the growth rate.

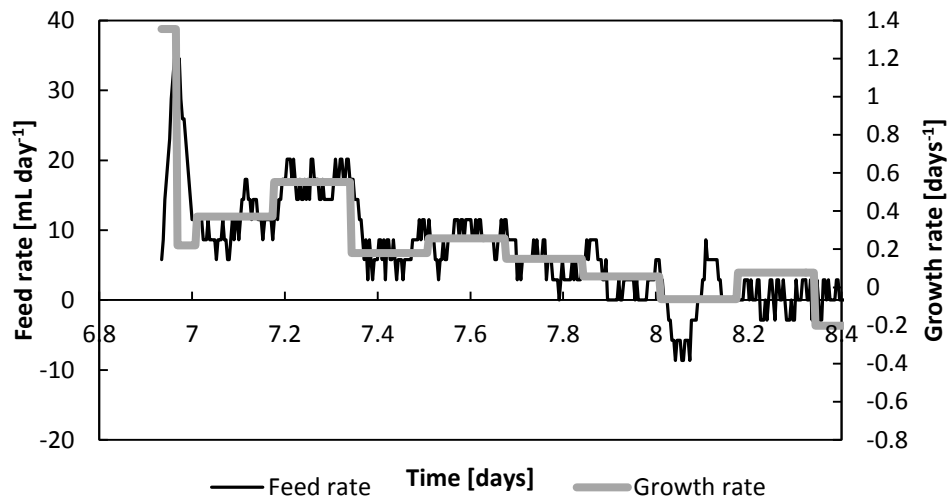


Figure 7.6 Comparison between the feed and growth rates calculated in LabVIEW and recorded in the data acquisition text file during the fed-batch phase of the culture

The analysed metabolites were quantified on a daily basis and revealed the cell to glucose and cell to L-glutamine yields to be highly comparable to previous cultures with respectively $Y_{cell/glc} = 1.45 \cdot 10^8 \text{ cell} \cdot \text{mM}^{-1}$ and $Y_{cell/gln} = 1.03 \cdot 10^9 \text{ cell} \cdot \text{mM}^{-1}$. When the fed-batch phase of the culture commenced, after 6.9 days, the expected amounts of glucose and L-glutamine had been consumed. Thus, 9.7 mM of D-glucose and 0.5 mM L-glutamine remained. On day 8, after 24 hours of continuous feed, the substrates of interest were found at 7.2 mM and 0.6 mM, meaning the cells were not likely to have been glucose or L-glutamine limited. The feed was observed to have stabilised at these substrate concentration levels, Figure 7.7.

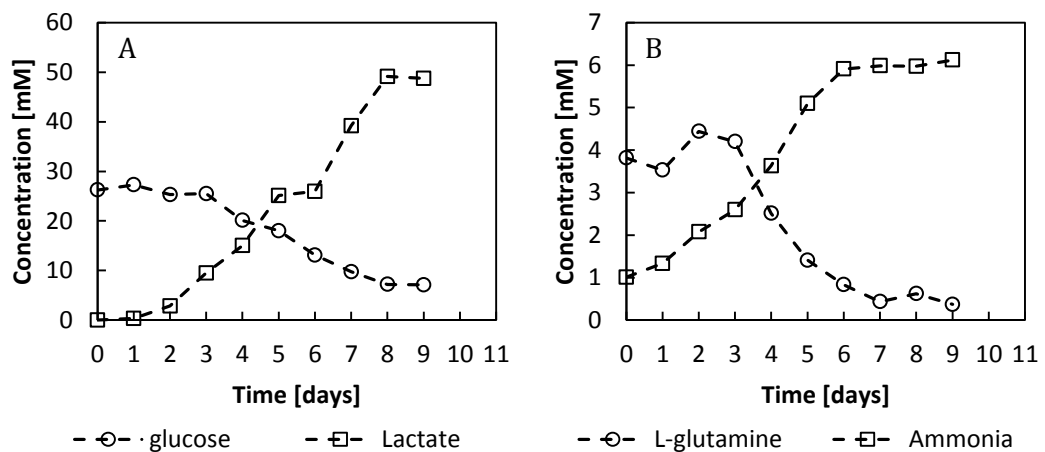


Figure 7.7 Evolution of the glucose and lactate concentrations (A) and L-glutamine and ammonia concentrations (B) throughout the first controlled feed fed-batch culture

Though glucose and L-glutamine were provided in sufficient amounts, cell growth inhibition was observed. This cell inhibition may have been caused by either the depletion

of an essential nutrient that was not analysed, or by an accumulation of metabolic by-products. The second explanation was the preferred case scenario as it would have been unlikely in the early stages of the fed-batch that the cells were limited by the absence of a nutrient, since no limitations were clearly observed during the perfusion cultures. The latter cause, the accumulation of an inhibitive metabolic product in fed-batch cultures, has been reported elsewhere. The cell growth inhibition effects caused by the accumulation of lactate and ammonia are well known and have been reported by many, and different groups have suggested alternative strategies to reduce their production (Altamirano et al., 2006; Cruz et al., 2000; Lao and Toth, 1997; Liangzhi Xie and Weichang Zhou, 2005; Sun et al., 2013; Xie and Wang, 1997).

7.3.3. Implications of lactate concentrations upon the cell development

CHO cell metabolism is characterised by rapid glycolysis, breakdown of glucose to pyruvate, and glutaminolysis, pathway lysing L-glutamine into glutamate, ammonia, aspartate, CO₂, pyruvate, lactate, alanine and citrate, Figure 7.8, (Altamirano et al., 2006). Consequently, Lactate and ammonia are two of the main products which accumulate within CHO cell fed-batch cultures (Ahn and Antoniewicz, 2011).

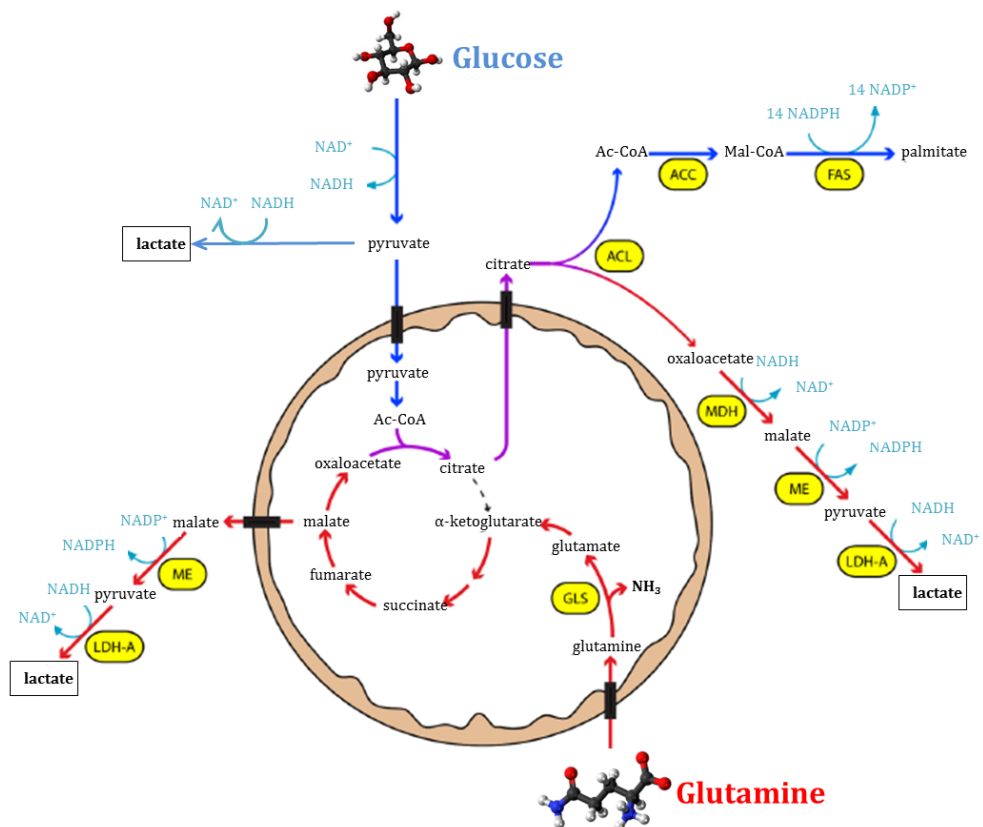


Figure 7.8 Glucose and L-glutamine catabolic pathways, which take place in the mitochondrion, lysing glucose and L-glutamine into lactate and ammonia. ACL, ATP-citrate lyase; ACC, acetyl-CoA carboxylase; FAS, fatty acid synthase; ME, malic enzyme; Ac-CoA, acetyl-CoA; Mal-CoA, malonyl-CoA; MDH, malate dehydrogenase; LDH-A, lactate dehydrogenase-A; GLS, glutaminase. Adapted from (Zagari, 2012)

In the literature, many articles discuss the toxic effects of both lactate and ammonia generated by hamster- derived cell lines and offer different strategies to reduce production from genetic engineering to metabolite substitution (glutamate instead of glutamine or galactose instead of glucose) (Chee Fung Wong et al., 2005; Kuwae et al., 2005; Lao and Toth, 1997; Sun et al., 2013; Zhou et al., 2011). However, the inhibition concentration levels of these two metabolic products cannot be clearly defined as the harmful levels of lactate and ammonia vary from one cell line to another. A previous study showed that an initial concentration of 15 mM ammonia reduced the growth rate of the CHO-DP12 cells by 33% in contrast to that obtained from cultures starting with a 5 mM ammonia concentration (Byrne, 2014). However, these levels had not been reached during the preliminary fed-batch culture (6 mM), suggesting that ammonia had little effect. On the other hand, the inhibitive lactate levels have not been previously evaluated for that cell line under the culture conditions employed.

To study the effect of lactate concentration on cell development, 5 different flasks, each containing different initial lactate concentrations, ranging from 0 to 100 mM were prepared. Each 125 mL Erlenmeyer flask with vent cap flask (Corning®, USA) was seeded with $0.3 \cdot 10^6$ $\nu_{\text{cell}} \cdot \text{mL}^{-1}$, in 30 mL EXCELL CHO DHFR^r medium (Sigma Aldrich, USA). The 5x30 mL medium was supplemented with 0, 25, 50, 75 or 100 mM lactate. A 1 mL sample was aseptically removed daily to determine the viable and dead cell densities, and to quantify the glucose and lactate present in the culture.

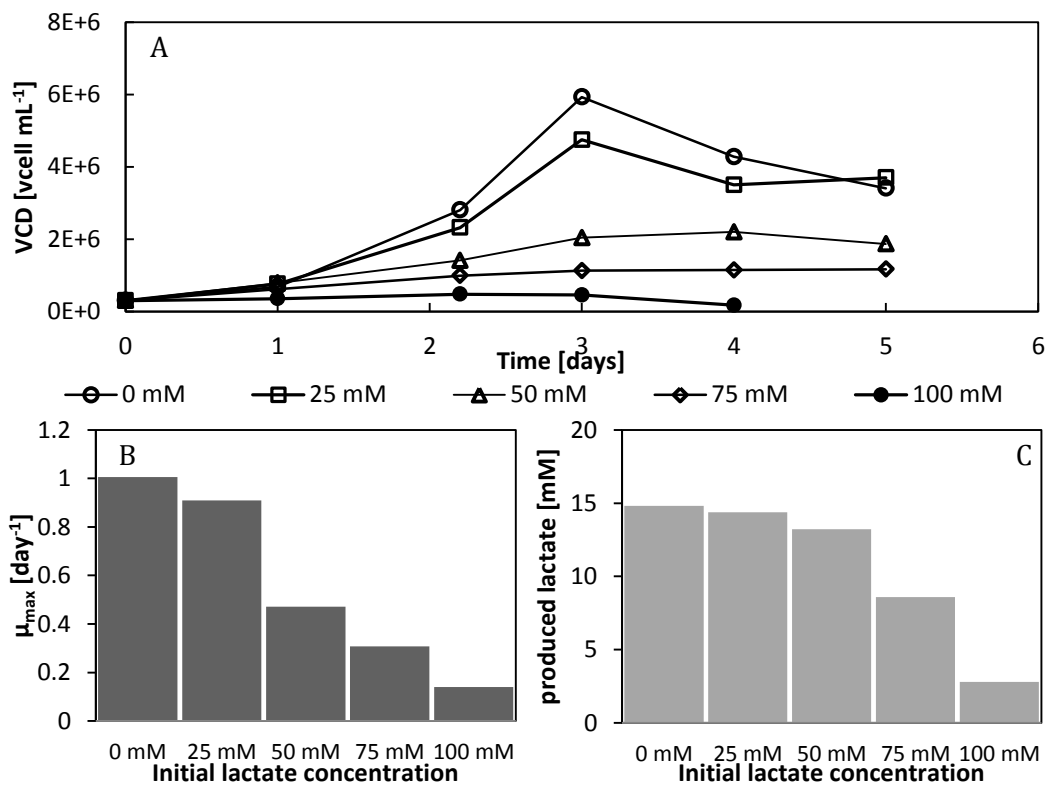


Figure 7.9 Effect of the initial lactate concentration on viable cell density (A), growth rate (B) and the produced lactate (C)

The experiment demonstrated how the CHO cell cultures are influenced by the presence of lactate and more importantly by the concentration of the metabolic by-product. The negative control flask that was not supplemented with lactate, grew to a maximum cell density of $5.93 \cdot 10^6 \text{ }_{\mu}\text{cell} \cdot \text{mL}^{-1}$, at a growth rate of 1.01 day^{-1} and produced 14.8 mM lactate. The maximum cell densities and growth rates observed in the lactate- spiked flasks were all inferior to the negative control and decreased with the initial lactate concentration, Figure 7.9. The cells in the presence of 50 mM lactate could only reach $2.2 \cdot 10^6 \text{ }_{\mu}\text{cell} \cdot \text{mL}^{-1}$, a density 63% inferior to the density generated in the negative control. Moreover, the growth rate evaluated in the 50 mM flask was reduced by 53% to 0.47 day^{-1} . Finally, the amounts of lactate produced in the spiked flasks were inferior to the control flask, and diminished with the initial lactate concentrations, Figure 7.9.

Lactate has a non-negligible, negative impact upon the development of the cells. In this experiment 100 mM lactate completely inhibited cell growth. Yet, these levels of lactate were not measured in the fed-batch culture (maximum measured 50 mM). In the flask cultures, the pH was not adjusted, and a drop in the pH was visually noticed with the changing colouration of the phenol red indicator. On the other hand, the pH in the fed-batch culture was maintained at $\text{pH} = 7.2 \pm 0.2$, with the addition of NaOH 2.5 M. Therefore, in addition to important concentrations of lactate, the NaOH addition caused an increase in osmolality, which may also have been detrimental to the cells (Lao and Toth, 1997; Zagari, 2012).

7.3.4. *Culture outcome*

Though the culture did not reach the targeted cell densities, and full microcapsule colonisation, it allowed to test the developed feed control feature inserted in the LabVIEW data acquisition VI, and to define culture condition limitations. The study showed that the CHO-DP12 cells, cultured in the EXCELL-CHO DHFR- medium, produced inhibitive amounts of lactate and after full conversation of the available glucose, that have not been previously observed in either the previous batch or perfusion operated cultures. The cell growth inhibition study demonstrated that the growth rate was reduced by 50 % in the presence of an initial lactate concentration of 50 mM. This concentration of lactate was measured on day 8, when the cell density plateaued. It must be noted that the test was undertaken in flask suspension cultures and results may vary from similar tests performed in microencapsulated mode or when cultivated in a bioreactor, with and without pH control.

Nevertheless, accurate real-time data was acquired in LabVIEW from the biomass monitor. Consequently, the feed was automatically initiated when the density achieved the preset value of $2.5 \cdot 10^6 \text{ }_{\nu}\text{cell} \cdot \text{mL}_{WV}^{-1}$, and from then on continuously delivered to the cells over a 28 hour period at a rate dictated primarily by the growth rate, and the viable cell density at time t . Though it seemed to have sustained the glucose and L-glutamine concentrations over the time frame, a longer controlled feed period would be necessary to prove the concept of the chosen control strategy to feed the CHO-DP12 cells (and applicable to other mammalian cells), based on the capacitance signal evolution.

7.4. Reduction of the initial glucose concentration to increase duration of control

The fourth section of this chapter involves designing a CHO-DP12 fed-batch culture with a controlled feed lasting a minimum of 2 days. This time frame would allow the collection of at least 3 off-line data points, including metabolite quantification and microcapsule stability analysis, to prove the concept of the feed strategy implemented in LabVIEW.

7.4.1. Culture method and simulation

The aim of this experiment was to extend the feeding period of the fed-batch culture by reducing the available glucose concentration of the medium in the first stage of the culture. The EXCELL CHO DHFR^r medium, composed of approximately $5.6 \text{ g} \cdot \text{L}^{-1}$ glucose was therefore replaced by the EXCELL 325 PF CHO (Sigma Aldrich, USA), which contains a lower glucose concentrations ($3.45 \text{ g} \cdot \text{L}^{-1}$ glucose). The culture was operated in two distinct phases: an initial batch phase, allowing the cells to proliferate, and a fed-batch phase which would be activated automatically once the viable cell density, estimated by dielectric spectroscopy, exceeded $1.25 \cdot 10^6 \text{ }_{\nu}\text{cell} \cdot \text{mL}_{WV}^{-1}$. At this stage of the culture, predicted to be day 3, the cells would have consumed 47% of the available glucose and 80% of the L-glutamine. Consequently, 10 mM glucose and 0.8 mM L-glutamine would be predicted to remain in the culture by the end of the batch phase, Figure 7.10. These concentrations are similar to the predicted and obtained values in the first feed controlled fed-batch, Figure 7.4 and Figure 7.7. Moreover, the initial culture volume was reduced to 1.2 L, and the feed medium the glucose and the L-glutamine concentrations were only enriched up to $30 \text{ g} \cdot \text{L}^{-1}$ (instead of $200 \text{ g} \cdot \text{L}^{-1}$) and 58.72 mM (instead of 148 mM), respectively. The choice of reducing the initial culture volume, the glucose and L-glutamine was taken to increase the potential dilution effect of the feed on the waste by-products and culture time.

If the cell growth inhibitive effect of the accumulated lactate concentration is correct, the cell growth would have stabilised by day 5.5, at $6.05 \cdot 10^6 \text{ } \nu_{\text{cell}} \cdot \text{mL}_{\text{WV}}^{-1}$. At this stage of the culture, the lactate would have accumulated to 50 mM, Figure 7.10B. This would allow a feed duration of 2.5 days. However, the prediction was extended to day 7, when the culture volume would have been filled to the full capacity of the eRC1 vessel. In this experiment, the microcapsules would not have been fully colonised, but up to $64.4 \cdot 10^6 \text{ } \nu_{\text{cell}} \cdot \text{mL}_{\text{capsules}}^{-1}$, representing 48.6% of the theoretical maximum cell density per packed microcapsule volume, based on an initial microcapsule to medium volume ratio of 25%.

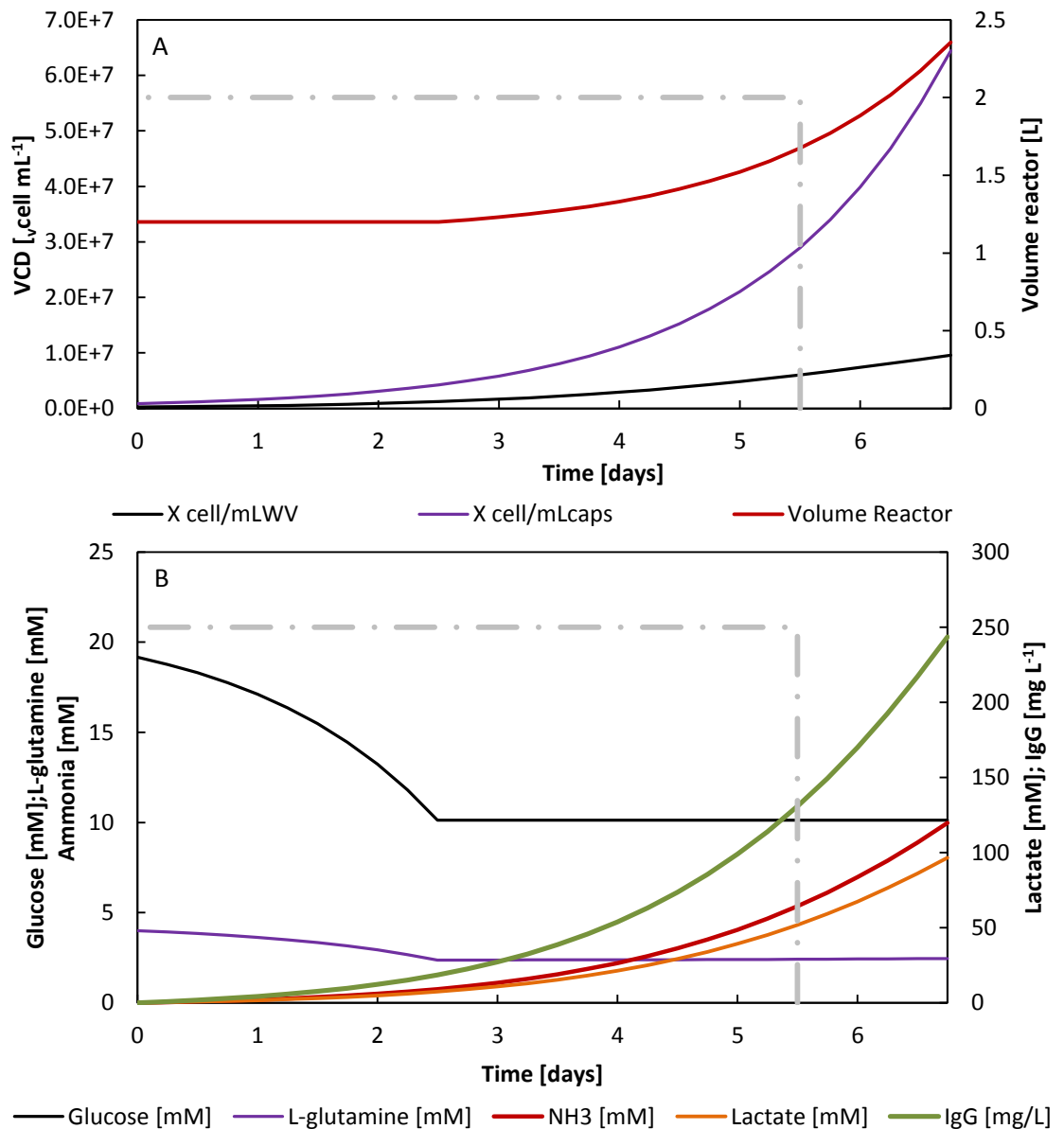


Figure 7.10 Predicted evolution of the culture variables throughout the second feed controlled culture, from inoculation until when the reactor would be completely filled. The model was constructed admitting that no lag phase or growth inhibition could be observed. The grey dashed-dot-dashed line represents the expected culture time based on the produced lactate concentration when would have reached 50 mM

7.4.2. Culture results

After encapsulating the CHO-DP12 cells and inoculating the pre-sterilised eRC1 vessel, the culture underwent a 1-day lag phase. Hence, the culture development was delayed by a day from the prediction. 3.64 days after inoculation, the viable cell density, estimated by continuous capacitance measurements at 580 kHz, set to dual frequency and with the polarisation correction switched on, was evaluated at $1.25 \cdot 10^6 \text{ }_{\nu}\text{cell} \cdot \text{mL}_{\text{WV}}^{-1}$, Figure 7.11A. Exceeding the pre-set density, initiated the controlled feeding protocol of the LabVIEW VI. In total, 76 mL of feed was supplemented to the culture, representing a feed volume 6.73-fold higher than previously, Figure 7.5B and Figure 7.11B. This result confirmed the model predictions and that it is possible to extend the fed-batch culture duration by reducing the glucose content of the initial medium, combined with increasing the time necessary to achieve inhibitory concentrations of lactate.

The feed was once again dependant on acquire dielectric signal and the evaluated cellular growth rate. A small drop in the estimated viable cell density was observed on day 4.16, which led to a short stabilisation of the supplied feed until the capacitance measurement increased once more, Figure 7.11. The culture reached a maximum cell density of $2.14 \cdot 10^6 \text{ }_{\nu}\text{cell} \cdot \text{mL}_{\text{WV}}^{-1}$, 6.3 days after inoculation. With the stationary and decline phases, the feeding of the culture ceased.

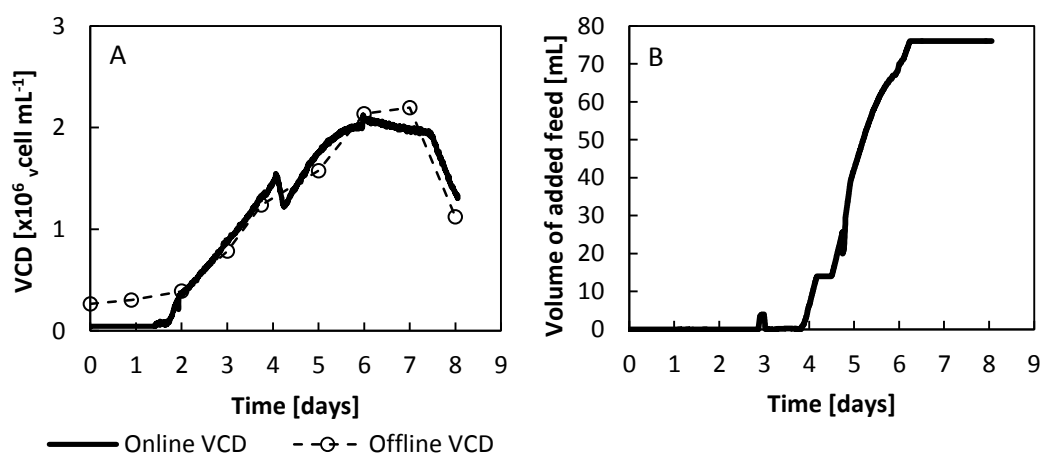


Figure 7.11 Evolution of the cell density and feed supplementation throughout the entire culture time of the second fed-batch culture. A: Development of the viable cell density estimated by dielectric spectroscopy and off line microscopic cell counts; B: Volume of feed medium added to the culture during the fed-batch phase

The metabolite analysis indicated that the cells had not suffered from glucose or L-glutamine limitation. As expected, by the end of the batch phase of the culture, 8.26 mM glucose and 1.45 mM L-glutamine remained, Figure 7.12. These levels of the two limiting substrates were then maintained by the controller during the feeding period. As illustrated in Figure 7.12, neither the glucose nor the L-glutamine accumulated to any significant degree. Once the feed stopped, on day 6, both glucose and L-glutamine concentrations fell.

As a consequence of metabolising the available glucose and L-glutamine, both lactate and ammonia were produced. The ammonia concentration increased continuously throughout the culture and by day 8 attained 6 mM. This concentration is less than the 15 mM that had been determined to initiate growth inhibition. The lactate was produced at a rate of $4.93 \cdot 10^{-9} \text{ day} \cdot \text{cell}^{-1} \cdot \text{mL}^{-1}$, which is similar to the value calculated for the batch cultures presented in Chapter 5. On day 6, the lactate concentration was 35 mM. To ensure that the pH was kept constant at $\text{pH} = 7.2 \pm 0.2$, the pH controller had to supply a total of 6.9 mL NaOH 2.5 M and 6.6 mL CaCl_2 125 mM, contributing to a rise in osmolality of the culture. Combined with the lactate concentration, this may once again have inhibited the cell growth.

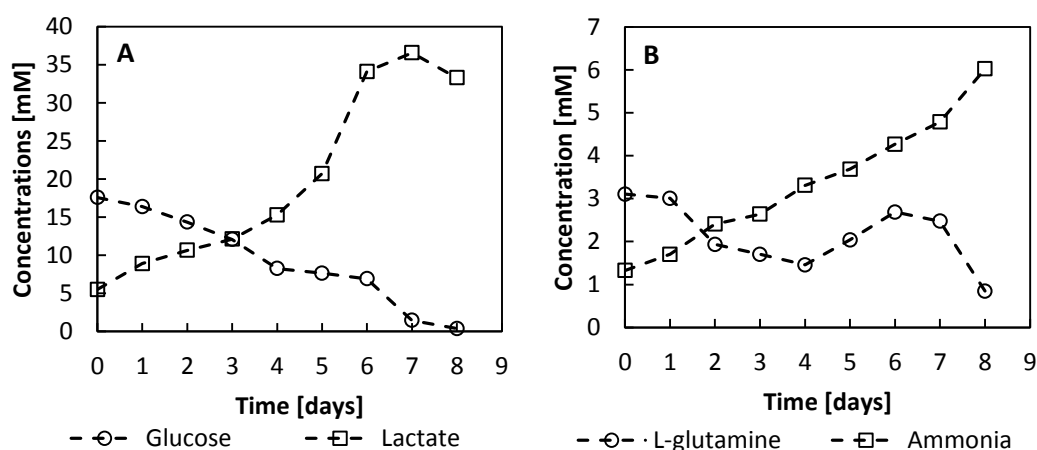


Figure 7.12 Evolution of glucose and lactate concentrations (A) and L-glutamine and ammonia concentrations (B) throughout the second adapted controlled feed fed-batch culture

The recombinant IgG₁ protein was synthesised at a rate of $29.8 \text{ pg} \cdot \text{cell}^{-1} \cdot \text{day}^{-1}$ during the exponential phase, from day 1 to day 5. By the end of the culture, the production then dropped to $15.6 \text{ pg} \cdot \text{cell}^{-1} \cdot \text{day}^{-1}$. The overall amount of product formed during the controlled fed-batch was 322 mg ($0.27 \text{ mg} \cdot \text{mL}^{-1} \cdot 1200 \text{ mL}$), Figure 7.13A.

In parallel to verifying the use of dielectric spectroscopy to monitor and control a feed, the aim for operating fed-batch cultures was to evaluate the microcapsule resistance to a nutrient feed. Though only, 76 mL of feed was supplemented, a small reduction in the packed microcapsule to working culture volume ratio and extracapsular cells were noticeable after day 6, during the stationary and decline phase, Figure 7.13. The reduction in microcapsules stability may be caused by the secretion of cellular metabolic products. In the literature, it is said that lactate, being a chelating agent, could destabilises the mechanical resistance of alginate gels (Thu et al., 1996b). Therefore, further investigation should be undertaken in order to determine

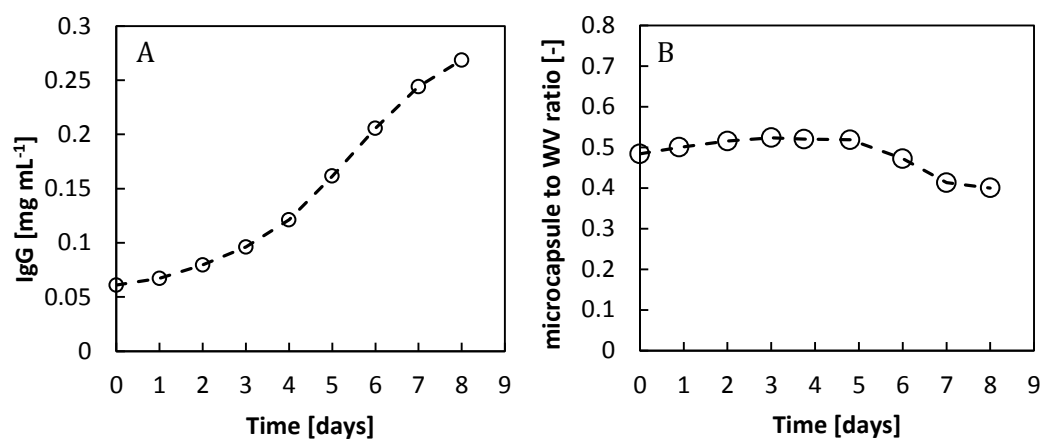


Figure 7.13 Production of rIgG1 (A), and evolution of the packed microcapsule to working volume (B) of the second adapted fed-batch.

7.5. Conclusions and outlook

The microencapsulated fed-batch cultures were continuously followed in real-time by dielectric spectroscopy. The capacitance measurements were continuously acquired within the tailored LabVIEW VI and computed into viable cell density values, based on the model previously conceived in Chapter 5. Besides the viable cell density, the online data was used to also accurately estimate the cellular growth rate. The same LabVIEW program then applied the online viable cell density and growth rate values to determine and output the required feed rate. The offline metabolite quantification demonstrated the cells were neither glucose nor glutamine limited. Instead, the concentrations of the two analysed limiting substrates were found to have stabilised, as foreseen in the prediction models.

It can be concluded that dielectric spectroscopy and the designed feeding strategy can be used to successfully control the supply of nutrients to microencapsulated CHO-DP12 cultures. The cells appear to be inhibited by the presence of metabolic by-products, probably lactate, and not from the exhaustion of an essential nutrient. Due to their nature, fed-batch cultures are often limited by the accumulation of harmful metabolic substances. Nevertheless, to optimise the outcome of the fed-batch, to increase the longevity of a culture and the overall productivity, numerous strategies can be undertaken. The proposed strategies in the literature vary from medium and feed optimisation, by substituting glucose and L-glutamine by galactose and glutamate, to cloning the gene of interest within a *glutamine synthetase* gene coding transfection plasmid and with a stringent clone selection (Liangzhi Xie and Weichang Zhou, 2005).

Chapter 8 Outcome, Outlook and Conclusion

Summary: This chapter closes the thesis. It introduces the problem questions once more before reviewing the findings of this work. The findings of this research answer all three questions that were stated in the introduction. The discussion then focuses on the contributions of the thesis to the current knowledge. Prior to this work, little or nothing was written on monitoring methods to estimate online the viable cell density of microencapsulated cultures, and therefore, the gap has been bridged. Next, the limitations of the study are discussed with recommendations for future investigation and process optimisation. Like many others, this work was faced with microcapsule instability and cell growth inhibition caused by the accumulation of metabolic waste products. Finally, this chapter concludes with stating that dielectric spectroscopy, from inoculation ($0.3 \cdot 10^6$ v cells \cdot mL $_{WV}^{-1}$), and biocalorimetry, in the eRC1, from densities above 10^7 v cells \cdot mL $_{WV}^{-1}$ are valid monitoring techniques, and dielectric spectroscopy can be used to control a feed rate of fed-bath cultures.

8.1. Introduction

This study set out to investigate the possibility of monitoring microencapsulated mammalian cell cultures. Microencapsulation not only has the potential for implanting cells into foreign bodies (Orive et al., 2004b; Zhang et al., 2008), but has also shown promising results for enhancing product quality and quantity in recombinant therapeutic manufacturing processes (Breguet et al., 2007b; Gugerli, 2003a). Microcapsules provide a semi-permeable shield, protecting the cells from mixing and gassing of the bulk in stirred tank reactors, whilst allowing the diffusion of metabolites, O₂ and CO₂ (Pajić-Lijaković et al., 2007; Zhao et al., 2013). The technology is nevertheless limited by the long-term instability of the microcapsules and by the lack of means to monitor cell growth, activity and viability.

Nowadays, regulations for producing therapeutic proteins are getting more and more stringent. Drug regulatory agencies are encouraging industries to use different monitoring methods in therapeutic drug production to have quick, continuous access to the different culture variables. This proposed manufacturing strategy has the aim of reducing manufacturing risks and batch-to-batch variability, by reacting as soon as a variable shifts from the desired trajectory. Thus, it would ensure product quality production reproducibility (Bakeev, 2005; Gnoth et al., 2007). As described in Chapter 2, many techniques are available for monitoring different variables of a culture, ranging from biomass, metabolites, O₂ consumption and CO₂ production to heat generation. Because the cells are not accessible to allow the use of some techniques such as turbidimetry or fluorometry, and because CO₂ is used to control the pH, dielectric spectroscopy and biocalorimetry were the two proposed methods in this thesis. Dielectric spectroscopy directly measures the biovolume of a culture, whilst biocalorimetry indirectly evaluates the cell density by determining the heat generated by the metabolic activity of the live cells. The study sought to answer these three primary questions:

1. Can we monitor encapsulated cells by dielectric spectroscopy? And are there any necessary mathematical corrections to make?
2. Can we monitor the cell metabolic activity in a bench calorimeter, the Bio-RC1?
3. Can either dielectric spectroscopy or biocalorimetry be used as monitoring method to provide in real-time precise and accurate biomass information for control of nutrient feed to cultures?

Each question was answered in their respective chapter, chapter 5, chapter 6 and chapter 7. For the manufacturing of a therapeutic recombinant protein, it is desired to achieve high cell densities to enhance the overall productivity of the process. Therefore, a

secondary goal that the study aimed to fulfil was to see to what extent can the microcapsules be colonised by the CHO-DP12 cells, and how does the viability evolve when the microcapsules are fully colonised?

This final chapter of the thesis will first summarise the findings of the study, present the limitations of the study before recommending different focus areas future research should consider before drawing a final conclusion.

8.2. Findings of the study

8.2.1. Elaboration of an automated monitoring and feed control program

The need for a tailored data acquisition program for monitoring microencapsulated CHO-cell cultures, with the potential to add a feed control feature, was first designed and discussed in Chapter 3. The data acquisition system was designed in LabVIEW. LabVIEW is renowned for facilitating the creation of robust data acquisition and instrumental control programs. The elaborated data acquisition VI was graphically coded and proved itself to be easily transferred from the Minifors bioreactor to the Bio-RC1 setups. Not only was it capable of acquiring data from the different instruments in parallel to monitor different culture variables (capacitance, conductivity, pH, reactor and jacket temperatures, etc.). The VI was also capable of mathematically modelling the data received from each frequency scan to draw out further information: the cell size and cell number. Moreover, as the work progressed, the VI was easily modified in order to add a feed control feature. The implemented feed control calculates the necessary feed rate based on the real-time viable cell density, computed from the measured online capacitance, and the growth rate. The growth rate was estimated by plotting the calculated natural logarithm of the capacitance against the culture time and calculating the slope of the linear regression, after the operator set period of time ($t_{\mu,calc} = 4 \text{ hours} = 15\% \cdot t_d$). The determined feed rate was then converted into voltage which was then output to the connected feed pump.

8.2.2. Are dielectric spectroscopy and macrocalorimetry valid methods to monitor microencapsulated CHO cell cultures?

Both dielectric spectroscopy and biocalorimetry permitted to follow in real-time the evolution of the viable cell density of microencapsulated CHO-DP12 cell cultures. The acquired capacitance and heat flow rate measurements, plotted against the viable cell density determined offline by microscopy, generated well correlated linear regressions. These correlations were then applied as calibration models and also provided additional cell line characteristics information (specific capacitance and specific heat flow rate).

As presented in chapter 2 and chapter 5, dielectric spectroscopy is linearly proportional to the viable cell density, and more precisely to the biovolume. The specific capacitance of the CHO-DP12 cell line of $1.44 \cdot 10^6 \frac{pF \cdot mL}{cm \cdot cell}$ did not vary from suspension to microencapsulated cultures. The limit of detection of this online monitoring method is $0.26 \cdot 10^6 \nu_{cell} \cdot mL_{WV}^{-1}$, similar to what was found in preceding studies (Ducommun et al., 2002a). Frequency scans, modelled using the Cole-Cole equation in LabVIEW, at densities superior to $2 \cdot 10^6 \nu_{cell} \cdot mL_{WV}^{-1}$ not only gave information upon the biovolume, but also defined the cell size and cell number per unit volume.

The continuous capacitance measurements of the CHO-DP12 cell culture at 580 kHz, dual frequency and with the polarisation correction switched on, gave easily accessible and immediate information upon the evolution of the viable cell density. Additionally, as presented in chapter 7, the feed rate of the fed-batch cultures was controlled based on the viable cell density and growth rate. The feed was continuous, yet the rate was determined by estimating the amounts of glucose and L-glutamine required by the cells. The feed rate was shown to be dependent upon the estimated growth rate and lasted for 2.5 days. Though the feed period was short, it was sufficiently long enough to demonstrate the effectiveness of the feed strategy: both glucose and L-glutamine concentrations remained stable throughout the feeding period, proving the cells were not glucose nor L-glutamine limited.

In chapter 6, the heat flow rate, produced by the cells grown and assessed by the Bio-RC1 biocalorimeter was used, in combination with dielectric spectroscopy, as a cell growth monitoring tool. The cells, during the exponential phase, growing at a specific growth rate of 0.62 days^{-1} generated a heat at $74.77 \text{ pW} \cdot \text{cells}^{-1}$. This method, at a scale of 1.4 L working volume, in the Bio-RC1 equipped for perfusion culture, had a limit of detection of $8.87 \cdot 10^6 \nu_{cell} \cdot mL_{WV}^{-1}$, and a limit of quantification of $26.88 \cdot 10^6 \nu_{cell} \cdot mL_{WV}^{-1}$. The heat flow rate is dependent upon the growth rate, and others have written about applying this cell culture propriety to control the growth rate of microbial cultures (Biener et al., 2012; Schuler and Marison, 2012). Similar to what has been described in the literature, the diminution of the growth rate from 0.62 days^{-1} to 0.29 days^{-1} resulted in a reduction in specific heat flow rate, and consequently in a stabilisation in the heat signal.

8.3. Theoretical implications

The literature reviews in Chapter 2 demonstrated that both dielectric spectroscopy and macrocalorimetry have been successfully used to monitor and control microbial cultures (Biener et al., 2012; Dabros et al., 2010; Schuler et al., 2012), and dielectric spectroscopy and microcalorimetry were reported to be valid methods to monitor and control mammalian cell cultures (Carvell and Dowd, 2006a; Ducommun et al., 2002a; Guan et al., 1998; Justice et al., 2011a). However, two voids existed. On the one hand, though microencapsulating cells seems to be a promising method to culture mammalian cells for glycosylated recombinant therapeutic protein manufacturing purposes, yet no evidence of any real-time cell development monitoring techniques had been reported. On the other hand, bench scale calorimetry seemed to have never been investigated nor proposed to monitor cell cultures. As a matter of fact, it is true that at bench scale, cell densities above $1 \cdot 10^7 \text{ cell} \cdot \text{mL}^{-1}$ are realistically required to obtain a significant signal, above the limit of detection. Nevertheless, in larger vessels, and even 15m^3 production tanks, the surface area to volume ratio is much smaller, thus the heat loss to the environment is less. Therefore, $T_r - T_j$ would be greater and would significantly overcome the signal to noise ratio.

This work demonstrates that dielectric spectroscopy is a reliable tool to monitor cell development and to continuously estimate the viable cell density of microencapsulated cultures. As a result, the method also provides the online information needed to control the feed rate necessary to provide the cells with a sufficient amount of nutrients to proliferate. It also shows the potential biocalorimetry could have in either monitoring high cell density cultures at bench scale or to monitor the cell activity at a much larger scale, in manufacturing processes.

8.4. Limitations of the study and recommendations for future research

The three set-out research questions have been positively answered in chapter 5, 6 and 7. However, the study was limited by two important factors. In chapter 6, a loss in microcapsule stability was noticed after 2 to 3 days of perfusion feed. Different studies have reported the benefits of microencapsulating cells, but have also faced microcapsule instability issues (Breguet et al., 2007b; Orive et al., 2004b). The calcium-alginate-poly-L-lysine-alginate microcapsules are formed by the poly-L-lysine electrostatically interacting with the alginate core. It was hypothesised that the high perfused feed rate may have destabilised this electrostatic interaction equilibrium by gradually washing out the structural components. As the microcapsules lost their mechanical resistance, they

ruptured and were removed with the released cells by the outflow of spent media. To reach the full microcapsule colonisation or the targeted cell densities superior to $10^8 \text{ } \nu\text{cell} \cdot \text{mL}_{\text{WV}}^{-1}$, and exceed the limit of quantification of the Bio-RC1 of $26.88 \cdot 10^6 \text{ } \nu\text{cell} \cdot \text{mL}_{\text{WV}}^{-1}$ (equipped for perfusion cultures), further investigation into microcapsule stabilisation would be required. The polyelectrolyte microcapsules could be strengthened by exchanging the poly-L-lysine by another polycation, such as poly-ornithine or chitosan (Bartkowiak and Hunkeler, 1999; Darrabie et al., 2005). Another alternative would be replacing the polyelectrolyte microcapsules by covalently bound microcapsules, which appear to be mechanically more resistance (Edwards-Lévy and Lévy, 1999).

The first encountered limitation, lead the work towards feeding the microencapsulated cells by operating the feed in fed-batch to limit the polyelectrolyte dilution effect. To avoid important fluctuations in nutrients caused by manual pulse feeds, an exponential feed strategy was chosen. The feed rate, controlled in LabVIEW, based on the viable cell density and the growth rate, lasted 2.5 days. In spite of the culture not being glucose or L-glutamine limited, the cell growth was inhibited. According to the literature and to the lactate study, the accumulation of waste by-products, essentially lactate, was a deemed as a probable cause for the cells to prematurely enter the stationary and decline phases. To further extend the feed time and the maximum cell density, a medium optimisation would be recommended, to reduce the production rate of the harmful metabolic by-products.

Finally, in this work, a suspension cell line was selected in order to enable a comparison study between suspension and microencapsulated cultures and more importantly the influence of the presence of microcapsules upon the dielectric signal. However, microcapsules potentially offer a surface, necessary for the development of adherent cell lines. Transferring the developed method to monitor microencapsulated cell cultures in a stirred tank reactor to the culturing of an adherent cell line or even a stem cell line would increase the potential of such cultures and overall productivity.

8.5. Conclusion

Microcapsules offer cells a prosperous environment, similar to the cells' original natural environment. Microcapsules also create a barrier to the cells in perfusion cultures, and can be separated from the outflow of spent media using a simple wire mesh. The cells being entrapped, however, are inaccessible for monitoring purposes. This work proved that both dielectric spectroscopy, from inoculation, and biocalorimetry, with viable cell densities above $10^7 \text{ } \nu\text{cells} \cdot \text{mL}_{\text{WV}}^{-1}$ are valid methods to monitor microencapsulated CHO cell cultures. Furthermore, a simple controlled feed strategy can be implemented in

LabVIEW, with dielectric spectroscopy providing the necessary biomass information, to feed the cells adequately, in fed-batch cultures. This brings microencapsulation one step forward towards an industrial application for the manufacturing of therapeutics.

References

- Ahn, W.S., Antoniewicz, M.R., 2011. Metabolic flux analysis of CHO cells at growth and non-growth phases using isotopic tracers and mass spectrometry. *Metab. Eng.* 13, 598–609. doi:10.1016/j.ymben.2011.07.002
- Altamirano, C., Illanes, A., Becerra, S., Cairó, J.J., Gòdia, F., 2006. Considerations on the lactate consumption by CHO cells in the presence of galactose. *J. Biotechnol.* 125, 547–556. doi:10.1016/j.jbiotec.2006.03.023
- Altamirano, C., Paredes, C., Illanes, A., Cairó, J.J., Gòdia, F., 2004. Strategies for fed-batch cultivation of t-PA producing CHO cells: substitution of glucose and glutamine and rational design of culture medium. *J. Biotechnol.* 110, 171–179. doi:10.1016/j.jbiotec.2004.02.004
- Andò, B., Carbone, D., 2009. A LabVIEW environment to compensate temperature-driven fluctuations in the signal from continuously running spring gravimeters. *Comput. Geosci.* 35, 2129–2136. doi:10.1016/j.cageo.2008.12.007
- Bakeev, K.A., 2005. Process analytical technology: spectroscopic tools and implementation strategies for the chemical and pharmaceutical industries. Blackwell Pub, Ames, Iowa.
- Bartkowiak, A., Hunkeler, D., 1999. Alginate–Oligochitosan Microcapsules: A Mechanistic Study Relating Membrane and Capsule Properties to Reaction Conditions. *Chem. Mater.* 11, 2486–2492. doi:10.1021/cm9910456
- Biener, R., Steinkämper, A., Hofmann, J., 2010. Calorimetric control for high cell density cultivation of a recombinant *Escherichia coli* strain. *J. Biotechnol.* 146, 45–53. doi:10.1016/j.jbiotec.2010.01.004
- Biener, R., Steinkämper, A., Horn, T., 2012. Calorimetric control of the specific growth rate during fed-batch cultures of *Saccharomyces cerevisiae*. *J. Biotechnol.* 160, 195–201. doi:10.1016/j.jbiotec.2012.03.006
- Brandon Downey, Lisa Graham, 2013. The Use of Dielectric Scanning to Probe for Cellular Biomass, Viability, and Morphology In Laboratory, Pilot, and Industrial Bioreactors.
- Breguet, V., Gugerli, R., von Stockar, U., Marison, I.W., 2007a. CHO immobilization in alginate/poly-l-lysine microcapsules: an understanding of potential and limitations. *Cytotechnology* 53, 81–93. doi:10.1007/s10616-007-9045-8
- Breguet, V., Gugerli, R., von Stockar, U., Marison, I.W., 2007b. CHO immobilization in alginate/poly-l-lysine microcapsules: an understanding of potential and limitations. *Cytotechnology* 53, 81–93. doi:10.1007/s10616-007-9045-8
- Breguet, V., Stockar, U. von, Marison, I.W., 2007c. Characterization of Alginate Lyase Activity on Liquid, Gelled, and Complexed States of Alginate. *Biotechnol. Prog.* 23, 1223–1230. doi:10.1021/bp070150e

- Byrne, K., 2014. High density CHO cell cultures: Improved productivity and product quality (doctoral). Dublin City University. School of Biotechnology.
- Cacciuttolo, M., 2007. Perfusion or fed-batch? A matter of perspective, in: *Cell Culture and Upstream Processing*. Taylor & Francis, pp. 173–183.
- Cairó, J.J., Gódiá, F., 2005. Cell Metabolism, in: *Cell Culture Technology for Pharmaceutical and Cell-Based Therapies, Biotechnology and Bioprocessing*. CRC Press, pp. 81–112.
- Cannizzaro, C., Gügerli, R., Marison, I., von Stockar, U., 2003a. On-line biomass monitoring of CHO perfusion culture with scanning dielectric spectroscopy. *Biotechnol. Bioeng.* 84, 597–610. doi:10.1002/bit.10809
- Cannizzaro, C., Gügerli, R., Marison, I., von Stockar, U., 2003b. On-line biomass monitoring of CHO perfusion culture with scanning dielectric spectroscopy. *Biotechnol. Bioeng.* 84, 597–610. doi:10.1002/bit.10809
- Carloni, A., Turner, A.P.F., Flickinger, M.C., 2009. Bioprocess Monitoring, in: *Encyclopedia of Industrial Biotechnology*. John Wiley & Sons, Inc.
- Carvell, J.P., Bhat, A., Patel, P.M., Markx, G.H., 2006. Recent developments in using scanning radio-frequency impedance measurements on cell culture processes. *Bioprocessing* 44–47.
- Carvell, J.P., Dowd, J.E., 2006a. On-line Measurements and Control of Viable Cell Density in Cell Culture Manufacturing Processes using Radio-frequency Impedance. *Cytotechnology* 50, 35–48. doi:10.1007/s10616-005-3974-x
- Carvell, J.P., Dowd, J.E., 2006b. On-line Measurements and Control of Viable Cell Density in Cell Culture Manufacturing Processes using Radio-frequency Impedance. *Cytotechnology* 50, 35–48. doi:10.1007/s10616-005-3974-x
- Catena, R., Santos, E., Orive, G., Hernández, R.M., Pedraz, J.L., Calvo, A., 2010. Improvement of the monitoring and biosafety of encapsulated cells using the SFGNESTGL triple reporter system. *J. Controlled Release* 146, 93–98. doi:10.1016/j.jconrel.2010.05.018
- Chee Fung Wong, D., Tin Kam Wong, K., Tang Goh, L., Kiat Heng, C., Gek Sim Yap, M., 2005. Impact of dynamic online fed-batch strategies on metabolism, productivity and N-glycosylation quality in CHO cell cultures. *Biotechnol. Bioeng.* 89, 164–177. doi:10.1002/bit.20317
- Chen, Z., Lovett, D., Morris, J., 2011. Process analytical technologies and real time process control a review of some spectroscopic issues and challenges. *J. Process Control* 21, 1467–1482. doi:10.1016/j.jprocont.2011.06.024
- Chisti, Y., 2000. Animal-cell damage in sparged bioreactors. *Trends Biotechnol.* 18, 420–432. doi:10.1016/S0167-7799(00)01474-8
- Chu, L., Robinson, D.K., 2001. Industrial choices for protein production by large-scale cell culture. *Curr. Opin. Biotechnol.* 12, 180–187. doi:10.1016/S0958-1669(00)00197-X
- Cruz, H.J., Freitas, C.M., Alves, P.M., Moreira, J.L., Carrondo, M.J.T., 2000. Effects of ammonia and lactate on growth, metabolism, and productivity of BHK cells. *Enzyme Microb. Technol.* 27, 43–52. doi:10.1016/S0141-0229(00)00151-4
- Dabros, M., Amrhein, M., Bonvin, D., Marison, I.W., von Stockar, U., 2009a. Data reconciliation of concentration estimates from mid-infrared and dielectric spectral measurements for improved on-line monitoring of bioprocesses. *Biotechnol. Prog.* 25, 578–588. doi:10.1002/btpr.143
- Dabros, M., Dennewald, D., Currie, D.J., Lee, M.H., Todd, R.W., Marison, I.W., Stockar, U. von, von Stockar, U., 2009b. Cole–Cole, linear and multivariate modeling of capacitance data for on-line monitoring of biomass. *Bioprocess Biosyst. Eng.* 32, 161–173. doi:10.1007/s00449-008-0234-4
- Dabros, M., Dennewald, D., Currie, D., Lee, M., Todd, R., Marison, I., von Stockar, U., 2009c. Cole–Cole, linear and multivariate modeling of capacitance data for on-line monitoring of biomass. *Bioprocess Biosyst. Eng.* 32, 161–173. doi:10.1007/s00449-008-0234-4

- Dabros, M., Schuler, M., Marison, I., 2010. Simple control of specific growth rate in biotechnological fed-batch processes based on enhanced online measurements of biomass. *Bioprocess Biosyst. Eng.* 33, 1109–1118. doi:10.1007/s00449-010-0438-2
- Darrabie, M.D., Kendall Jr., W.F., Opara, E.C., 2005. Characteristics of Poly-l-Ornithine-coated alginate microcapsules. *Biomaterials* 26, 6846–6852. doi:10.1016/j.biomaterials.2005.05.009
- Davey, C., 1993. *The Biomass Monitor Source Book*. Aber Instruments Ltd (Science Park, Aberystwyth).
- Davey, C.L., Davey, H.M., Kell, D.B., 1992a. On the dielectric properties of cell suspensions at high volume fractions. *J. Electroanal. Chem.* 343, 319–340. doi:10.1016/0022-0728(92)85097-M
- Davey, C.L., Davey, H.M., Kell, D.B., 1992b. On the dielectric properties of cell suspensions at high volume fractions. *J. Electroanal. Chem.* 28, 319–340. doi:10.1016/0302-4598(92)80023-A
- Davey, C.L., Davey, H.M., Kell, D.B., Todd, R.W., 1993. Introduction to the dielectric estimation of cellular biomass in real time, with special emphasis on measurements at high volume fractions. *Anal. Chim. Acta* 279, 155–161. doi:10.1016/0003-2670(93)85078-X
- Davidovich-Pinhas, M., Bianco-Peled, H., 2010. A quantitative analysis of alginate swelling. *Carbohydr. Polym.* 79, 1020–1027. doi:10.1016/j.carbpol.2009.10.036
- Demain, A.L., Vaishnav, P., 2009. Production of recombinant proteins by microbes and higher organisms. *Biotechnol. Adv.* 27, 297–306. doi:10.1016/j.biotechadv.2009.01.008
- Doran, P.M., 1995a. 9 - Mass Transfer, in: Doran, P.M. (Ed.), *Bioprocess Engineering Principles*. Academic Press, London, pp. 190–217.
- Doran, P.M., 1995b. 5 - Energy Balances, in: Doran, P.M. (Ed.), *Bioprocess Engineering Principles*. Academic Press, London, pp. 86–109.
- Doran, P.M., 1995c. 8 - Heat Transfer, in: Doran, P.M. (Ed.), *Bioprocess Engineering Principles*. Academic Press, London, pp. 164–189.
- Doran, P.M., 1995d. 13 - Reactor Engineering, in: Doran, P.M. (Ed.), *Bioprocess Engineering Principles*. Academic Press, London, pp. 333–391.
- Dorresteyn, R.C., Numan, K.H., de Gooijer, C.D., Tramper, J., Beuvery, E.C., 1996. On-line estimation of the biomass activity during animal-cell cultivations. *Biotechnol. Bioeng.* 51, 206–214. doi:10.1002/(SICI)1097-0290(19960720)51:2<206::AID-BIT10>3.0.CO;2-K
- Ducommun, P., Kadouri, A., von Stockar, U., Marison, I.W., 2002a. On-line determination of animal cell concentration in two industrial high-density culture processes by dielectric spectroscopy. *Biotechnol. Bioeng.* 77, 316–323. doi:10.1002/bit.1197
- Ducommun, P., Kadouri, A., von Stockar, U., Marison, I.W., 2002b. On-line determination of animal cell concentration in two industrial high-density culture processes by dielectric spectroscopy. *Biotechnol. Bioeng.* 77, 316–323. doi:10.1002/bit.1197
- Edwards-Lévy, F., Lévy, M.-C., 1999. Serum albumin–alginate coated beads: mechanical properties and stability. *Biomaterials* 20, 2069–2084. doi:10.1016/S0142-9612(99)00111-8
- El Wajgali, A., Esteban, G., Fournier, F., Pinton, H., Marc, A., 2013a. Impact of microcarrier coverage on using permittivity for on-line monitoring high adherent Vero cell densities in perfusion bioreactors. *Biochem. Eng. J.* 70, 173–179. doi:10.1016/j.bej.2012.11.001
- El Wajgali, A., Esteban, G., Fournier, F., Pinton, H., Marc, A., 2013b. Impact of microcarrier coverage on using permittivity for on-line monitoring high adherent Vero cell densities in perfusion bioreactors. *Biochem. Eng. J.* 70, 173–179. doi:10.1016/j.bej.2012.11.001

- Ferrer-Mirallas, N., Domingo-Espín, J., Corchero, J.L., Vázquez, E., Villaverde, A., 2009. Microbial factories for recombinant pharmaceuticals. *Microb. Cell Factories* 8, 17. doi:10.1186/1475-2859-8-17
- García-Payo, M.C., Ampuero, S., Liu, J.S., Marison, I.W., von Stockar, U., 2002. The development and characterization of a high resolution bio-reaction calorimeter for weakly exothermic cultures. *Thermochim. Acta* 391, 25–39. doi:10.1016/S0040-6031(02)00161-2
- Gnoth, S., Jenzsch, M., Simutis, R., Lübbert, A., 2007. Process Analytical Technology (PAT): Batch-to-batch reproducibility of fermentation processes by robust process operational design and control. *J. Biotechnol., Advances in Biochemical Engineering Science* 132, 180–186. doi:10.1016/j.jbiotec.2007.03.020
- Gombotz, W.R., Wee, S., 1998. Protein release from alginate matrices. *Adv. Drug Deliv. Rev.* 31, 267–285. doi:10.1016/S0169-409X(97)00124-5
- Guan, Y., Evans, P.M., Kemp, R.B., 1998. Specific heat flow rate: An on-line monitor and potential control variable of specific metabolic rate in animal cell culture that combines microcalorimetry with dielectric spectroscopy. *Biotechnol. Bioeng.* 58, 464–477. doi:10.1002/(SICI)1097-0290(19980605)58:5<464::AID-BIT2>3.0.CO;2-B
- Guan, Y.H., Kemp, R.B., 1999. On-line heat flux measurements improve the culture medium for the growth and productivity of genetically engineered CHO cells. *Cytotechnology* 30, 107–120. doi:10.1023/A:1008038515285
- Gugerli, R., 2003a. Polyelectrolyte-complex and covalent-complex microcapsules for encapsulation of mammalian cells: potential and limitations (PhD). EPFL, Lausanne, Switzerland.
- Gugerli, R., 2003b. Polyelectrolyte-complex and covalent-complex microcapsules for encapsulation of mammalian cells: potential and limitations. Lausanne, Switzerland.
- Han, W.S., Stillman, G.A., Lu, M., Lu, C., McPherson, B.J., Park, E., 2010. Evaluation of potential nonisothermal processes and heat transport during CO₂ sequestration. *J. Geophys. Res. Solid Earth* 115, B07209. doi:10.1029/2009JB006745
- Heinzen, C., Berger, A., Marison, I., 2004. Use of Vibration Technology for Jet Break-Up for Encapsulation of Cells and Liquids in Monodisperse Microcapsules, in: Nedović, V., Willaert, R. (Eds.), *Fundamentals of Cell Immobilisation Biotechnology, Focus on Biotechnology*. Springer Netherlands, pp. 257–275.
- Hernández, L.Y., Castro, D., de la A Vitón, P., Pérez, O., Rodríguez, M., 2009. Modelation of growth kinetics of mammalian cells in perfusion culture. *Biotechnol. Apl.* 26, 232–236.
- Hübner, H., Buchholz, R., Flickinger, M.C., 2009. Microencapsulation, in: *Encyclopedia of Industrial Biotechnology*. John Wiley & Sons, Inc.
- Janssen, M., Patiño, R., Stockar, U. von, 2005. Application of bench-scale biocalorimetry to photoautotrophic cultures. *Thermochim. Acta* 435, 18–27. doi:10.1016/j.tca.2005.04.024
- Johnston, W.M., Hanna, J.R.P., Millar, R.J., 2004. Advances in Dataflow Programming Languages. *ACM Comput Surv* 36, 1–34. doi:10.1145/1013208.1013209
- Justice, C., Brix, A., Freimark, D., Kraume, M., Pfromm, P., Eichenmueller, B., Czermak, P., 2011a. Process control in cell culture technology using dielectric spectroscopy. *Biotechnol. Adv.* 29, 391–401. doi:10.1016/j.biotechadv.2011.03.002
- Justice, C., Brix, A., Freimark, D., Kraume, M., Pfromm, P., Eichenmueller, B., Czermak, P., 2011b. Process control in cell culture technology using dielectric spectroscopy. *Biotechnol. Adv.* 29, 391–401. doi:10.1016/j.biotechadv.2011.03.002
- Kang, A., Park, J., Ju, J., Jeong, G.S., Lee, S.-H., 2014. Cell encapsulation via microtechnologies. *Biomaterials* 35, 2651–2663. doi:10.1016/j.biomaterials.2013.12.073

- Keane, J.T., Ryan, D., Gray, P.P., 2003. Effect of shear stress on expression of a recombinant protein by Chinese hamster ovary cells. *Biotechnol. Bioeng.* 81, 211–220. doi:10.1002/bit.10472
- Kemp, R.B., 2000. “Fire burn and cauldron bubble” (W. Shakespeare): what the calorimetric–respirometric (CR) ratio does for our understanding of cells? *Thermochim. Acta* 355, 115–124. doi:10.1016/S0040-6031(00)00442-1
- Kiviharju, K., Salonen, K., Moilanen, U., Eerikäinen, T., 2008. Biomass measurement online: the performance of in situ measurements and software sensors. *J. Ind. Microbiol. Biotechnol.* 35, 657–665. doi:10.1007/s10295-008-0346-5
- Kong, D., Gentz, R., Zhang, J., 1998. Long-term stable production of monocyte-colony inhibition factor (M-CIF) from CHO microcarrier perfusion cultures. *Cytotechnology* 26, 131–138. doi:10.1023/A:1007997412002
- Kuwae, S., Ohda, T., Tamashima, H., Miki, H., Kobayashi, K., 2005. Development of a fed-batch culture process for enhanced production of recombinant human antithrombin by Chinese hamster ovary cells. *J. Biosci. Bioeng.* 100, 502–510. doi:10.1263/jbb.100.502
- Lao, M.-S., Toth, D., 1997. Effects of Ammonium and Lactate on Growth and Metabolism of a Recombinant Chinese Hamster Ovary Cell Culture. *Biotechnol. Prog.* 13, 688–691. doi:10.1021/bp9602360
- Liangzhi Xie, Weichang Zhou, 2005. Fed-Batch Cultivation of Mammalian Cells for the Production of Recombinant Proteins, in: *Cell Culture Technology for Pharmaceutical and Cell-Based Therapies, Biotechnology and Bioprocessing*. CRC Press, pp. 349–386.
- Liu, J.-S., Marison, I.W., von Stockar, U., 2001. Microbial growth by a net heat up-take: A calorimetric and thermodynamic study on acetotrophic methanogenesis by *Methanosarcina barkeri*. *Biotechnol. Bioeng.* 75, 170–180. doi:10.1002/bit.1176
- Luellau, E., Fenge, C., 2005. Cell Culture Bioreactors, in: *Cell Culture Technology for Pharmaceutical and Cell-Based Therapies, Biotechnology and Bioprocessing*. CRC Press, pp. 155–224.
- Ma, J., Qi, W.T., Yang, L.N., Yu, W.T., Xie, Y.B., Wang, W., Ma, X.J., Xu, F., Sun, L.X., 2007. Microcalorimetric study on the growth and metabolism of microencapsulated microbial cell culture. *J. Microbiol. Methods* 68, 172–177. doi:10.1016/j.mimet.2006.07.007
- Marison, I., Liu, J.-S., Ampuero, S., Von Stockar, U., Schenker, B., 1998. Biological reaction calorimetry: Development of high sensitivity bio-calorimeters. *Thermochim. Acta* 309, 157–173. doi:10.1016/S0040-6031(97)00424-3
- Mark Riley, 2005. Instrumentation and Process Control, in: *Cell Culture Technology for Pharmaceutical and Cell-Based Therapies, Biotechnology and Bioprocessing*. CRC Press, pp. 249–297.
- Marks, D.M., 2003. Equipment design considerations for large scale cell culture. *Cytotechnology* 42, 21–33. doi:10.1023/A:1026103405618
- Markx, G.H., Davey, C.L., 1999a. The dielectric properties of biological cells at radiofrequencies: applications in biotechnology. *Enzyme Microb. Technol.* 25, 161–171. doi:10.1016/S0141-0229(99)00008-3
- Markx, G.H., Davey, C.L., 1999b. The dielectric properties of biological cells at radiofrequencies: applications in biotechnology. *Enzyme Microb. Technol.* 25, 161–171. doi:10.1016/S0141-0229(99)00008-3
- Markx, G.H., Davey, C.L., Kell, D.B., 1991. To what extent is the magnitude of the Cole-Cole α of the β -dielectric dispersion of cell suspensions explicable in terms of the cell size distribution? *Bioelectrochem. Bioenerg.* 25, 195–211. doi:10.1016/0302-4598(91)87003-Y
- Martínez, J.L., Liu, L., Petranovic, D., Nielsen, J., 2012. Pharmaceutical protein production by yeast: towards production of human blood proteins by microbial fermentation. *Curr. Opin. Biotechnol.* 23, 965–971. doi:10.1016/j.copbio.2012.03.011

- Maskow, T., Paufler, S., n.d. What does calorimetry and thermodynamics of living cells tell us? *Methods*. doi:10.1016/j.ymeth.2014.10.035
- Meghrou, J., Mahmoud, W., Jacob, D., Chubet, R., Cox, M., Kamen, A.A., 2009. Development of a simple and high-yielding fed-batch process for the production of influenza vaccines. *Vaccine* 28, 309–316. doi:10.1016/j.vaccine.2009.10.048
- Nienow, A.W., 2006. Reactor Engineering in Large Scale Animal Cell Culture. *Cytotechnology* 50, 9–33. doi:10.1007/s10616-006-9005-8
- Noll, T., Biselli, M., 1998a. Dielectric spectroscopy in the cultivation of suspended and immobilized hybridoma cells. *J. Biotechnol.* 63, 187–198. doi:10.1016/S0168-1656(98)00080-7
- Noll, T., Biselli, M., 1998b. Dielectric spectroscopy in the cultivation of suspended and immobilized hybridoma cells. *J. Biotechnol.* 63, 187–198. doi:10.1016/S0168-1656(98)00080-7
- Opel, C.F., Li, J., Amanullah, A., 2010a. Quantitative modeling of viable cell density, cell size, intracellular conductivity, and membrane capacitance in batch and fed-batch CHO processes using dielectric spectroscopy. *Biotechnol. Prog.* 26, 1187–1199. doi:10.1002/btpr.425
- Opel, C.F., Li, J., Amanullah, A., 2010b. Quantitative modeling of viable cell density, cell size, intracellular conductivity, and membrane capacitance in batch and fed-batch CHO processes using dielectric spectroscopy. *Biotechnol. Prog.* 26, 1187–1199. doi:10.1002/btpr.425
- Orive, G., Maria Hernández, R., Rodríguez Gascón, A., Calafiore, R., Swi Chang, T.M., Vos, P. de, Hortelano, G., Hunkeler, D., Lacík, I., Luis Pedraz, J., 2004a. History, challenges and perspectives of cell microencapsulation. *Trends Biotechnol.* 22, 87–92. doi:10.1016/j.tibtech.2003.11.004
- Orive, G., Maria Hernández, R., Rodríguez Gascón, A., Calafiore, R., Swi Chang, T.M., Vos, P. de, Hortelano, G., Hunkeler, D., Lacík, I., Luis Pedraz, J., 2004b. History, challenges and perspectives of cell microencapsulation. *Trends Biotechnol.* 22, 87–92. doi:10.1016/j.tibtech.2003.11.004
- Ozturk, S., Hu, W.-S., 2005. *Cell Culture Technology for Pharmaceutical and Cell-Based Therapies*. CRC Press.
- Ozturk, S., Kompala, D., 2005a. Optimization of High Cell Density Perfusion Bioreactors, in: Ozturk, S., Hu, W.-S. (Eds.), . CRC Press, pp. 387–416.
- Ozturk, S., Kompala, D., 2005b. Optimization of High Cell Density Perfusion Bioreactors, in: Ozturk, S., Hu, W.-S. (Eds.), *Cell Culture Technology for Pharmaceutical and Cell-Based Therapies*. CRC Press, pp. 387–416.
- Pajić-Lijaković, I., Bugarski, D., Plavšić, M., Bugarski, B., 2007. Influence of microenvironmental conditions on hybridoma cell growth inside the alginate-poly-L-lysine microcapsule. *Process Biochem.* 42, 167–174. doi:10.1016/j.procbio.2006.07.023
- Párta, L., Zalai, D., Borbély, S., Putics, Á., n.d. Application of dielectric spectroscopy for monitoring high cell density in monoclonal antibody producing CHO cell cultivations. *Bioprocess Biosyst. Eng.* 1–13. doi:10.1007/s00449-013-0998-z
- Patel, P., Markx, G.H., 2008. Dielectric measurement of cell death. *Enzyme Microb. Technol.* 43, 463–470. doi:10.1016/j.enzmictec.2008.09.005
- Pollock, J., Ho, S.V., Farid, S.S., 2013. Fed-batch and perfusion culture processes: Economic, environmental, and operational feasibility under uncertainty. *Biotechnol. Bioeng.* 110, 206–219. doi:10.1002/bit.24608
- Potvin, G., Ahmad, A., Zhang, Z., 2012. Bioprocess engineering aspects of heterologous protein production in *Pichia pastoris*: A review. *Biochem. Eng. J.* 64, 91–105. doi:10.1016/j.bej.2010.07.017
- Read, E. k., Park, J. t., Shah, R. b., Riley, B. s., Brorson, K. a., Rathore, A. s., 2010. Process analytical technology (PAT) for biopharmaceutical products: Part I. concepts and applications. *Biotechnol. Bioeng.* 105, 276–284. doi:10.1002/bit.22528

- Sadettin S Ozturk, Dhinakar S Kompala, 2005. Optimization of High Cell Density Perfusion Bioreactors, in: Cell Culture Technology for Pharmaceutical and Cell-Based Therapies, Biotechnology and Bioprocessing. CRC Press, pp. 387–416.
- Schubert, T., Breuer, U., Harms, H., Maskow, T., 2007. Calorimetric bioprocess monitoring by small modifications to a standard bench-scale bioreactor. *J. Biotechnol.* 130, 24–31. doi:10.1016/j.jbiotec.2007.02.013
- Schuler, M.M., Marison, I.W., 2012. Real-time monitoring and control of microbial bioprocesses with focus on the specific growth rate: current state and perspectives. *Appl. Microbiol. Biotechnol.* 94, 1469–1482. doi:10.1007/s00253-012-4095-z
- Schuler, M.M., Sivaprakasam, S., Freeland, B., Hama, A., Hughes, K.-M., Marison, I.W., 2012. Investigation of the potential of biocalorimetry as a process analytical technology (PAT) tool for monitoring and control of Crabtree-negative yeast cultures. *Appl. Microbiol. Biotechnol.* 93, 575–584. doi:10.1007/s00253-011-3507-9
- Sivaprakasam, S., Mahadevan, S., Bhattacharya, M., 2007. Biocalorimetric and respirometric studies on metabolic activity of aerobically grown batch culture of *Pseudomonas aeruginosa*. *Biotechnol. Bioprocess Eng.* 12, 340–347. doi:10.1007/BF02931054
- Sun, Y., Zhao, L., Ye, Z., Fan, L., Liu, X., Tan, W.-S., 2013. Development of a fed-batch cultivation for antibody-producing cells based on combined feeding strategy of glucose and galactose. *Biochem. Eng. J.* 81, 126–135. doi:10.1016/j.bej.2013.10.012
- Tharmalingam, T., Sunley, K., Spearman, M., Butler, M., 2011. Enhanced Production of Human Recombinant Proteins from CHO cells Grown to High Densities in Macroporous Microcarriers. *Mol. Biotechnol.* 49, 263–276. doi:10.1007/s12033-011-9401-y
- Thu, B., Bruheim, P., Espevik, T., Smidsrød, O., Soon-Shiong, P., Skjåk-Bræk, G., 1996a. Alginate polycation microcapsules: I. Interaction between alginate and polycation. *Biomaterials* 17, 1031–1040. doi:10.1016/0142-9612(96)84680-1
- Thu, B., Smidsrød, O., Skjåk-Bræk, G., 1996b. Alginate gels - Some structure-function correlations relevant to their use as immobilization matrix for cells, in: R.H. Wijffels, R.M.B., C. Bucke and J. Tramper (Ed.), *Progress in Biotechnology, Immobilized Cells Basics and Applications Proceedings of an International Symposium Organized under Auspices of The Working Party on Applied Biocatalysis of the European Federation of Biotechnology Noordwijkerhout*. Elsevier, pp. 19–30.
- Travis, J., 2002. *LabVIEW for everyone: Graphical Programming Made Easy and Fun*, 2nd ed. ed. Prentice Hall, Upper Saddle River, NJ.
- Türker, M., 2004. Development of biocalorimetry as a technique for process monitoring and control in technical scale fermentations. *Thermochim. Acta* 419, 73–81. doi:10.1016/j.tca.2004.01.036
- Uludag, H., De Vos, P., Tresco, P.A., 2000. Technology of mammalian cell encapsulation. *Adv. Drug Deliv. Rev.* 42, 29–64. doi:10.1016/S0169-409X(00)00053-3
- Verica, M., Branko, B., Viktor, N., Flickinger, M.C., 2009a. Immobilized Cells, in: *Encyclopedia of Industrial Biotechnology*. John Wiley & Sons, Inc., Hoboken, NJ, USA, pp. 2899–2916.
- Verica, M., Branko, B., Viktor, N., Flickinger, M.C., 2009b. Immobilized Cells, in: *Encyclopedia of Industrial Biotechnology*. John Wiley & Sons, Inc.
- Voisard, D., Claivaz, C., Menoud, L., Marison, I.W., von Stockar, U., 1998. Use of reaction calorimetry to monitor and control microbial cultures producing industrially relevant secondary metabolites. *Thermochim. Acta* 309, 87–96. doi:10.1016/S0040-6031(97)00370-5
- Voisard, D., Meuwly, F., Ruffieux, P.-A., Baer, G., Kadouri, A., 2003. Potential of cell retention techniques for large-scale high-density perfusion culture of suspended mammalian cells. *Biotechnol. Bioeng.* 82, 751–765. doi:10.1002/bit.10629

- Voisard, D., Pugeaud, P., Kumar, A.R., Jenny, K., Jayaraman, K., Marison, I.W., von Stockar, U., 2002a. Development of a large-scale biocalorimeter to monitor and control bioprocesses. *Biotechnol. Bioeng.* 80, 125–138. doi:10.1002/bit.10351
- Voisard, D., von Stockar, U., Marison, I.W., 2002b. Quantitative calorimetric investigation of fed-batch cultures of *Bacillus sphaericus* 1593M. *Thermochim. Acta* 394, 99–111. doi:10.1016/S0040-6031(02)00243-5
- Von Stockar, U., Maskow, T., Liu, J., Marison, I.W., Patiño, R., 2006. Thermodynamics of microbial growth and metabolism: An analysis of the current situation. *J. Biotechnol.* 121, 517–533. doi:10.1016/j.jbiotec.2005.08.012
- Wagner, C., Armenta, S., Lendl, B., 2010. Developing automated analytical methods for scientific environments using LabVIEW. *Talanta* 80, 1081–1087. doi:10.1016/j.talanta.2009.08.018
- Wahab, Y., Bakar, N.A., Zainol, M.Z., Anuar, A.F.M., Fazmir, H., Mazalan, M., 2014. Labview-based Gait Analysis System for Rehabilitation Monitoring. *Procedia Comput. Sci., Medical and Rehabilitation Robotics and Instrumentation (MRR2013)* 42, 54–61. doi:10.1016/j.procs.2014.11.033
- Wali, W.A., Hassan, K.H., Cullen, J.D., Shaw, A., Al-Shamma'a, A.I., 2013. Real time monitoring and intelligent control for novel advanced microwave biodiesel reactor. *Measurement* 46, 823–839. doi:10.1016/j.measurement.2012.10.004
- Walsh, G., 2014. Biopharmaceutical benchmarks 2014. *Nat. Biotechnol.* 32, 992–1000. doi:10.1038/nbt.3040
- Wang, W., Li, C., Tollner, E.W., Rains, G.C., 2012. Development of software for spectral imaging data acquisition using LabVIEW. *Comput. Electron. Agric.* 84, 68–75. doi:10.1016/j.compag.2012.02.010
- Warnock, J., Al-Rubeai, M., 2005. Production of Biologics from Animal Cell Cultures, in: Nedović, V., Willaert, R. (Eds.), . Springer Netherlands, pp. 423–438.
- Wrobel, P., Czyżycki, M., Furman, L., Kolasinski, K., Lankosz, M., Mrenca, A., Samek, L., Wegrzynek, D., 2012. LabVIEW control software for scanning micro-beam X-ray fluorescence spectrometer. *Talanta* 93, 186–192. doi:10.1016/j.talanta.2012.02.010
- Wurm, F.M., 2004. Production of recombinant protein therapeutics in cultivated mammalian cells. *Nat. Biotechnol.* 22, 1393–1398. doi:10.1038/nbt1026
- Xiao, J., Zhang, Y., Wang, J., Yu, W., Wang, W., Ma, X., 2010. Monitoring of Cell Viability and Proliferation in Hydrogel-Encapsulated System by Resazurin Assay. *Appl. Biochem. Biotechnol.* 162, 1996–2007. doi:10.1007/s12010-010-8975-3
- Xie, L., Wang, D.I.C., 1997. Integrated approaches to the design of media and feeding strategies for fed-batch cultures of animal cells. *Trends Biotechnol.* 15, 109–113. doi:10.1016/S0167-7799(97)01014-7
- Yang, W.C., Lu, J., Kwiatkowski, C., Yuan, H., Kshirsagar, R., Ryll, T., Huang, Y.-M., 2014. Perfusion seed cultures improve biopharmaceutical fed-batch production capacity and product quality. *Biotechnol. Prog.* 30, 616–625. doi:10.1002/btpr.1884
- Zagari, F., 2012. Multidisciplinary Analysis of the Metabolic Shift to Lactate Consumption in CHO Cell Culture. EPFL, Lausanne, Switzerland.
- Zamorano, F., Wouwer, A.V., Bastin, G., 2010. A detailed metabolic flux analysis of an underdetermined network of CHO cells. *J. Biotechnol.* 150, 497–508. doi:10.1016/j.jbiotec.2010.09.944
- Zhang, Y., Wang, W., Xie, Y., Yu, W., Lv, G., Guo, X., Xiong, Y., Ma, X., 2008. Optimization of microencapsulated recombinant CHO cell growth, endostatin production, and stability of microcapsule in vivo. *J. Biomed. Mater. Res. B Appl. Biomater.* 84B, 79–88. doi:10.1002/jbm.b.30847
- Zhao, W., Zhang, Y., Liu, Y., Tan, M., Yu, W., Xie, H., Ma, Y., Sun, G., Lv, G., Zhao, S., Ma, X., 2013. Oxygen diffusivity in alginate/chitosan microcapsules. *J. Chem. Technol. Biotechnol.* 88, 449–455. doi:10.1002/jctb.3845
- Zhou, M., Crawford, Y., Ng, D., Tung, J., Pynn, A.F.J., Meier, A., Yuk, I.H., Vijayasankaran, N., Leach, K., Joly, J., Snedecor, B., Shen, A., 2011. Decreasing lactate level and

- increasing antibody production in Chinese Hamster Ovary cells (CHO) by reducing the expression of lactate dehydrogenase and pyruvate dehydrogenase kinases. *J. Biotechnol.* 153, 27–34. doi:10.1016/j.jbiotec.2011.03.003
- Zhou, T.-C., Zhou, W.-W., Hu, W., Zhong, J.-J., Flickinger, M.C., 2009. Bioreactors, Cell Culture, Commercial Production, in: *Encyclopedia of Industrial Biotechnology*. John Wiley & Sons, Inc.
- Zhu, J., 2012. Mammalian cell protein expression for biopharmaceutical production. *Biotechnol. Adv.* 30, 1158–1170. doi:10.1016/j.biotechadv.2011.08.022

A. Appendix

a. Publications

Cole HE, Demont A, and Marison IW, The Application of Dielectric Spectroscopy and Biocalorimetry for the Monitoring of Biomass in Immobilized Mammalian Cell Cultures, *Processes*, 2015 (Accepted)

Demont A, Cole HE, Marison IW, An understanding of potential and limitations of alginate/PLL microcapsules as a cell retention system for perfusion cultures, *Journal of Microencapsulation*, 2015 (Submitted-under review)

b. Oral presentations

Research Day of School of Biotechnology, Dublin City University, Dublin, *The Application of dielectric spectroscopy for the monitoring of encapsulated CHO cell cultures*, February 2014

BioProcess Analytics and Sensor Technology, Zurich University of Applied Sciences, Wädenswil, Switzerland, *Monitoring and Control of high cell density cultures*, September 2014 (Presentation given by Prof. Marison IW).

c. Posters

ESBES-ISSSP 2012, Istanbul, Turkey, *Microencapsulation, an innovative technology for increasing cell growth: Dielectric spectroscopy for online cell density monitoring*, September 2012

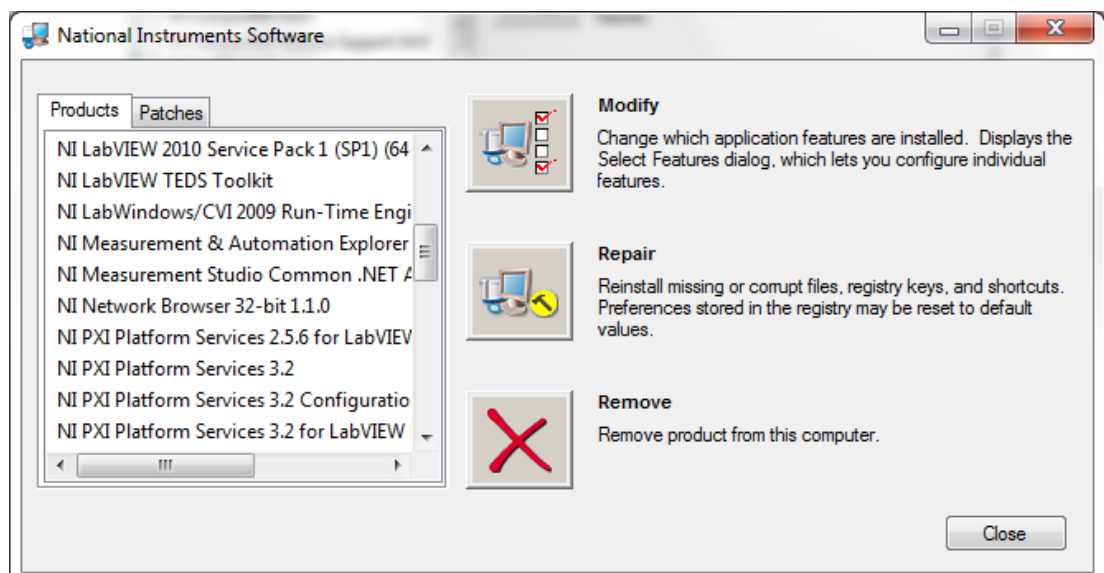
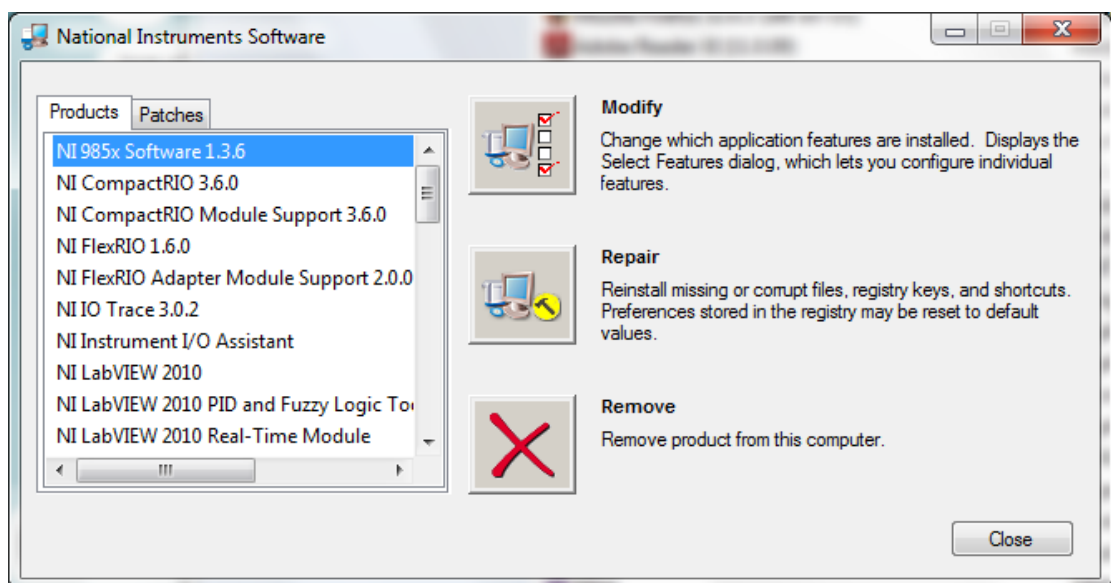
d. The LabVIEW monitoring and control VI

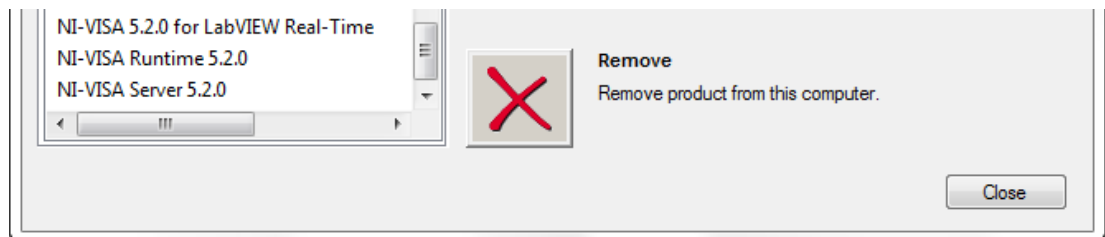
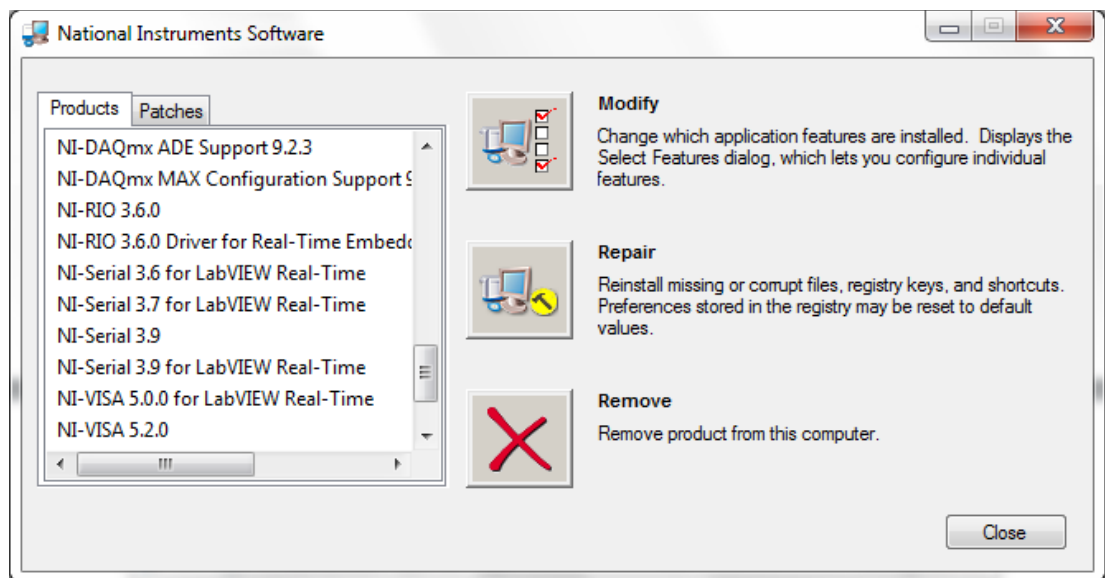
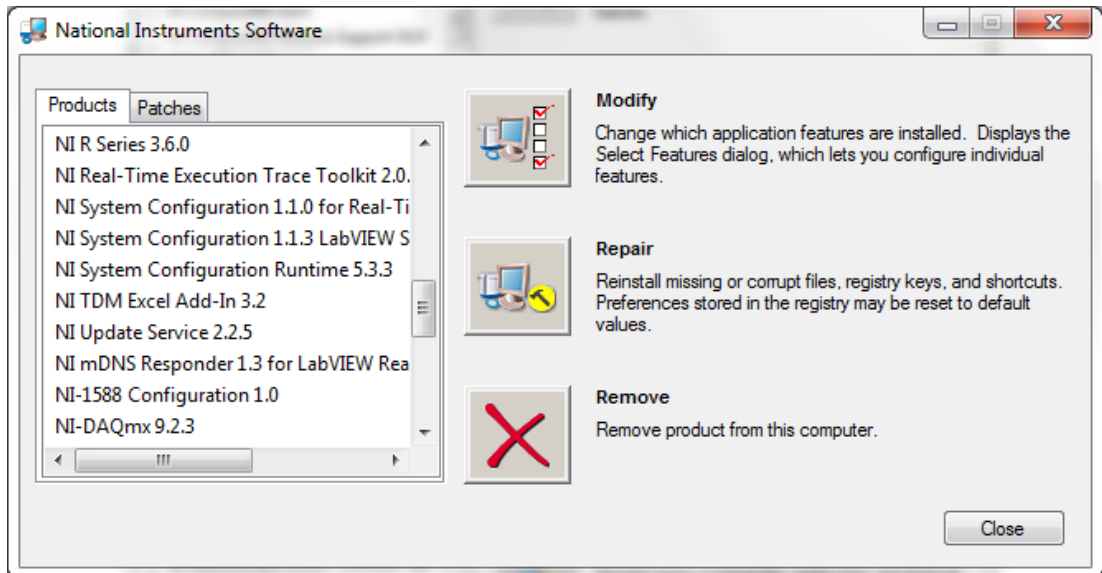
i. The necessary software installed on the computer

For the communication between computer, CompactRIO and instruments functions well, the following software must be installed the user computer (Windows 7, 32-bit Operating system):

- NI-LabVIEW 2010 SP1
- RealTime 2010 SP1
- NI-RIO 3.6.0
- NI VISA 5.0.3

ii. Necessary software and sub-modules installed on CompactRIO

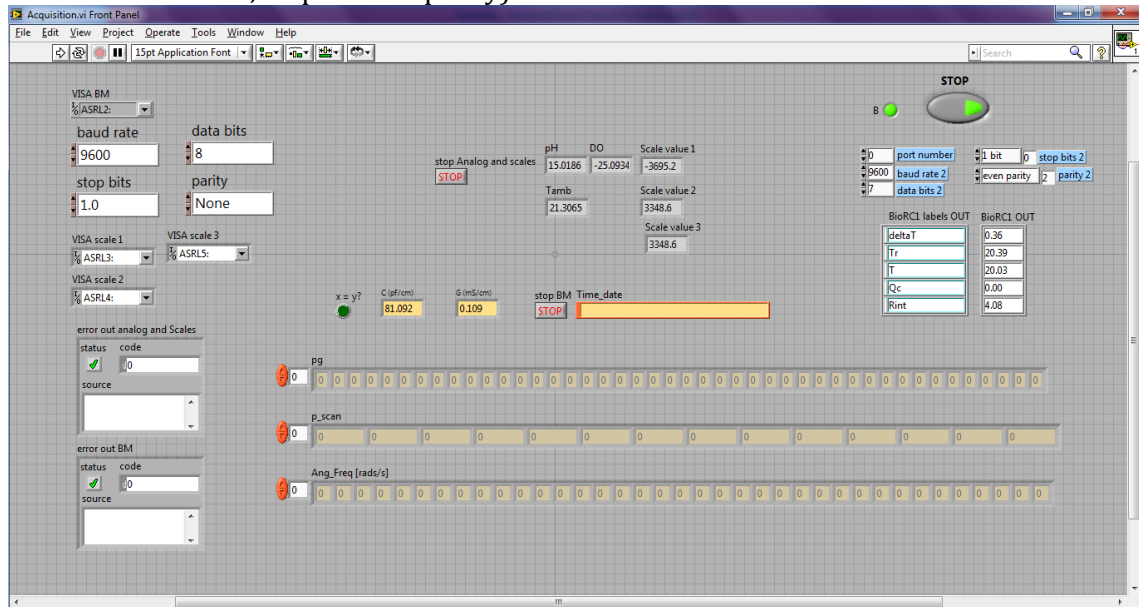




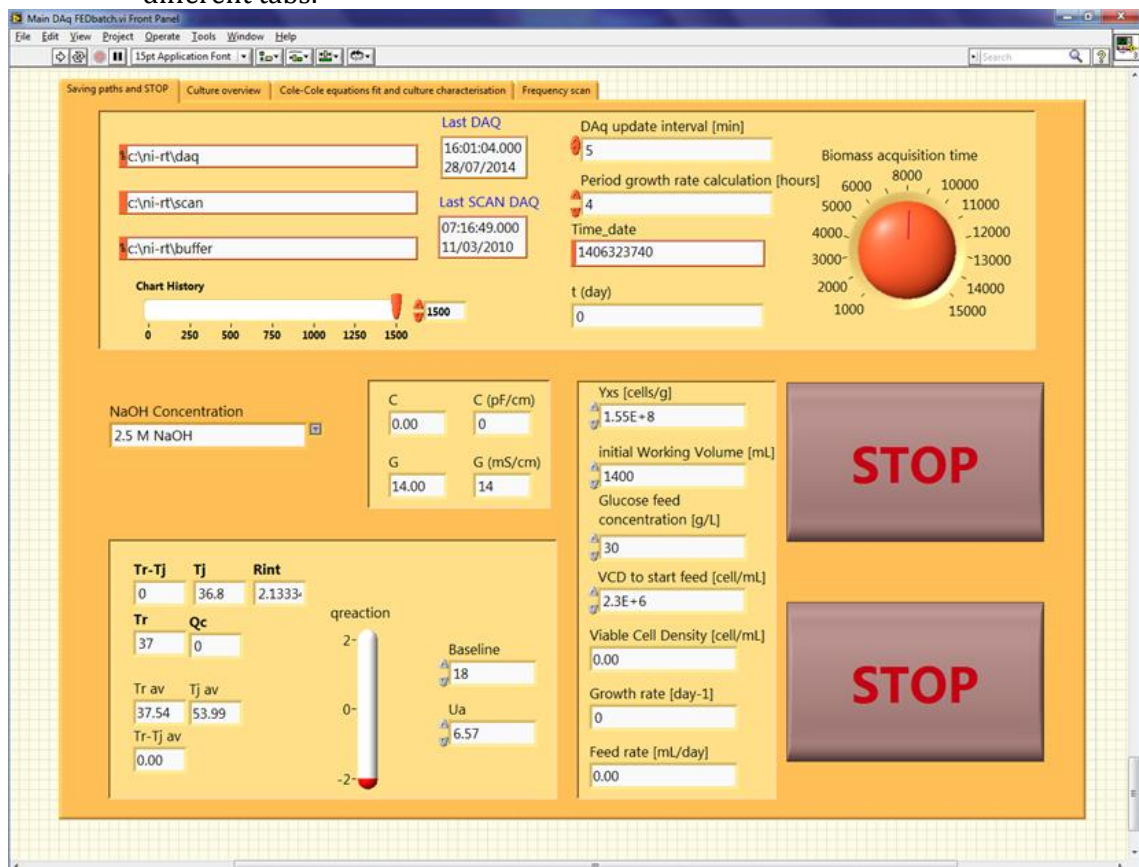
iii. *User manual (for Fed-Batch cultures, more complete version)*

1. Switch on the CompactRIO and computer
2. Check all necessary instruments are connected to the CompactRIO, switched on and functioning.
3. Open the LabVIEW project entitled *RC1e-BM DAq HEC* project. Verify the CompactRIO is visible in the project. If no communication is established between the CompactRIO and computer, open NI MAX and start trouble shooting.
4. In the LabVIEW project, open the *Acquisition VI*. In this VI, the communication parameters with the digital instruments must be entered in their respective

numeric control boxes (COM port (ASRL port on CompactRIO), baud rate, data bits, stopbits and parity).



5. Run the VI by clicking on the white arrow in the task bar
6. Ensure data is being received from each connected instrument.
7. Then open the *Main DAq FEDbatch* VI. The front panel appears and contains 4 different tabs.



8. In the first tab, enter the file path to the desired location where the files are to be saved. This also consists in naming all three files.
9. Select the base concentration, the data acquisition time period, the time frame for determining the growth rate, enter the cells to substrate yield, initial working volume, the substrate concentration in the feed medium, the cell

density at which to start the feed into their respective numeric control box. It is also possible to change the chart history length (number of data points per chart) and the time necessary for the biomass monitor to send data (this varies with the software update).

- View the *Cole-Cole equations fit and culture characterisation* tab. Enter the specific membrane capacitance C_m and the cytoplasm conductivity σ_i . Make sure the save to file button is OFF.



- Go to the *Culture overview* tab to view all the time charts. In this tab, the culture progression can be observed by any operator. To start the VI, click on the Run button (white arrow). The text files are created as soon as the VI is initiated. In these textfiles, the different headings are inserted, the files are saved, and closed. After the set data acquisition time, the files are opened, the last values are inserted, after the previous saved valued. The files are then saved and closed once again.



12. To perform a frequency scan, go back to the Cole-Cole equations fit and culture characterisation tab. Start the frequency scans on the biomass monitor and let the signal equilibrate. This is important, especially at the beginning of the culture. Once no variations can be observed on the biomass monitor screen, click on the save to file button. This will save the permittivity and conductivity values to the frequency scan file. Once sufficient frequency scans have been saved, switch off the save to file function, and go back to the single frequency screen on the biomass monitor.
13. At the end of the culture, to end the acquisition of the data and the output of the signal to the pump, go back to the *Saving paths and STOP* tab and click on the two STOP buttons. It takes a while for the VI to stop (one full acquisition time cycle). Then go back to the *Acquisition VI*, and click on the two STOP buttons. Close all VIs.
14. To view the acquired data, go to the saved files location, and open the desired text file to view. The data can be copied and pasted into a Microsoft Excel spreadsheet.

iv. Acquisition VI Code

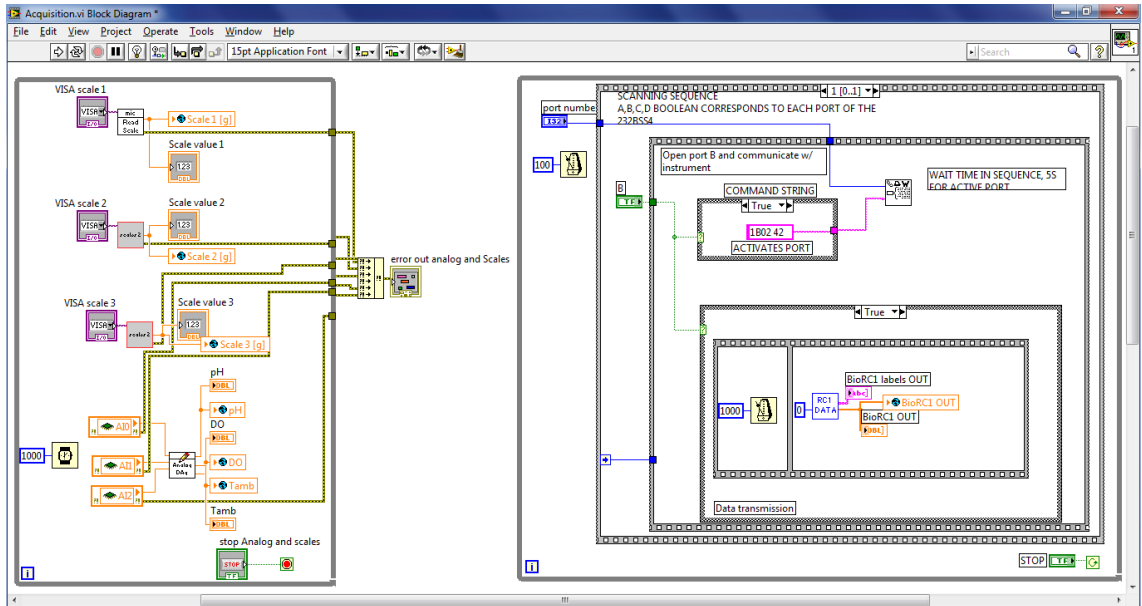


Figure A.1 Code for the acquisition of the signals received from the pH controller, DO controller, ambient temperature pt100 and calorimeter eRC1

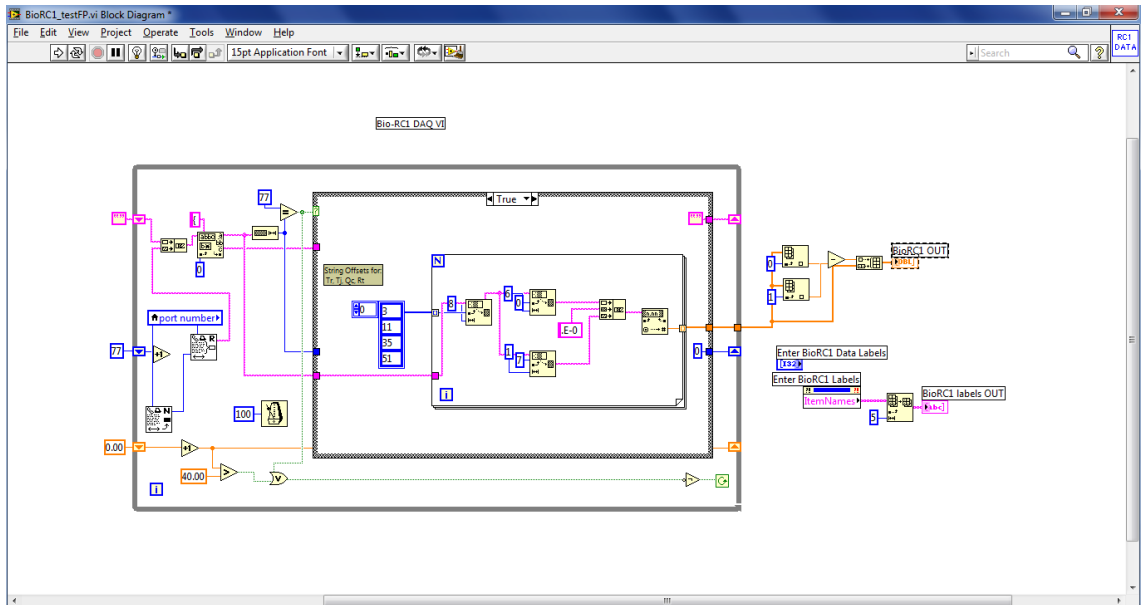


Figure A.2 Sub-VI to obtain and read the signal sent by the eRC1

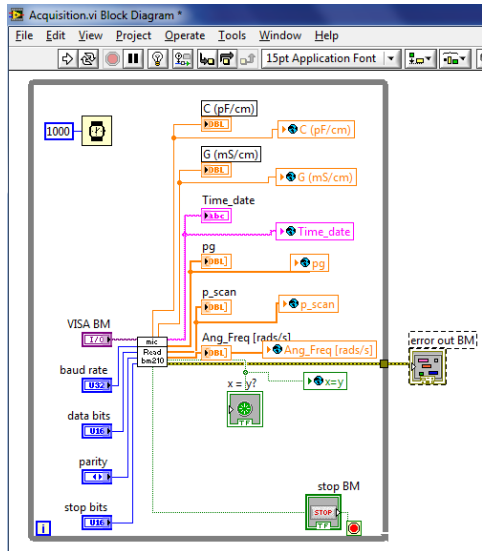


Figure A.3 Code for the acquisition of the signals received from the Biomass Monitor

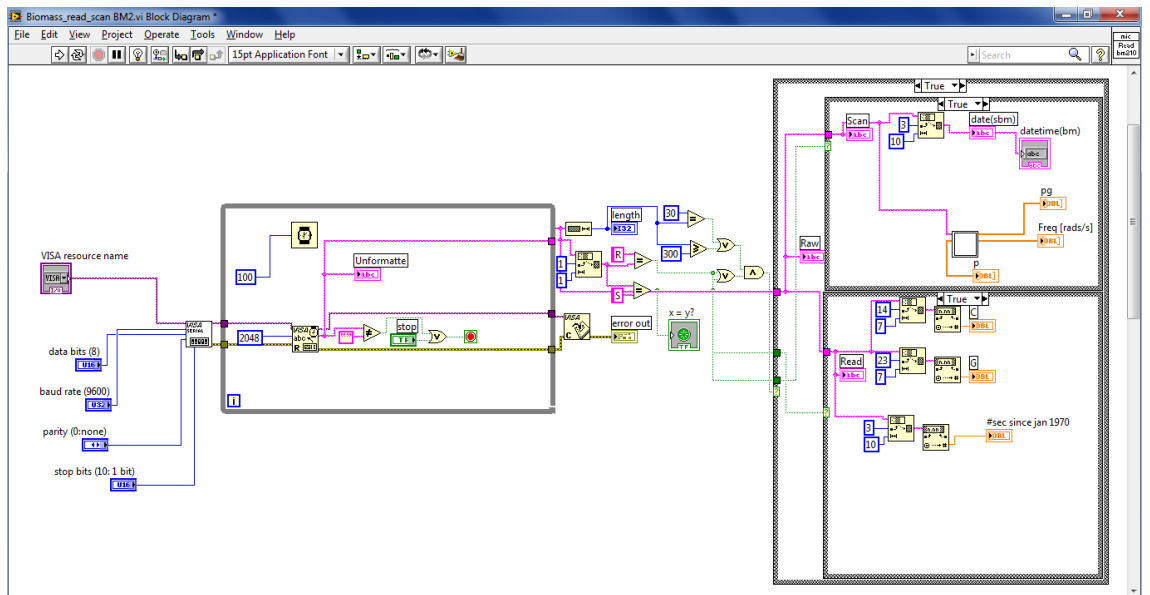


Figure A.4 Sub-VI to obtain and read the signal sent by the Biomass Monitor from ABER Instruments

v. Main DAq FEDBatch VI

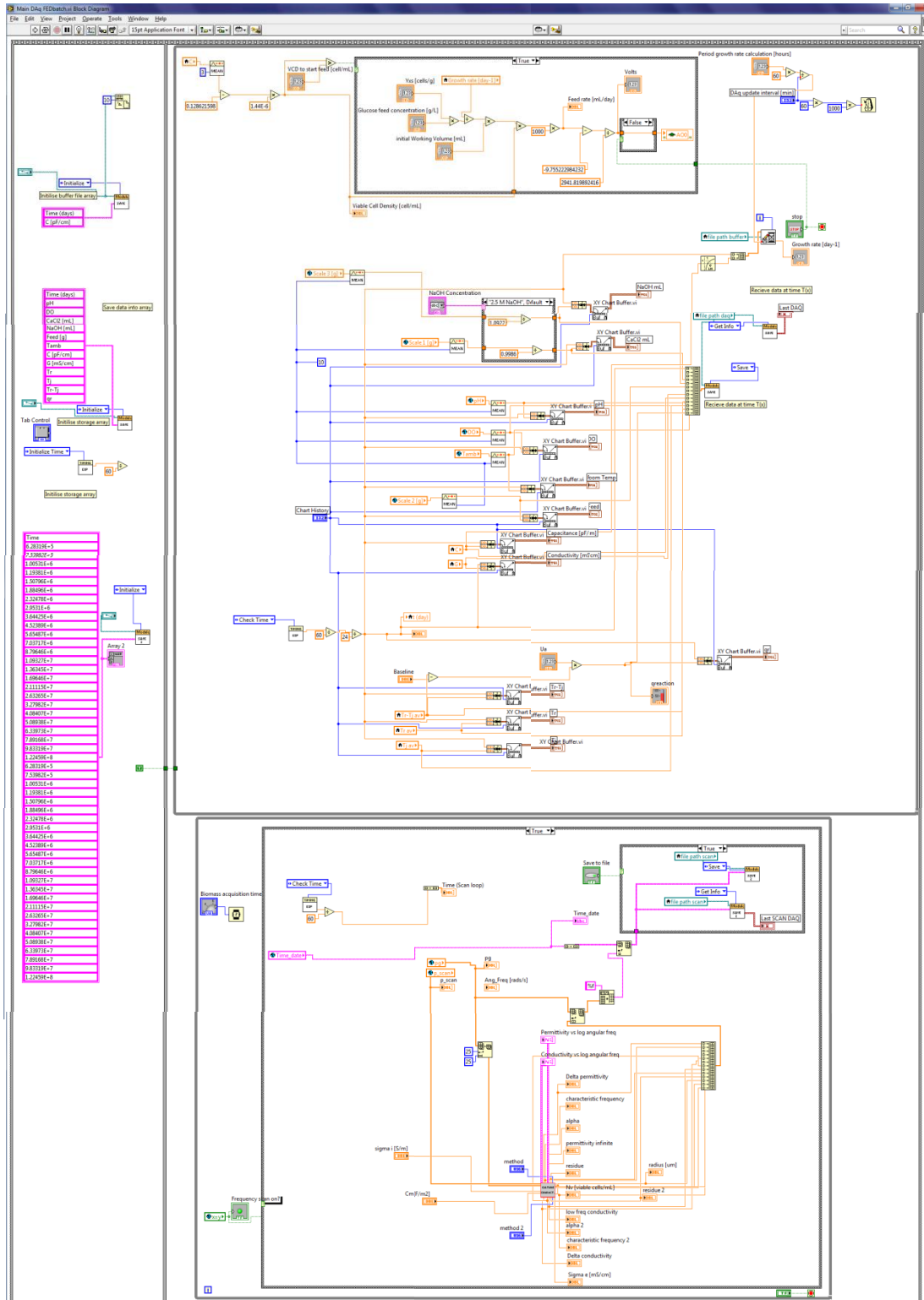


Figure A.5 Code of the Main Data Acquisition VI. This VI codes for saving the data into a text file after calculating an average and adding the new data point to the time chart. In addition, in the FEDbatch VI, the growth rate and the feed rate are calculated

vi. Cole Cole modelling of frequency scans

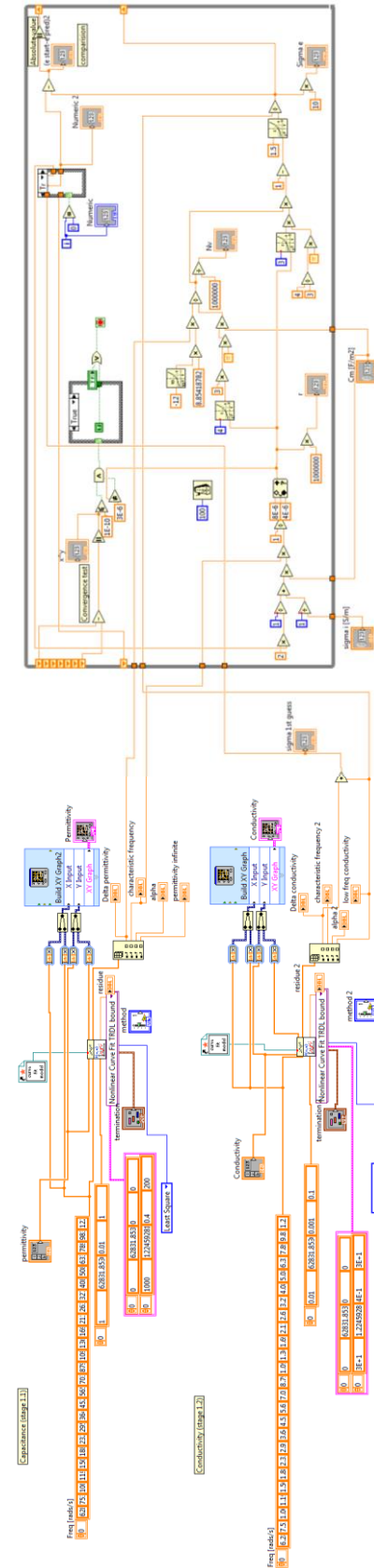


Figure A.6 Code for the frequency scans modelling using the Cole Cole equations, and iteration to determine the cell radius, cell number per unit volume and the conductivity of the medium

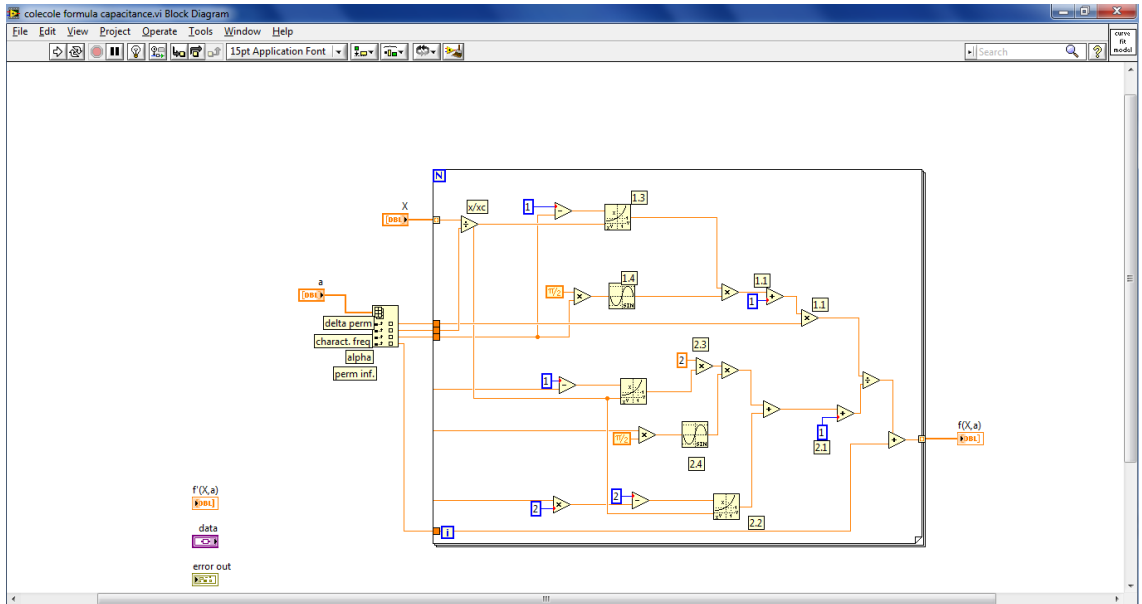


Figure A.7 Code of the Cole Cole formula used to fit capacitance values

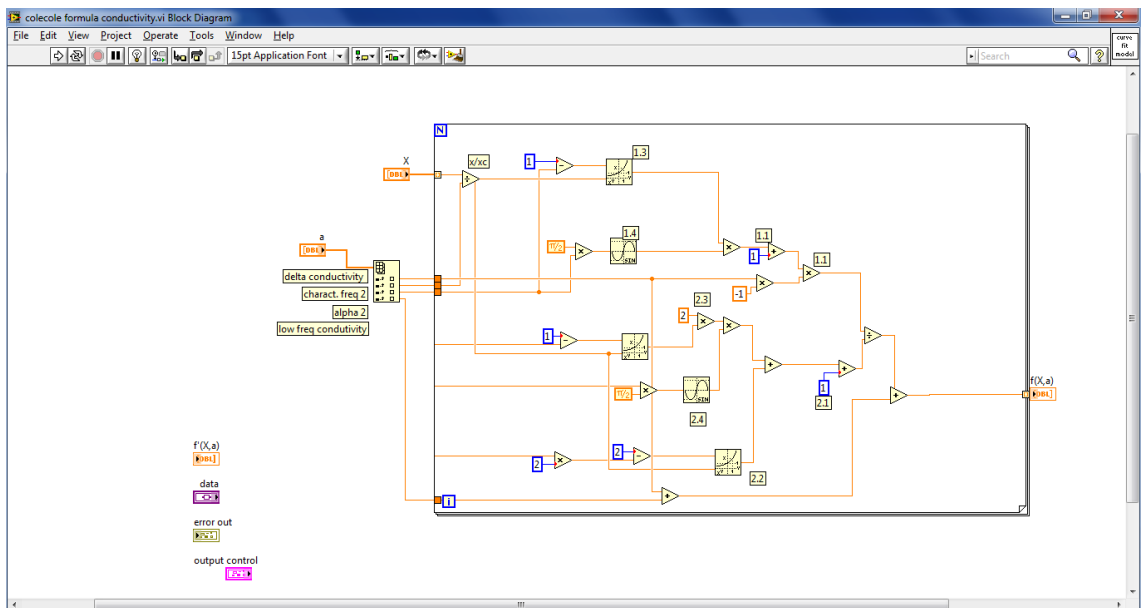


Figure A.8 Code of the Cole Cole formula used to fit conductivity values